Chameleon stars: diffusion and spectroscopic transformations in white dwarfs

by

Benjamin T. Dehner

A dissertation submitted to the graduate faculty

in partial fulfillment of the requirements for the degree of

DOCTOR OF PHILOSOPHY

Department: Physics and Astronomy

Major: Astrophysics

Major Professor: Steven D. Kawaler

Iowa State University

Ames, Iowa

1996

Graduate College
Iowa State University

This is to certify that the doctoral dissertation of

Benjamin T. Dehner

has met the requirements of Iowa State University

Signature was redacted for privacy.

Major Professor

Signature was redacted for privacy.

For the Major Department

Signature was redacted for privacy.

For the Graduate College

DEDICATION

To my parents, who made it possible;

and to Susan, who made it worthwhile.

TABLE OF CONTENTS

LIST OF TABLES

LIST OF FIGURES

ACKNOWLEDGEMENTS

In the time and work it took to get to this point, there are many people who helped me, both professionally and personally. On the professional side, there are those who helped educate me, and teach about science and its methods. On the personal side, there are those who helped me learn that life isn't all about school, and that there is far more to learn than can be gained by sitting in front of a computer or in a classroom.

For the professional part, my advisor, Steve, who helped me get started; the NSF, who paid my salary while I did this. Jim Liebert, who pointed me in a good direction. Don, who got me started, even though I did something else. Roger Alexander, who's forgotten more about numerical methods than I know, and gave me lots of help. And not to forget Bonnie, Erlene, Lori, Eva, Joyce, the only ones in the department who do any real work.

Personally, there are many, many people I have to thank during my career here at Iowa State. Jerry Mathews, my first instructor here, who was always a help. Golbon, who it was a pleasure and honor to know. The clan - Charley, Jeff, Susan (S.), Ken, Mark, Rich, Steve, Vandy. The slugs - Scott, Anthony (Dad!), Mikey, Karen, Doug, Kathy, Phil, and Matt. Chuck, Bruce, Kevin, Ralph, the bastards. A special thanks to Susan K., for, well, being Susan. Max, for getting me started on

mystic; Athen, for getting me started on netrek. Don, for being that humble and modest sort of guy he is, and for showing me how to golf. Can't forget to mention the group - Doug, Andy, Dan (the originals), Paul, Kurt (in spirit, anyway), Curt, Brian (once or twice,) John, Theresa, Jim, Ginger, Kari, and Jennifer.

Life is a crap sandwhich -

the more bread you got, the less crap you gotta take

- Tom Servo

ABSTRACT

White dwarfs stars are the end product of stellar evolution, generating no energy by nuclear fusion, slowly cooling over time. As they cool, their intense gravity causes the lightest element – either hydrogen or helium – to float to the surface. This "gravitational settling" is responsible for the observed nearly pure surface composition of white dwarfs. In this investigation, I model this settling process in these stars by constructing a sequence of models which represent the star at different stages as it cools.

As white dwarfs cool, at certain temperatures they undergo nonradial pulsations. Most importantly, a change in the composition as a function of the depth within the star causes differences in the pulsations of the star. Pulsations are then a natural way of measuring the depth of surface layers of pure composition formed by gravitational settling.

I calculated a sequence of models representing the evolution of white dwarfs. The initial model was of a young, hot white dwarf at a surface temperature of $T_{eff} \sim$ 130,000K, representing the pulsating white dwarf PG 1159. The model has a surface layer of mixed He, C, and O containing about 10^{-3} of the stellar mass. This model was evolved until it cooled to 25,000K, where it again undergoes pulsations. By this temperature, settling causes the formation of a surface layer of helium containing

about 10^{-6} of the stellar mass. Observations of GD 358, a pulsating helium-rich white dwarf at $T_{eff} \sim 25,000K$, show that it has a surface helium layer of roughly this thickness. This indicates that stars like PG 1159 may evolve to stars like GD 358, despite the incongruity in surface layer mass.

Finally, there exists a range of temperature, from 45,000K to 30,000K, where all observed white dwarfs have hydrogen dominated surfaces. I added hydrogen to the PG 1159 models to investigate its effects. The calculations show that hydrogen diffuses very quickly to the surface, and would be present at the surface in detectable quantities. This contradiction with observations of PG 1159, which shows no detectable hydrogen, implies some other mechanism, such as mass loss, which alters the surface abundance of white dwarfs.

CHAPTER 1. WHITE DWARFS: THE CAST OF CHARACTERS

Strange objects which persist in showing a type of spectrum utterly out of keeping with their luminosity may ultimately teach us more than a host which radiate according to the rule.

A. Eddington (1922)

This dissertation concerns the modeling of the evolution of white dwarf stars. However, before addressing *what* is to be done, it is even more important to ask *why* it is to be done at all. What broader questions exist, and where, in the framework of astronomy, does this work fit in? First, therefore, I start with the history of white dwarf stars, and the solution to the initial puzzle posed by their very existence. I then give a modern perspective on the role of white dwarfs in contemporary stellar astrophysics. Finally, I preview the work presented in this dissertation, and how it fits into this framework.

1.1 A Historical Perspective

In the quote at the beginning of this Chapter, Eddington was referring to the then recently discovered class of white dwarf stars. The debut of this strange class of faint stars was in 1783, when 40 Eri B was "discovered" by William Herschel (Herschel, 1783, 1785). This was followed by the discovery of Sirius B in 1862 by Clark

(Bond 1862). Though known to be underluminous for their mass in comparison with normal stars, they were not thought to be otherwise unusual until spectroscopic measurements were made early in the twentieth century. They were then both classified as spectral type A, i.e., hotter than the Sun, with the observations of 40 Eri B in 1910 (Hertzsprung 1915), and Sirius B in 1914 (Adams 1915). This presented a mystery, since simple radiative theory indicates that such hot stars must be faint because of very small size – nearly the size of the Earth. This, in turn implies a mean density of over 100,000 times greater than the Sun!

Some of the properties of these first white dwarfs and their companions are summarized in Table 1.1,[1] which gives the effective (surface) temperature $T_{\rm eff}$, the mass and luminosity in solar units, $M_\odot$ and $L_\odot$, and the distance in parsecs from the Sun. As can be seen, the white dwarf stars are very low luminosity, but have masses similar to the Sun and a much higher temperature.

The numbers given in Table 1.1 are shown more graphically in Figure 1.1,[2] which shows the location of the main sequence of hydrogen burning stars and the white dwarfs. The location of two special stars – PG 1159–035 and GD 358 – are also marked in this diagram. These stars play an important role in my investigation.

An understanding of the internal structure of white dwarfs developed in 1926 when R. Fowler speculated that the interiors of white dwarfs were governed by the (then novel) Fermi–Dirac statistics (Fowler 1926). He speculated that the central support of the star against gravity came from electron degeneracy pressure. This idea

[1]Data on the white dwarfs taken from McCook & Sion (1987), and data on the main sequence stars from Hoffleit (1982)

[2]Main sequence data taken from Bowers & Deeming (1984) Table 3.1 while the white dwarf data is from stellar models used in this investigation.

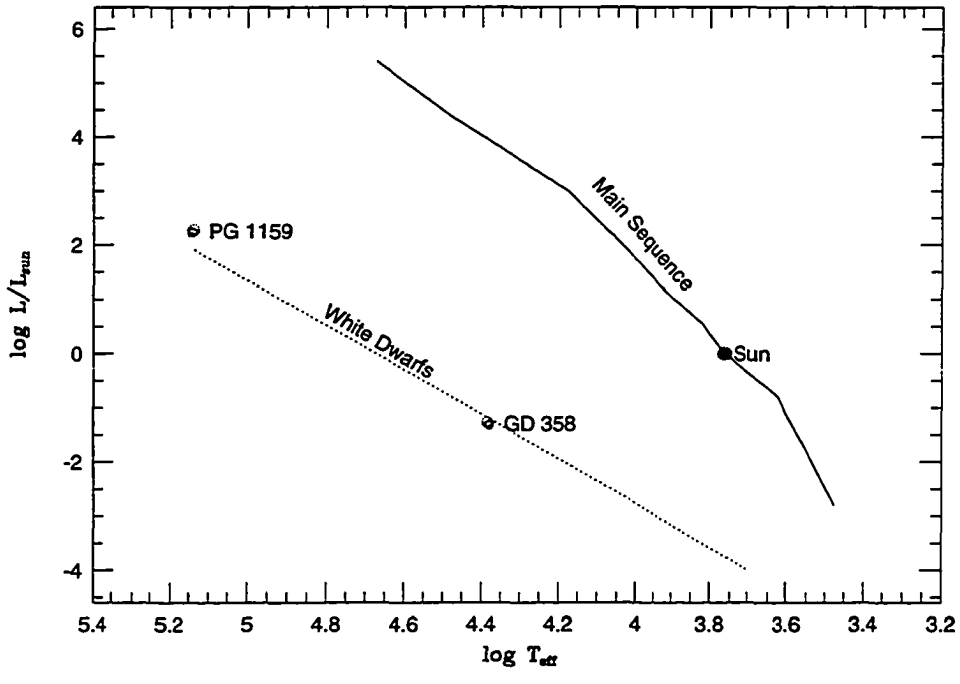

Figure 1.1: HR Diagram, with the main sequence and white dwarfs.

Table 1.1: Properties of the "first" white dwarfs

Star	m_v	L ($L_\odot$)	T_{eff}(K)	M ($M_\odot$)	Distance (parsecs)
40 Eri A	4.5	0.3	5,080	0.75	4.8
40 Eri B	9.7	0.0027	12,700	0.44	
Sirius A	-1.5	23.0	9,130	2.35	2.6
Sirius B	8.3	0.002	25,400	0.98	

was further elaborated upon in 1939 by S. Chandrasekhar who further demonstrated that white dwarfs could never exceed approximately $1.4M_\odot$ in mass; this was the largest mass that could be supported by electron degeneracy pressure (Chandrasekhar 1939).

As more white dwarfs were discovered, it was found that nearly all had pure elemental surface composition, with that surface being either hydrogen or helium. In the early 1950's, Evry Schatzman showed that this purity results from gravitational settling; heavier elements sink to the center of the star, and the lightest elements float to the surface (Schatzman, 1958). However, it still remained a mystery as to why some retained hydrogen at their surface while others did not. And, further, the question of the origins of white dwarfs remained unanswered.

Schatzman (1958) and Schwarzchild (1958) both speculated that the degenerate configuration of white dwarfs may follow the exhaustion of all available nuclear fuel. A main sequence star supports itself against gravity by generating energy through nuclear fusion, and so perhaps, they argued, when a star runs out of fuel, it would collapse into the degenerate configuration of a white dwarf. While this is correct in a broad sense, we now know that the true path that a star take to becoming a

white dwarf is much more convoluted, as will be discussed in more detail in the next Chapter.

1.2 Modern Perspectives and Problems

Two fundamental aspects of white dwarfs have direct bearing on this investigation. First, white dwarfs come in two major "flavors", with either helium or hydrogen dominated surfaces. The origins of this dichotomy are still not well understood. Second, white dwarfs have been established as the end stage of stellar evolution for stars between 0.8 and 8 times the mass of the Sun (see Chapter 2 for details.) This implies that the properties of both individual white dwarfs and the aggregate properties of the population place some conditions on their predecessor stars. In particular, the white dwarf population contains a history of star formation in the galaxy, and so understanding white dwarf evolution is a link to understanding galactic star formation, as shown by, for example, Wood (1992).

1.2.1 The "DB gap"

As stated, white dwarfs usually have either pure H or pure He surface layers. This dichotomy is the basis of the spectroscopic classification now in use for these stars. The three main categories are the DA stars, with surfaces rich in hydrogen; the DB stars, which show neutral helium (He I) surface features; and the DO stars, which show ionized helium (He II) surfaces. While white dwarfs have a wide range of surface temperatures, from $\gtrsim$100,000K down to $\sim$5000K, there are no helium-rich white dwarfs between 45,000K and 30,000K, as described by Liebert (1986). Helium rich stars are found at temperatures both above and below this gap, however. Given

that white dwarfs generate no energy, and therefore must cool, one must ask "Where are the helium white dwarfs between 45,000K and 30,000K?" This "DB Gap" implies that there must be some mechanisms or processes that hide the surface helium at 45,000K and re-introduce it at 30,000K in some white dwarfs, such as discussed by Liebert, Fontaine, & Wesemael (1987).

1.2.2 The coolest white dwarfs

As the ultimate remnants of most normal stars, white dwarfs can provide an archaeological record of the history of star formation in the galaxy. Most importantly, as the coolest white dwarfs are the oldest objects in the galactic disk, identification of the low luminosity white dwarfs provides a time limit on star formation in the galaxy. This facet of white dwarfs has been explored extensively following the work of Winget et al.(1987); see for example Iben & Laughlin (1989) and Wood (1992). Obviously, there are uncertainties inherent in this approach; despite these difficulties, Liebert et al.(1988), using data from several surveys, have determined that there are essentially no white dwarfs fainter than ~0.00003 solar luminosities. Models of cooling white dwarfs by Wood (1992) which match the luminosity function cutoff have indicated an age for the galactic disk of 8 to 10 Gyr. This *range* reflects our remaining uncertainties about white dwarf structure, the principle one being the surface compositional structure.

1.3 Purpose and Direction of This Work

The goal of this dissertation is to examine the diffusive processes that alter the surface layer composition during white dwarf evolution. Diffusion may play a role

in producing the observed phenomenon of the DB gap, as well in determining evolutionary links between various types of white dwarfs. Most of the work on diffusion in white dwarfs over the past four decades has focused on specific phenomena of white dwarf atmospheres. However, only a very few comprehensive computations of white dwarf evolution incorporating time-dependent diffusion have been done, and none have been made since the remarkable results that have come from the studies of the pulsating white dwarfs. In this work, I construct white dwarf evolutionary sequences that include time-dependent diffusion and compare them directly with the new observations.

In the next Chapter, I will review the modern view of white dwarf origin and evolution. In chapter 3, I discuss the evolution code and the numerical methods used to solve the equations governing white dwarf structure and evolution, and in Chapter 4 I elaborate on the treatment of diffusion used in the evolution code. Chapter 5 describes the results for helium-rich surface models, and Chapter 6 explores the behavior of hydrogen-rich models. In Chapter 7, I summarize the results and examine the accomplishments of this investigation.

CHAPTER 2. WHITE DWARF EVOLUTION: A LIFE STORY

What is their history? What their destiny? What their function in the universal scheme of things?

– Agnes M. Clerke (1903)

In this Chapter, I will review some of the conventional ideas of stellar evolution, concentrating on the formation of white dwarfs. This review provides the background against which the investigation presented in the following chapters was conducted. Further, I wish to pose some of the questions and point out uncertainties in current thinking; these are the motivation for this investigation. Finally, I will also discuss how the properties of observed white dwarfs may be related to their progenitor stars.

2.1 Stellar Evolution: A Brief Description

An anonymous astronomer once quipped "A star is nature's way of making a white dwarf." This is at best an oversimplification of stellar evolution and white dwarf formation, although it is relevant to the description of evolution in this Chapter. Most, but not all, stars will become white dwarfs. For stars which do become white dwarfs, there may be several possible evolutionary paths to that end. Some general introduction to stellar evolution is available in such texts as Clayton (1983) and Hansen & Kawaler (1994). Here, I will focus on those stars which become white

dwarfs, and, on what appears to be the most common paths they take. Some excellent reviews, on which this chapter is based, can be found in Iben & Renzini (1983, 1984), and Iben & Tutukov (1984).

The story of evolution is an account of the conflict within a star of internal pressure against gravitational collapse. For most of a star's life, while it is on the main sequence, the nuclear fires in the core of the star convert hydrogen into helium and energy, heating the core and providing long-term support against gravity. Eventually, though, the hydrogen fuel becomes exhausted; the evolutionary path taken by the star at this point depends on the mass.

When the core of the star runs out of hydrogen, the (now helium) core begins to contract, and hydrogen fusion continues in a shell surrounding the core. This is accompanied by expansion and cooling of the star; this maintains and then increases its luminosity as the shell thins. The star is now a "red giant", and, with its changed state, has ascended the "red giant branch" (RGB). Along with the ascent of the red giant branch comes the "first dredge-up." A convection zone forms, which reaches down from the outer layers to convectively mix underlying material which has undergone nuclear processing. The results of this dredge-up are discussed by Becker & Iben (1979) and summarized by Iben & Renzini (1984).

For stars greater than about 3 $M_{\odot}$, the helium core will begin to undergo fusion quiescently. This helium core-burning star will descend the red giant track, and begin to burn helium in the core at higher temperatures and lower luminosities along helium burning loops, as shown in Iben & Renzini (1984).

The cores of stars less massive than 2-3 $M_{\odot}$, however, do not have the internal pressure to ignite helium fusion at moderate densities; instead, these stars will develop

a electron degenerate helium core, where the gravitational pressure is balanced by the quantum mechanical interaction of the closely packed electrons. In this state, the pressure exerted by the electrons depends only on the density, and is independent of the temperature.

Eventually, these degenerate cores reach a sufficiently high temperature to begin helium fusion in a "helium flash". The fusing helium releases energy and heats up the core, but the increased temperature does not affect the pressure, due to the degeneracy. The temperature increase does, however, increase the energy generation rate, thus further raising the temperature. This runaway cycle continues until the temperature in the core is high enough to remove the degeneracy condition. Given that this helium flash can happen on a timescale of minutes, as shown by the calculations of Cole & Dupree (1980, 1981), it is somewhat of a mystery that the star as a whole does not explode. However, such stars do not catastrophically explode, since low mass stars, which must have undergone a helium flash, are observed quietly burning helium in their cores as horizontal branch stars in globular clusters.

Finally, regardless of the ignition conditions, the following stages occur when the helium fuel in the core becomes exhausted. Similar to the earlier stage, where a shell burning hydrogen source ignited, a helium–burning shell surround the carbon-oxygen core. The star expands and cools in a manner similar to the first ascent of the red giant branch, and ascends the asymptotic giant branch (AGB). As it ascends the AGB, the surface convection zone deepens in star, contributing to the "second dredge up."

High mass stars may then ignite carbon in their cores, and continue with nuclear reaction with elements of increasing atomic number. These stars typically continue

until producing iron in their core; at this point, these stars can undergo a supernova explosion. These high mass ($> 9M_{\odot}$) stars are beyond the scope of this dissertation. I focus on less massive objects which have a less catastrophic end to their lives.

2.1.1 The Asymptotic Giant Branch

The asymptotic giant branch (AGB) represents the final throes of a dying star. One of the most important processes in this phase of the stars life (or death) is that the star may lose much of its mass during this time. As discussed by Weidemann (1990), it has become increasingly apparent that stars of up to 9 (possibly more) $M_{\odot}$ are the predecessors of white dwarf stars, which must be less than the Chandrasekhar limit of $1.4M_{\odot}$.

Models by Bowen & Willson (1991) demonstrate how mass loss driven by large-amplitude pulsation on the AGB leads to the inevitable formation of a "superwind". Their models show how the superwind may naturally increase to very large values, thus terminating the AGB.

AGB evolution is naturally divided into two periods, the "early AGB" (E-AGB) and the "thermally pulsing AGB" (TP-AGB); see, for example, Iben & Renzini (1983) & Iben (1991). During the early part of a star's life on the AGB, it derives most of its luminosity from an outer hydrogen burning shell. However, as the hydrogen burns, it deposits the resultant helium "ash" in a shell beneath it. Eventually, this helium ash reaches high enough density to ignite at its base, where it is mildly degenerate, in an event referred to as a thermal pulse. When the helium shell undergoes fusion, the energy generated causes it to expand, pushing out the outer hydrogen shell and extinguishes hydrogen burning. The helium shell deposits its carbon ash onto

the growing degenerate core. Eventually, the helium burning subsides by expansion and cooling, followed by re-ignition of the hydrogen-burning shell in the subsequent relaxation. These episodes of helium burning add mass to the carbon/oxygen core.

The luminosity of a star with a degenerate carbon/oxygen core and a hydrogen shell source, i.e., on the AGB, is determined primarily from the mass of the core, and is independent of the envelope. As originally demonstrated by Paczynski (1970), the AGB luminosity is given by

$$\frac{L}{L_\odot} \approx 60,000\left(\frac{M_c}{M_\odot} - 0.5\right), \tag{2.1}$$

where M_c is the mass of the degenerate core. This "core mass–luminosity relation" holds for all but the most luminous AGB stars, as discussed by (for example) Blöcker & Schönberner (1991). Hence on the AGB the star's position in the H–R diagram is determined by the core mass, and not the total mass, and the evolution of the core and envelope are to a large extent decoupled. However, once the AGB star has lost enough mass, it leaves the AGB to regions of higher temperatures as the hot core becomes exposed. Most white dwarf stars are assumed to form from such "post-AGB" objects, which have ascended the AGB, and then moved off of the AGB to regions of higher temperature, losing most of their outer envelope. The models of Paczynski (1970), Iben & Tutukov (1984) and Schönberner (1983) show how post-AGB evolution can lead to the development of the white dwarfs through this channel.

There is another channel into the white dwarf cooling track for stars in which the envelope is not massive enough to ascend the AGB. Such objects instead evolve to white dwarfs through the subdwarf (sd) phase. Vauclair and Liebert (1987) discuss this scenario in the context of white dwarf formation, while models by Dorman, Rood & O'Connell (1993) and others display evolutionary tracks. This channel into the

white dwarf region produces white dwarfs at the low-mass end of the distribution (between 0.50 and 0.55 $M_{\odot}$) and is not thought to be a major contributor to the total white dwarf population. Hence, these objects will not be considered here. I will instead concentrate on stars which proceed through the thermally–pulsing AGB to a possible planetary nebula nuclei (PNNi) stage, where they then cool (possibly as a "PG 1159" star) before settling on the white dwarf cooling track.

As an AGB star loses mass the luminosity increases and the mass loss rate increases. Initially, the effect of the mass loss on T and L is small; see the models of Bowen & Willson (1993). However, as discussed by Paczynski (1970) and Schönberner (1983), when the envelope is thin enough due to mass loss, at about $10^{-3}M_{\odot}$, the effective temperature strongly depends on the remaining envelope mass. Essentially, as long as the envelope is thick enough, the core is hidden from view. However, as the envelope further thins, the inner core becomes exposed and the effective temperature of the star increases dramatically.

If a star leaves the AGB during a thermal pulse, then the extended envelope – with the remnant hydrogen – can be entirely lost, implying this newly formed star will have a helium rich surface. If, however, the star leaves the AGB during the hydrogen burning phase, it will still retain a hydrogen rich surface. Iben (1984) notes that an AGB model spends about 80% of its lifetime in the hydrogen burning phase, so, therefore, approximately 80% of the white dwarfs formed as post-AGB object should be hydrogen rich white dwarfs. This scenario implies that a white dwarf is "born" as either a hydrogen-rich (DA) white dwarf, or a helium-rich (DB/DO) white dwarf, and thereafter remains that way.

2.1.2 Planetary nebulae

Whether or not a proto-white dwarf will form a planetary nebula depends on the competition between the mass loss rate and the evolution rate of the star. During this stage of evolution, the star becomes hotter, as the outer envelope is lost and more of the hotter core is exposed. As the outer envelope expands to the radius of a planetary nebula, the star must be hot enough (T_{eff} ~30,000K) to ionize the material to form the nebula. If the star evolves to higher temperatures too slowly, the expanding material will expand and disperse before it can become ionized by the central star. The age of a planetary nebula can be estimated by measuring the size and the expansion velocity of the nebula; these dynamical ages consistently disagree with the theoretical models. This disagreement between the observationally determined ages of planetary nebulae and the theoretical ages is discussed by Gathier & Pottasch (1989).

A recent explanation for this has been forwarded by Blöcker (1995). He demonstrates that the cooling timescale is also dependent on the initial mass of the object while it is on the AGB. A more massive object will have a higher internal temperature, and will have a less degenerate core. This lesser degree of degeneracy in turn leads to a shorter cooling timescale than would otherwise be expected.

At the core of a planetary nebula is an object referred to, obviously enough, as a "planetary nebula nucleus", or PNN (plural = PNNi). (Sometimes these are referred to as "central stars of planetary nebulae", or CSPN, or, occasionally, "central stars".) Gathier & Pottasch (1989) discuss some of the properties of PNNi; these objects typically have a surface gravity somewhat less then the white dwarfs, with $\log g \sim 6$, and have temperature ranging from roughly 30,000K to over 100,000K. These objects

are often considered intermediates between white dwarfs and the AGB.

2.2 White Dwarfs

In the first Chapter, white dwarfs were introduced as being very small, hot stars, maintaining themselves against gravitational collapse with electron degeneracy pressure. Now I will go into more detail about their structure, and properties as a class.

2.2.1 Masses

The "typical" white dwarf is an object about the mass of the sun and the size of the earth. As reviewed by Weidemann (1990), white dwarfs have a strong uniformity in mass, with the bulk of them being at or near 0.6 $M_\odot$. For a sample of 126 hydrogen-rich white dwarfs, Bergeron, Saffer, and Liebert (1992) determine a mean mass of 0.56 $M_\odot$, with a standard deviation of 0.137 $M_\odot$. The distribution is more sharply peaked than a Gaussian, with a tail extending to the high mass end. Their mean surface gravity is determined to be $\log g = 8.0$, which implies a radius of approximately 10^{-2} times that of the sun, or about the size of the Earth.

This strong uniformity in white dwarf masses is itself curious. Since white dwarf predecessors on the main sequence may be as large as 9 $M_\odot$, this is indicative of the amount of mass that these stars must somehow loose on the way to becoming a white dwarf. The narrowness of this distribution can be understood, at least qualitatively, as resulting from the feedback between the Paczynski (1970) core mass–luminosity relation and the steep luminosity dependence of the Bowen & Willson (1993) mass loss description (e.g. Kawaler 1996.) This convergence of evolutionary paths of white

dwarfs simplifies their modeling in certain respects, though it complicates their use as archaeological specimens.

2.2.2 Spectral classification

The spectral classification for white dwarf stars as described by Sion (1986), which is summarized here. Also included are the variable white dwarf types not considered by Sion (1986). The basic properties and classification scheme is given in Table 2.1.

Table 2.1: White Dwarf Spectral Classifications

Type	T_{eff} (K)	features
DA	< 80,000	H lines
DB	< 30,000	HeI lines
DO	>47,000	HeII or HeII lines
DC	<5000	no lines
DQ	<10,000	carbon
DZ	anywhere	metals
DAV (ZZ Ceti)	10,000-13,000K	pulsation
DBV (GD 358)	20,000K - 27,000K	"
DOV (GW Vir)	>80,000	"

A graphical representation of Table 2.1 is shown in Figure 2.1, with the temperature regions inhabited by each variety of white dwarf indicated. The pulsational instability strips of variable stars are also noted. One may be tempted to think of the stars in the diagram as "evolving" from left to right, as they cool. While essentially correct, this simple picture may easily mislead; white dwarf evolution will be more fully discussed in the next Section.

The DA stars have a surface rich in hydrogen, with an apparently pure surface

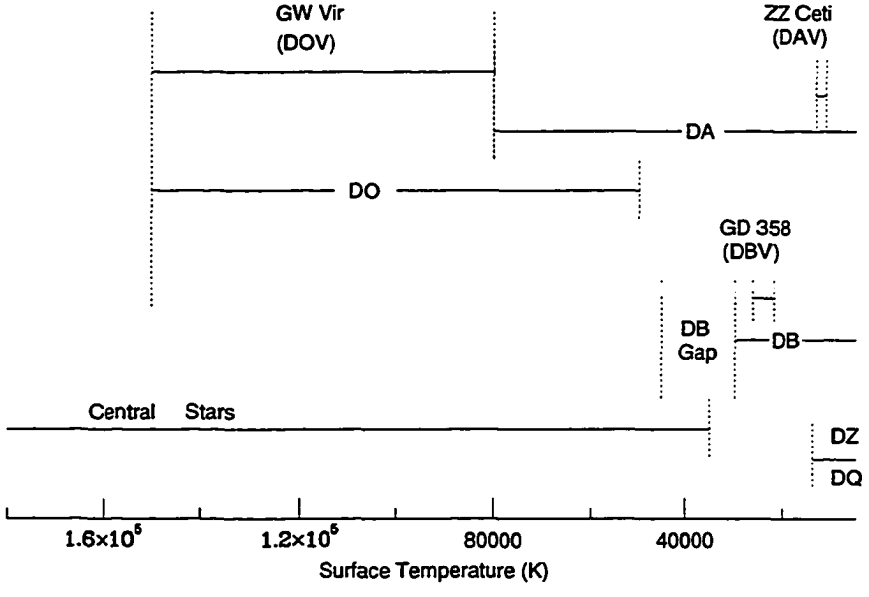

Figure 2.1: Approximate temperature distribution of white dwarfs

hydrogen layer (H/He $< 10^{-4}$.) The hottest known DA stars are at about 80,000K, while the coolest DAs are at about 6000K. Above 80,000K it is believed that hydrogen will be completely ionized, and thus spectroscopically invisible; likewise, below 5500K, hydrogen becomes spectroscopically invisible as well. The effective temperature range from roughly 12,230K to 10,300K, as determined by Kepler & Nelan (1993), is known as the ZZ Ceti instability strip, where almost all observed DAs pulsate. A few non-pulsating DAs have been found in this region as well by Kepler & Nelan (1993), which leads Kepler (1995) to speculate that the location of the instability strip may be mass dependent; this mass–dependence would require that higher mass stars pulsate within a higher temperature range.

The DB stars, which show lines of neutral helium, are found at T_{eff} between $\approx$ 30,000K and 12,000K, below which the helium lines disappear. Though such stars would easily be identifiable as DB white dwarfs, there are no helium–rich white dwarfs in the range between 30,000K and 45,000K; this is called the "DB gap", and will discussed in the next Section. Between approximately 20,000K to 28,000K (Thejll et al.1991) are found the pulsating DB stars, with the prototype being GD 358.

The DO stars, distinguished by the presence of He II lines, are among the hottest known white dwarfs, with temperatures as high as 180,000K down to roughly 47,000K. Some DO stars show evidence for large abundances of carbon and oxygen; these stars are known as the PG 1159 stars after their prototype. Some PG 1159 stars are also pulsating stars — the "GW Vir" stars, of which PG 1159 is again the prototype. The exact boundaries of the GW Vir instability region in the H–R diagram are uncertain due to large uncertainties in the surface temperatures of these stars. Atmospheric models by Werner et al.(1991a) indicate that if hydrogen is present in

the atmospheres of the DO stars, it must be at an abundance of less than 5% by mass.

The PG 1159 stars are often considered proto-white dwarfs, stars starting to make their way down the white dwarf cooling tracks. These stars are characterized by high surface temperatures (> 100,000K), strong metal abundances (mostly C, N, & O), and no detectable hydrogen. Given the above classification scheme, these stars could be classed as DOZQ stars. These objects are believed to be intermediate between the PNNi and the hot DO white dwarfs. Whether or not they are a link between the AGB and all white dwarf stars is still a somewhat open question; the answer depends on whether or not enough hydrogen remains in these stars to eventually turn them into DA stars.

Dreizler et al.(1995) discuss observations of "hybrid PG 1159" stars, which show spectra characteristic of the PG 1159 stars, except that these hybrid objects clearly show the presence of hydrogen. These stars appear to be to located midway between the PG 1159 stars and hot DO stars on the H-R diagram, but as yet few of these (three) have been discovered.

2.2.3 Pulsations

As seen in Table 2.1, some white dwarfs pulsate. These pulsating stars are extremely important, both in the general sense and in this investigation, because the pulsations are a probe into the interior structure of the star. The study of pulsating white dwarf stars has made many advances in recent years, due in large part to the advent of pulsational studies with the Whole Earth Telescope (WET), described by Nather et al. (1990). These studies allow a direct probe into the internal structure of

these objects, giving a solid observational foundation for structural and evolutionary models.

The location of the instability regions in the HR diagram are a matter of great debate. Temperature estimates are derived from comparison of observation with atmospheric models, with uncertainties of roughly several hundred degrees, and more for the DBV and DOV stars. Further, systematic uncertainties, such as errors in the the input physics of the models, can raise this substantially. Theoretical estimates of the location of the instability regions, i.e., from evolutionary models, depend heavily on assumptions made about convection within the star, such as the convective efficiency; see, for example, Tassoul et al.(1990.) A more precise temperature determination would perhaps be a useful way to calibrate models of convection.

Paradoxically, while this dissertation is concerned with chemical evolution, spectroscopy plays a very small part, since the spectroscopic differentiation between "pure hydrogen" and "pure helium" does not require sophisticated spectroscopic measurements. (Not, at least, at the temperatures of the objects in this dissertation.) On the other hand, while this is not a study of variable stars, stellar pulsations play a key role in this study, since these pulsations provide an essential probe of the internal structure of the star.

2.2.4 Cooling

Many of the aspects of white dwarf cooling are summarized in the review by D'Antona & Mazzitelli (1990). A white dwarf can well be described as "a hot brick surrounded by a blanket", a hot central core slowly losing energy through a surrounding insulating envelope. This basic model of a cooling white dwarf was first

introduced by Mestel (1952), in which he assumed a degenerate isothermal core (the brick) which cooled by radiative diffusion through a surrounding non-degenerate envelope (the blanket.) While this model neglects some of the relevant physics, it is still a good approximation to the cooling of white dwarfs.

Early in a white dwarf's cooling history, neutrino emission becomes an important mechanism for the star's cooling. As shown by Iben & Tutukov (1984), models of very young, hot white dwarfs at luminosities between $1.5 > \log(L_\gamma/L_\odot) > 0$, have a neutrino luminosity which exceeds the photon luminosity. Kawaler et al.(1985) show that higher mass white dwarfs should have a much more significant neutrino cooling over a larger range of luminosities. In general, neutrino cooling causes the cooling timescale to be faster than the classical Mestel time.

Lamb & Van Horn (1974), Iben & Tutukov (1984) and Wood (1992) also show that later in the white dwarf's life, when $\log(L/L_\odot) \sim -3$, other effects such as crystallization of the core, and Debye effects (a quantum mechanical effect which causes a decreased specific heat) will occur. When the core begins to crystallize, this will release latent energy from the interior, thus slowing the cooling of the white dwarf. After this, however, the now crystalline interior will have a lower specific heat then gaseous phase, and will tend to cool more quickly. While the details of white dwarf cooling are actively being investigated, this basic picture is clear.

2.3 Chemical Evolution and Changes in Surface Composition

The processes controlling the chemical evolution of white dwarfs are complex. As seen in Table 2.1 and Figure 2.1 there is a temperature range between roughly 45,000K down to 30,000K where there are no observed helium rich white dwarfs.

This phenomena, called the "DB gap" has been noted by Wesemael et al.(1985) and Liebert (1986). That this gap exists at all indicates that some dynamical mechanism must operate in at the hot helium-rich star which can change the surface composition. Liebert et al.(1987) suggest that the blue (high temperature) edge of the gap is caused by gravitational settling, which causes hydrogen to float to the surface of the star covering the helium as the star cools to 45,000K. Subsurface convection zones, which form at about 30,000K, reach from the hydrogen surface into the deeper helium layers, then mix the helium back to the surface to account for the red edge. While plausible, this scenario has yet to be demonstrated to occur in evolutionary models.

The red edge of the gap is defined by the star PG 0112+104, the hottest known DB below the gap. The temperature of this star is somewhat uncertain; several results are summarized by Thejll et al.(1991). While all results consistently list this star as the hottest DB below the gap, there is a discrepancy between the results of different researchers. The currently "accepted" value for the temperature of this star, by Thejll et al.(1991) is 27,000K $\pm$ 2000K.

Sion (1986) discusses a possible two-track evolutionary scheme for white dwarfs, supposing that DAs and DBs evolve along separate evolutionary tracks. Further, Sion speculates that there are possible tracks by which one type may change to another, consistent with the presence of the DB gap. This discussion by Sion points out many questions and uncertainties which are at the heart of current investigations in white dwarf evolution.

Further, the PG 1159 stars could be the precursors of all white dwarfs, if one can explain the transition from the metal-rich PG 1159 surface composition to the much more chemically pure DA and DB stars. At cooler temperatures, there is the high

metal abundances in the DQ and DZ stars. As noted by Sion (1984), the temperature-dependent distribution of these objects is additional evidence for the existence of some mechanism (or mechanisms) which can alter the surface abundance.

To model white dwarf chemical evolution correctly, there are five mechanisms which much be considered: mass loss, diffusion, convection, radiative levitation, and accretion of interstellar material. Each of these plays a significant role at one time or another in the "life" of a white dwarf. In this dissertation, while I focus on diffusion, I also address each of the others to see what insight my models may give concerning the importance of these mechanisms.

2.3.1 Convection

At some point in their lifetime, white dwarfs develop convective layers within their envelopes. The two main problems which need to be considered are the extent of the convection zone, and the efficiency of convective transport. The transport of energy through the convection zone from the core has obvious implications for the stellar energy loss and cooling timescale. The extent of the convection zone determines how much convective mixing may occur. Convective mixing can affect radiative opacities, and thus cooling timescale; convective mixing may also play a role in transformations from one spectral type to another.

The role of convection in white dwarf evolution has been most recently studied via a grid of white dwarf models by Tassoul, Fontaine, & Winget (1990). They discuss using the observed temperature limits on the pulsational instability strips to calibrate models of white dwarf convection.

2.3.2 Diffusion

Gravitational settling in white dwarf stars was discussed by Schatzman (1958), in which he demonstrated that differential force force on ions and electrons causes a small electric field, which in turn leads to separation of elements in white dwarf stars. This separation of elements is observed as the nearly pure elemental surface composition of most white dwarf stars, either hydrogen or helium. However, there have been few calculations of time-dependent diffusion in the literature. In most white dwarf studies, authors assert a layered compositional structure, presuming that diffusive equilibrium is reached very quickly, compared with evolutionary timescales. In such studies, an equilibrium composition profile (i.e. Arcoragi & Fontaine 1980) is frequently used to describe the structure, and this profile is maintained throughout the evolution of the model. There has been no comprehensive evolutionary modeling with time dependent diffusion for white dwarfs stars with realistic post-AGB models.

Vauclair and Reisse (1977) consider a situation where elemental separation is achieved relatively rapidly, resulting in a large gradient in the mean molecular weight μ. This gradient, or "μ-barrier", as they call it, would then remain stable by chemical diffusion processes. While this approach is similar to the equilibrium described above, they then consider possible disruption of the equilibrium gradient caused by meridonial circulation induced by stellar rotation. Their conclusion is that such circulation cannot significantly affect the shape of the μ-barrier.

Muchmore (1984) considers diffusion of heavy elements in white dwarfs, concerned with explaining anomalous metal abundances, with DA and DB models including C, Mg, Ca, and Fe. He calculates diffusion timescales for these elements, based on the diffusive velocities at the base of the convection zone. Further, he con-

siders the effects of thermal diffusion, and concludes that thermal effects will be small in white dwarf stars. Since Muchmore's investigation is concerned with cooler white dwarfs, starting at $T_{eff} \sim 23{,}000K$, he also includes the effects of multiple ionization states for the various heavy elements on the diffusion.

Iben & MacDonald (1985, IM) included a dynamical treatment of diffusion, with an approach similar to Muchmore (1984). IM consider a mixture of nine isotopes, ^{1}H, ^{3}He, ^{4}He, ^{12}C, ^{14}N, ^{16}O, ^{18}O, ^{22}Ne, and ^{22}Mg. Unfortunately, they did not treat diffusion throughout the evolutionary sequence. Rather, they "turned on" diffusion relatively late in the white dwarf evolution, at $T_{eff} \sim 30{,}000K$. Further, they did not have pulsational models – or data – with which to compare their results. The goal of their work was to investigate hydrogen burning on an inward diffusive tail in the latter stages of white dwarf evolution. Despite these limitations, IM contains many modeling techniques which are adapted in this work.

Pelletier et al.(1986) also present a sophisticated dynamical treatment of diffusion. Their methods included the effects of electron degeneracy and the presence of multiple ionization stages, and they also used a more powerful numerical method for solving the diffusion equation. However, their models considered only a binary mixture of helium and carbon. Further, their evolutionary models were started at $T_{eff} = 50{,}000K$, much cooler than the initial models used here. They were concerned with explaining the anomalous carbon abundances seen in the cooler DQ stars. Their main emphasis was examining a deep convection zone mixing material from a diffusive tail from the carbon core of a star.

Paquette et al.(1986b) calculate diffusion timescales based on their diffusion coefficient calculations in Paquette et al.(1986a). However, they are only concerned

about the settling of metals (C, N, O, Mg, Ca, and Fe) as trace constituents, and examining the possibility of radiative effects, which would maintain abundances of these elements in the photospheres of white dwarfs longer than gravitational settling would suggest.

2.3.3 Radiative levitation

In a certain sense, radiative levitation is a diffusive processes. Radiative forces acting on atoms in a plasma cause a differential force which can act to separate different species. It is treated separately here because radiative levitation studies typically require a completely different approach than other types of diffusion studies.

Many workers have addressed radiative levitation, invoking radiative forces in hot white dwarfs to explain anomalous metal abundances. Theses studies calculate the total radiative force on a given element, and compare this force to the gravitational force to see if this force can support an element against gravitation. Radiative levitation is related to diffusion, in that it is a differential force on the atoms, induced by a radiation field, can cause a separation of the elements involved. Chayer et al.(1989), Chayer et al.(1990), have addressed the purely radiative problem, and were unable to explain metal abundances in white dwarfs with purely radiative effects. Unglaub & Bues (1996) investigated radiative forces in PG 1159 stars, and were also unsuccessful in explaining the high metal abundances.

Radiative forces may be an important mechanism in diffusion in white dwarfs. A future goal is to include radiative forces within a diffusion calculation. Unfortunately, calculation of radiative forces requires detailed knowledge of the opacities and relative number densities of all ionization states of all elements present, and is beyond the

scope of this dissertation.

2.3.4 Accretion

The possibility of white dwarfs accreting material from the interstellar medium (ISM), especially hydrogen, has been discussed by MacDonald & Vennes (1991). Accretion from a cool interstellar medium is certainly possible, especially for cooler white dwarfs. As explained in MacDonald & Vennes (1991), the likelihood of hydrogen from a cool interstellar cloud being accreted onto a white dwarf surface depends on the hydrogen becoming ionized by the stellar radiation. Ionized particles undergo Coulomb force interaction and behave as a fluid. Thus, a younger, hotter white dwarf, with a larger Strömgren sphere (radius of surrounding material ionized by the star) would be more capable of accreting a larger fraction of hydrogen from the ISM. However, accretion of a small amount of hydrogen onto a DB white dwarf may result in the accreted hydrogen absorbing ionizing photons, and preventing further accretion.

Further, as discussed by MacDonald (1992), a very low mass loss rate may be sufficient to prevent accretion onto a white dwarf. Mass loss rates as low as $10^{-21}M_{\odot}$/yr in a hot ISM, or 10^{-18} - $10^{-17}M_{\odot}$/yr in a cold cloud could be enough to prevent accretion. While mass loss in white dwarfs is very speculative, as discussed in the next section, the younger, hotter stars which are most likely to accrete are also the most likely to lose mass.

Finally, according to Wesemael (1979), significant white dwarf accretion will occur during encounters with cold interstellar cloud, and the the mean time between encounters will be roughly 3.9×10^{7}yr. The objects studied in this dissertation are

not old enough to have encountered an interstellar cloud. Thus, the objects used in this study, it is believed that accretion will not be a factor.

2.3.5 Mass loss

While ample evidence exists for mass loss in PNNi, mass loss from white dwarf stars is very speculative. There has been no observed mass loss from even the hot PG 1159 stars, let alone any of the cooler white dwarfs. The current assumption is that such high surface gravities will prevent any significant mass loss. On the other hand, there is observed mass loss from the lower gravity PNN, on the order of $10^{-9}M_{\odot}$/yr. The central star Abell 78 was observed to have a mass loss as high as $10^{-7.6}M_{\odot}$/yr (Werner and Koester 1992, quoted in Werner et al.1992). Werner et al.(1995) discuss observations of hot DO white dwarfs which indicate a possible wind, although this is still a tentative conclusion.

There are also some theoretical calculations of the mass loss from PNNi. Pauldrach et al.(1988) present the results of calculations of radiation driven winds from PNNi. They calculate a grid of models with four masses, evolving away from the AGB, at temperatures ranging from 30,000K to 100,000K. Some of their results are summarized in Table [2.2]; they are in qualitative agreement with observations.

This leaves open the question of mass loss in ordinary white dwarfs. As we shall see, the diffusion velocities in white dwarfs are small, on the order of 10^{-6} cm/sec at the surface, so that a very small mass loss may prevent the onset of gravitational separation in the surface layers.

Table 2.2: PNNi Mass Loss, Pauldrach et al.(1988)

$M/M_\odot$	T_{eff} (10^3K)	$\dot{M}$ ($10^{-6}M_\odot$/yr)	$M/M_\odot$	T_{eff} (10^3K)	$\dot{M}$ ($10^{-6}M_\odot$/yr)
1.0	30	0.41	0.644	30	0.037
	100	0.18		100	0.020
0.565	30	0.0092	0.546	30	0.0016
	100	0.0037		80	0.00075

2.4 Things To Come

I have presented a background of stellar evolution. First, I presented the an overview of the stages of evolution leading to white dwarf formation, then a description of the changes white dwarfs go through. While the work in this dissertation focuses on white dwarfs, white dwarfs themselves are the result of previous stages of stellar evolution. The surface layer structure is, at least initially, a sensitive function of the point at which they depart from the AGB. We must keep in mind that modeling white dwarfs gives implications for earlier stages of evolution. Ironically, while this dissertation focuses on modeling the evolution of the surface composition of white dwarfs, the main observational tie not to spectroscopy, but to photometry. We wish to model not only the evolution of the surface abundance, but the thickness of the surface layers; and stellar pulsations are the key observation for this measurement, as described in Chapter 5.

CHAPTER 3. ISUEVO: THE DETECTIVE'S TOOLS

Comparing the methods now available for astronomical inquiries with those in use thirty years ago, we are at once struck with the fact that they have multiplied.

– Agnes M. Clerke (1887)

3.1 Introduction: Modeling Stellar Evolution

Groundbreaking calculations of the structure and evolution of stars using "modern" computers began nearly 40 years ago; pioneering studies of white dwarf evolution followed in the 1960's. Today, computational stellar evolution is a mature area, with many independently developed codes in active use. For the present investigation, models were needed that were as realistic as practical, with prior evolutionary phases accounted for and observational constraints met. In addition, pulsation calculations require numerical techniques which produce smooth models with well-behaved spatial and thermodynamic derivatives. The physical state of white dwarf interiors requires that the models accurately treat degeneracy, non-ideal effects on equations of state, and conductive opacities.

The evolution code used here known (for lack of a better name) as ISUEVO was designed for pulsation and evolution studies of a variety of types of stars; it was opti-

mized for white dwarfs and and PN central stars (Kawaler 1993, Dehner & Kawaler 1995). For this study, the code was further developed and refined; the major change was the inclusion of time dependent diffusion. In this chapter, I describe the details of ISUEVO as a "standard" stellar evolution code. The equations solved are reviewed in Section [3.2]. The details the input physics are then described, and Section [3.4] outlines the numerical techniques used to solve the structure equations. Discussion of the numerical treatment of diffusion is reserved for the following Chapter.

3.2 Equations of Stellar Structure

Since ISUEVO is essentially a traditional stellar evolution code, the reader is referred to basic texts, such as Hansen & Kawaler (1994), for the derivation of the basic equations. These equations describe the run of pressure, radius, luminosity, and temperature as a function of the mass fraction. For our application, these equations are first expressed in a Lagrangian reference frame. In this frame, the independent variable is the surface mass fraction q, which is the mass contained within a spherical shell bounded by the surface and the position of interest within the star. More precisely, q is given by

$$q = \frac{M_* - M_r}{\mathrm{M}_\odot}. \tag{3.1}$$

This defines $q = 0$ as the surface of the star, increasing to $q = M_*/\mathrm{M}_\odot$ at the center.

The equations of stellar structure, written in this form, become (all symbols defined in Appendix A)

$$\frac{d\ln R}{dq} = \frac{-\mathrm{M}_\odot}{4\pi \mathrm{R}_\odot^3}\frac{1}{R^3\rho} \tag{3.2}$$

$$\frac{d\ln P}{dq} = \frac{G\mathrm{M}_\odot^2}{4\pi \mathrm{R}_\odot^4}\left(\frac{M_*}{\mathrm{M}_\odot} - q\right)\frac{1}{PR^4} \tag{3.3}$$

$$\frac{d\ln T}{dq} = \frac{GM_\odot^2}{4\pi R_\odot^2}\left(\frac{M_*}{M_\odot} - q\right)\frac{\nabla}{PR^4} \tag{3.4}$$

$$\frac{dL}{dq} = -\frac{M_\odot}{L_\odot}\left[\epsilon + \frac{P}{\rho}\left.\frac{\partial \ln \rho}{\partial \ln T}\right|_P \left(\frac{1}{T\nabla_{ad}}\frac{dT}{dt} - \frac{1}{P}\frac{dP}{dt}\right)\right.$$
$$\left. + \frac{1}{s_{yr}}\frac{\dot{M}}{M_\odot}\left(C_P - \frac{dT}{dq} - \frac{\chi_T}{\chi_\rho}\frac{1}{\rho}\frac{dP}{dq}\right)\right] \tag{3.5}$$

The temperature gradient ∇ in equation [3.4] depends on the mode of heat transport, and, in general, is given by the minimum of the adiabatic and radiative gradients, so that

$$\nabla \equiv \frac{d\ln T}{d\ln P} = \min\left(\nabla_{ad}, \nabla_{rad}\right), \tag{3.6}$$

where

$$\nabla_{rad} = \left[\frac{3L_\odot}{16\pi acGM_\odot}\right]\frac{L\kappa P}{T^4}\frac{1}{\left(\frac{M_*}{M_\odot} - q\right)}, \tag{3.7}$$

and

$$\nabla_{ad} = \frac{\Gamma_2 - 1}{\Gamma_2}. \tag{3.8}$$

In addition to these equations for the stellar interior, four boundary conditions are also needed. The central and surface boundary conditions are as discussed in Hansen & Kawaler (1994). For the surface boundary conditions, ISUEVO uses the method of triangles described in Kippenhan et al.(1967).

3.3 Input Physics

In the solution of the equations as described above, expressions are required for the density, opacity, and energy generation rates in terms of the dependent variables P, T, L, and r. We must also identify conditions when convective instabilities occur,

and compute the temperature gradient in the presence of the resultant convective flux. This section discusses these constituitive relations and the treatment of convection.

3.3.1 Nuclear burning and neutrino emission

Though none of the models directly considered in this investigation are fueled by nuclear burning, these models are the results of an evolutionary sequence where burning does occur. The various reaction rates computed are from Harris, Fowler, Caughlan, & Zimmerman (1983) and references therein.

In the young, hot white dwarfs, energy loss from neutrinos is important, and may actually exceed energy loss from photons. Energy loss from neutrino emission is computed using rates by Munkata et al.(1985), and Beaudet et al.(1967).

3.3.2 Opacities

The dominant opacity source in the bulk of a white dwarf interior is that of electron conduction. Conductive opacities are obtained using an analytic fit to the Hubbard & Lampe (1967) tabulation, formulated by Iben (1975). More recent calculations from Itoh et al.(1993) are up to a factor of 2 higher; though this would be important if we were concerned with the precise time scales for cooling, the Hubbard and Lampe (1967) opacities are sufficient for the work presented here.

In the envelope, the radiative opacities from the OPAL tables of Rogers & Iglesias (1992) are used. These include tables for high C/O abundances, characteristic of evolved white dwarfs. These tables, and the routines used for interpolation, were kindly provided by Forrest Rogers and Carlos Iglesias of Lawrence Livermore National Laboratory.

3.3.3 Equation of State

The equation of state (EOS) quantities were obtained with an analytic EOS routine that includes solution of the Saha equation for H, He, C and a fictitious metal to represent all other species. Pressure ionization was treated in a very simple manner, assuming complete ionization at temperatures above $10^{5.5}$K. The fully ionized EOS is computed for arbitrary degrees of degeneracy and relativistic behavior using the method of Eggleton et al.(1973). Coulomb interactions between the ions at high densities were included using the prescription of of Iben & Tutukov (1984).

3.3.4 Convection and mixing

The presence of convection is determined using the Schwarzchild criterion, in which a zone is convective if

$$\nabla_{\rm ad} < \nabla_{\rm rad} \tag{3.9}$$

where $\nabla_{\rm rad}$ and $\nabla_{\rm ad}$ are defined in Equations [3.7] & [3.8]. The convective flux is determined from the mixing length theory, which assumes that a bubble of material rises adiabatically a length l before releasing its energy at a higher layer. This "mixing" length is usually expressed as a fraction of the pressure scale height H_P, which in turn is defined below.

The equations that describe the movement and energy transport of a convective bubble are put in the following form (from Cox & Giuli 1968, as in Tassoul, Fontaine, & Winget 1990), where the primed quantities represent values inside of the convective bubble.

The average speed of a convective cell is given by

$$v_c^2 = \frac{al^2 gQ(\nabla - \nabla')}{H_P}. \tag{3.10}$$

The average convective flux is given by

$$F_c = \frac{b\rho v_c C_P T l(\nabla - \nabla')}{H_P}. \tag{3.11}$$

The convective efficiency is given by

$$\frac{\nabla - \nabla'}{\nabla' - \nabla_{\rm ad}} = \frac{C_P \rho^2 l v_c \kappa}{c\sigma T^3} \tag{3.12}$$

where

$$\begin{aligned} l &= \text{mixing length,} \\ H_P &= \text{pressure scale height } \equiv \left(\frac{1}{P}\frac{dP}{dr}\right)^{-1}, \\ Q &= \text{heat content of convective element } \rho C_P T. \end{aligned}$$

The mixing length l is set equal to the pressure scale height H_P, and the constants a, b, and c are parameters which depend on the version of mixing length theory used. (The other symbols have their usual meanings.) For the standard ML-1 mixing length theory, Tassoul et al.(1990) give values of $a = \frac{1}{8}$, $b = \frac{1}{2}$, $c = 24$. For the ML-2 mixing length theory, which assumes a greater convective efficiency, they give $a = 1$, $b = 2$, and $c = 16$. The ML-3 version, described by Tassoul et al.(1990), has an even greater convective efficiency than ML-2. In this version, the a, b, and c parameters from ML-2 are used, but with a mixing length of twice the pressure scale height. This investigation assumes ML-2, since it has been shown to give a good approximation of the location of the blue edge of the DB instability strip.

We assume that in a convection zone, mixing occurs instantaneously and completely. The mass fraction of each element is presumed to be equal in all layers in the convective zone. If a convective zone exists between layers u and l, and the mass fraction of element i in layer j is $x_{j,i}$, then the convective mixing mass at each layer will then be given by

$$M_i = \sum_{l}^{u}(q_j - q_{j+1})x_{j,i}, \text{ total mass of element i in the convective zone;}$$

$$M_c = q_u - q_l \text{ mass of the convective zone;}$$

$$x_{j,i} = M_i/M_c,\ l \leq j \leq u, \text{ mass fraction in each convective zone.}$$

3.4 Solving the Equations

At each time step, the full set of equations [3.2]-[3.5] is solved using the relaxation method, with subroutines from Press et al.(1989). This method involves approximating the differential equation using backwards differences, then setting up a matrix of the difference system. Using an initial guess at the solution, a matrix of correction terms is then generated, and this process iterated on until the resulting corrections are adequately small. In this context, "adequately" means that the largest correction to any of the variables (T, L, P, or R) is less then 10^{-4} at all grid points.

Schematically, ISUEVO goes through the following steps in computing a sequence of stellar models:

1. Initialization
   (a) read input data and starting models
   (b) load arrays
   (c) determine timestep

2. Evolution loop
   (a) locate convection zones
   (b) calculate nuclear burning rates and changes in composition
   (c) compute composition in convective layers from mixing
   (d) rezone model as necessary
   (e) calculate changes in composition due to diffusion
   (f) solve equations of structure & generate new model
   (g) write out model summaries
   (h) find new timestep
   (i) *done - go to next model*
3. Final outputs
   (a) print out model summaries
   (b) calculate envelope for pulsational output.

Most of these steps have been described in the previous section, except for rezoning. Whenever the model grid becomes too coarse, or the change in any quantity from one zone to the next becomes to large, new zones are added as necessary resolve rapid changes in the quantity. This becomes especially important when the stellar models are used for pulsational modeling, since the pulsation properties depend strongly on the spatial derivatives of various thermodynamic quantities. If these derivatives cannot be smoothly calculated from the model parameters, numerical instabilities in the pulsation calculations may develop.

3.5 Calculation Results: Testing the Code

As the goal of this project was to investigate evolution in white dwarfs, all of the initial models in my sequences were representative of PG 1159, with structure

determined by the models of Kawaler and Bradley (1994); see that paper for details of the evolutionary history behind the starting model used here. First, I want to establish the reliability of ISUEVO as a working stellar evolution code by comparing white dwarf evolutionary models with those of other researchers. However, due to differences in the level of detail available in published results, I will not make a strongly quantitative comparison.

A sequence of dwarf models was computed without the use of diffusion for the purpose of comparison. I will compare these models with those of Tassoul et al.(1990, hereafter TFW), who constructed a sequence of white dwarfs for stellar pulsation studies. In particular, I will compare to their 60400L1 sequence, which is closest to my PG 1159 model. This sequence is a $0.6M_{\odot}$ model, with a helium layer with a thickness of $\log q = -4.0$, using the "Los Alamos" opacities, supplied by W.B. Heubner, and ML1 mixing length theory. This sequence spanned a temperature range of $103{,}039K > T_{eff} > 6266K$.

I will also compare with the models of Iben & Tutukov (1984, hereafter IT), who constructed a helium rich white dwarf sequence to study white dwarf cooling and the white dwarf luminosity function. Their helium model sequence used a $0.6M_{\odot}$ model with a helium layer of $0.016M_{\odot}$.

Finally, Wood (1992, hereafter Wood) also presents a sequence of models for calculating a white dwarf luminosity function. I will also make a comparison to some of his results. Wood ran a grid of DB models, with varying core composition (pure carbon, pure oxygen, and mixed) and helium envelopes of $10^{-3}M_{*}$ and $10^{-4}M_{*}$ for his $0.6M_{\odot}$ models. Most of Wood's computations are based on a variant of the code used by TFW, so this is not a truly independent test.

When comparing these model sequences, it must be kept in mind that the sequences of TFW, Wood, and IT were generated for a specific investigation. Wood and IT were trying to examine the white dwarf luminosity function, and did not discuss many details of specific models. TFW were presenting a grid of models for detailed pulsation investigations, and give a great many details, but, given the vast number of models generated, the details are not always on the most appropriate sequence for the purpose of my comparison. The starting models used by those authors differ from mine, since they presumed compositional stratification in their models, while mine has the mixed composition of PG 1159. They also presumed different surface layer thicknesses than I do. There is also an arbitrary offset in time, since each sequence has a different definition of the $t = 0$ start time. Therefore, a truly quantitative comparison of the different modeling codes is not possible with these models. I will instead demonstrate that the results are qualitatively similar.

The composition profile of the initial model is given in Figure [3.1]. The composition transition at $\log q = -3.5$ was determined by the pulsation data on PG 1159 by Nather et al.(1990). The evolutionary role of this model will be discussed in more detail in Chapter 5.

The evolution of the temperature profile as a function of effective temperature for a 0.58 $M_\odot$ sequence is shown in Figure [3.2]. The temperature inversion near the core for the hotter models is a result of neutrino cooling; this inversion gradually disappears as the star cools, disappearing at a temperature of 29803K, when the model reaches a luminosity of $0.12L_\odot$. The flattening of the temperature profile near the core at lower effective temperatures is due to the efficiency of electron conduction in the core. This inversion is not shown in the models of TFW, for the simple reason

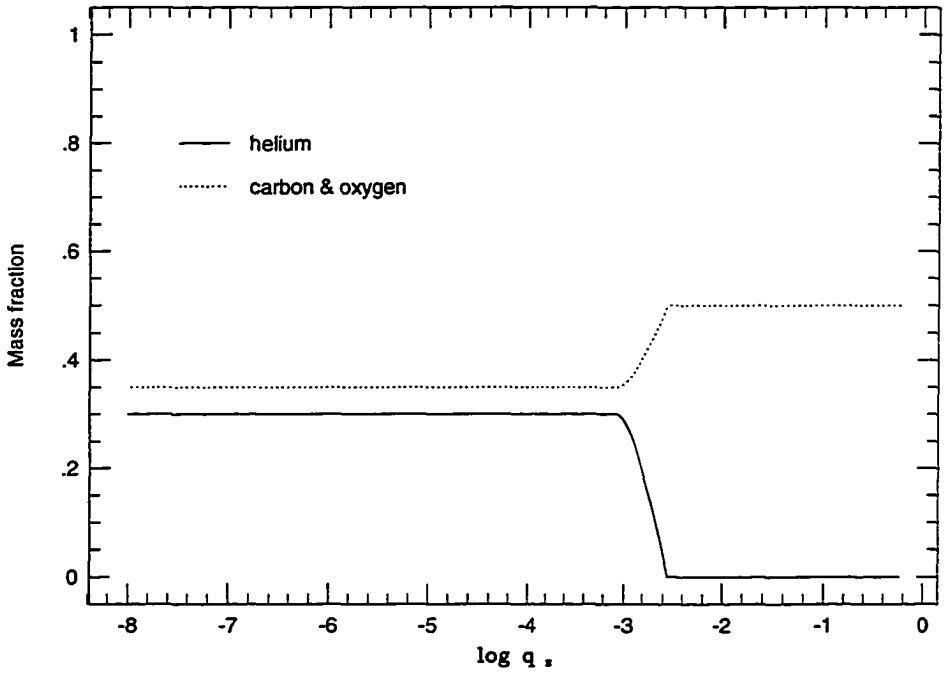

Figure 3.1: Composition profile of the initial PG 1159 model.

that they do not include neutrino emission; they were primarily interested in modeling white dwarfs at cooler temperatures. They do show the isothermal core as a result of the electron conduction. IT include neutrino losses, and show the temperature inversion; in their helium sequence, this inversion disappears when $L \sim 0.1 L_{\odot}$. Wood does not give structural detail to make a comparison.

The luminosity and the central temperature as a function of time are shown in Figure [3.3]. For a brief time, the luminosity is constant, as the model relaxes onto the cooling track. The model then drops in luminosity from $\log(L/L_{\odot}) \sim 1.5$ to $\log (L/L_{\odot}) = -1.4$ during the time $\log t = 5.5$ to $\log t = 7.5$yr. The TFW DA models[1] fade to this luminosity by about $\log t = 7.8$yr, and the IT models by 10^8yr. Wood's models reach this luminosity at about $\log t = 7.8$yr. The discrepancy with IT is due to their much thicker envelope; Wood demonstrates the effect of the envelope mass on the apparent age and the luminosity. The greater the envelope mass, the younger the apparent age and the greater the luminosity. Wood and TFW, however, match reasonably well.

The central temperature can easily be compared with the IT. In my models, the central temperature initially remains constant at 72×10^6K; this is mirrored in IT, although at a slightly higher temperature, $\sim 90 \times 10^6$K. The downturn in T_c being when $\log L/L_{\odot} = 1.5$; in IT this occurs much later, when $\log L/L_{\odot} = 0.1$. This is again because IT's models contain a much thicker envelope, so the core requires more time to lose its energy.

[1]TFW do not give a cooling curve for their DB models.

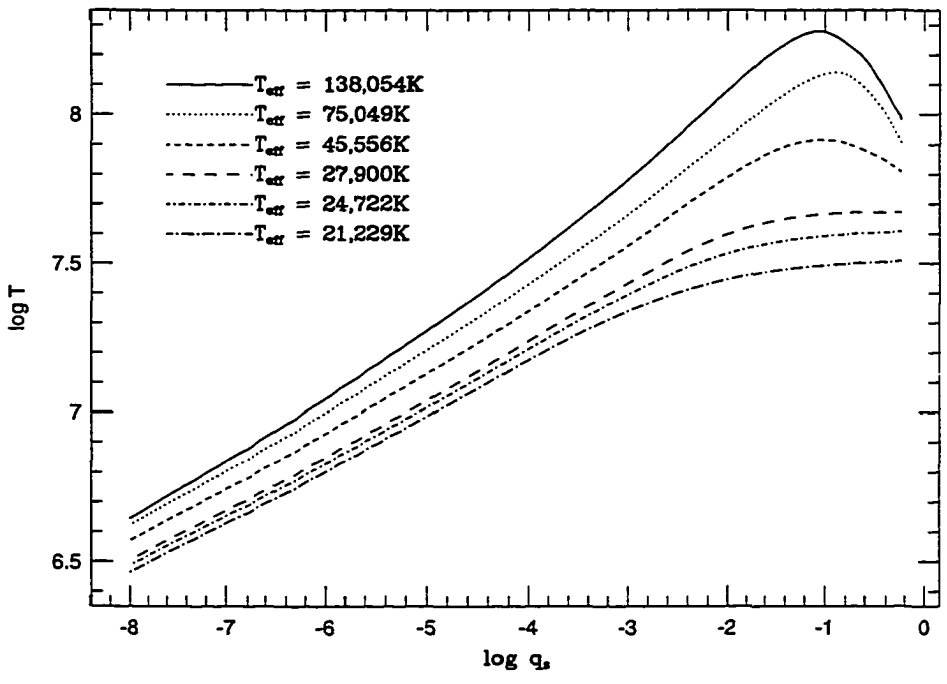

Figure 3.2: Temperature profile evolution

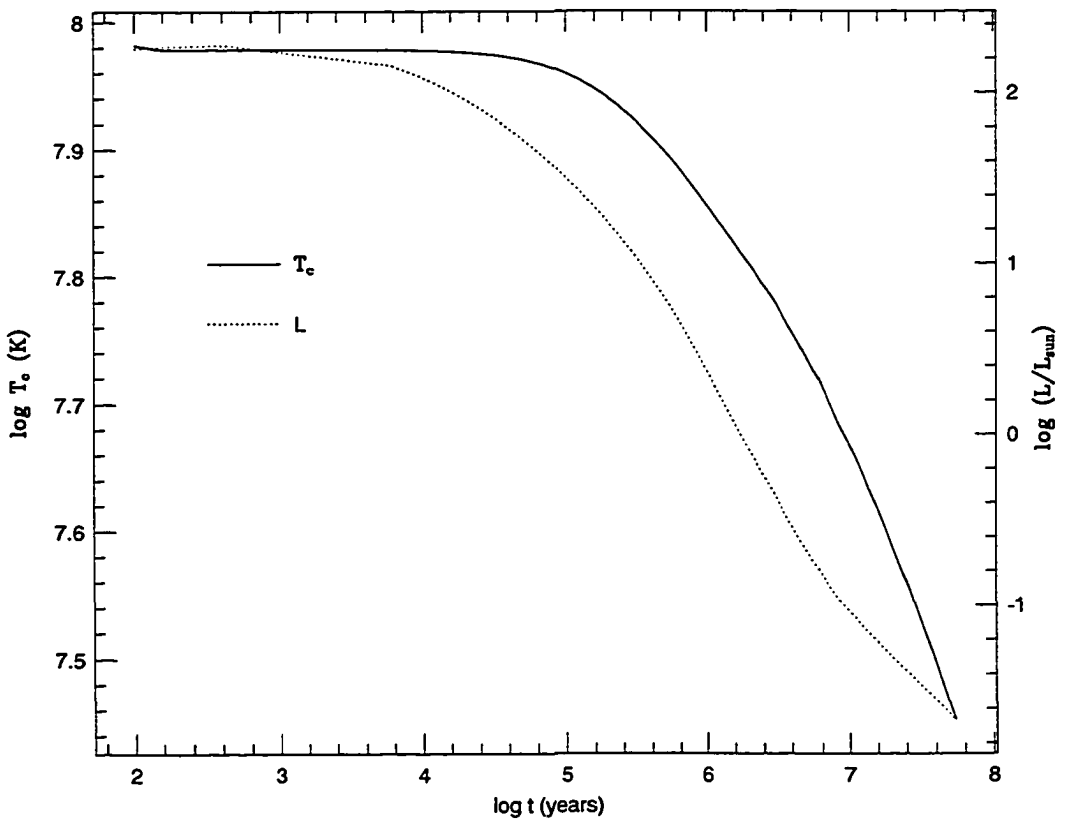

Figure 3.3: Luminosity and central temperature evolution.

3.6 Summary: What ISUEVO Does

The purpose of this chapter is twofold. First, to explain the techniques and the physics of models of stellar evolution. Second, and, most important, to establish ISUEVO as working, reliable code for computing such models. The physical principles used in these models are well understood, and the mathematical techniques have long been explored. Not only is the numerical work well established, but a sequence of white dwarf evolution from ISUEVO – without diffusion – gives results which are consistent with the results of other such efforts.

The innovations to ISUEVO important to this work are described in the next Chapter, where the techniques used to include diffusion are discussed. In discussing this work, comparison with other researchers is impossible because such an integrated evolution and diffusion computation, over such a span of white dwarf temperatures, has not previously been done. Instead, we must content ourselves with an analytic demonstration, that the results are physically plausible. Finally, after the background work in this Chapter and the next, where I establish the reliability of the code, in Chapter 5 I will examine the modeling of the evolution of PG 1159 with diffusion.

CHAPTER 4. ISUEVO II: CALCULATING DIFFUSION IN WHITE DWARFS

Any theory too complex to fit on a T-shirt is probably wrong.

- H. Shipman (1987)

As discussed in Chapter 2, the numerical solution of the time-dependent diffusion equation, has had very little treatment compared to that given the stellar structure equations. As described in the previous Chapter, we have used standard methods of solving them; the process of stellar evolution is understood well enough so that one can, at least qualitatively, know if the solution method is providing the "right" answer.

In this Chapter, I discuss the diffusion equation, and the methods to solve it within an evolving stellar model. First, I will discuss what is meant by the term "diffusion", and the various processes involved. I then discuss the historical approach, which is essentially the work of Evry Schatzman, and contrast this with the current approach. I then elaborate on the numerical methods used to solve this equation, and conclude with a discussion of the physical properties of its solution.

4.1 Nomenclature: What is diffusion?

There are often several different connotations applied to the word diffusion. Diffusion, in the astrophysical context, is often divided up into different categories, depending on the driving force. In this work, "diffusion" is *any* process which can cause a change of relative abundance of species within a mixture; most of the specific mechanisms that will be discussed are a subset of this broad category. By this definition, radiative levitation (discussed in Chapter 2) is also diffusion, although it is not included here.

The more specific types of diffusion are gravitational settling, which is caused by differential gravitational forces on ions. "Ordinary" or "chemical" diffusion is driven by fractional number density gradients in a mixture, e.g., an interface between two mixtures of differing composition. Finally, there is "thermal" diffusion, caused by temperature gradients between two mixtures. The distinction between these various flavors of diffusion will be made more clear as we examine the equations governing diffusion in detail.

4.2 History: A Schatzman Sampler

One of the first quantitative approaches to diffusion in white dwarfs was given by Schatzman in the 1950s and summarized in his classic book White Dwarfs (Schatzman 1958; hereafter simply "Schatzman"). Schatzman considered an electric field within a star caused by the gravitational separation of electrons and ions. This electric field is given by Schatzman's Equation [5-81] as

$$E = -(\mu m_h - m_e) g e^{-1} \tag{4.1}$$

where μ is the mean molecular weight, g is the gravitational acceleration, and the other terms have their usual meaning (see Appendix A.) The net force is then (Schatzman Eqn. [5-82])

$$Am_h g + ZeE = gm_h Z[(A/Z) - \mu], \tag{4.2}$$

where A is the atomic mass, Z is the atomic charge. The net force is dependent on the difference between the molecular weight and the mean molecular weight. Intuitively, this is as one expects; the light elements in a mixture should float to the top.

By using an analogy of viscous forces on stellar motions in a cluster, Schatzman then gives the following formulation for the diffusion velocity w of a heavy element in the hydrogen layer of a white dwarf: (Schatzman Eqn. [5-84]):

$$w = \frac{m_h g Z[(A/Z) - \mu] k^2 T^2}{\pi N_h m_h Z^2 e^4 [kT/m_h]^{1/2} \log\left\{1 + \frac{1+d_1^2 k^2 T^2}{Z^2 e^4}\right\}} \tag{4.3}$$

where d_1 is the average distance between hydrogen atoms. The log term is expanded in a Taylor series, requiring that

$$\frac{d_1^2 k^2 T^2}{Z^2 e^4} = 10^{-10.712} T^2 Z^{-2} \rho^{-2/3} \equiv \Delta < 1, \tag{4.4}$$

which is effectively assuming that the thermal energy is small with respect to the electrostatic energy.

Assuming that the outer hydrogen layer is in radiative equilibrium, Schatzman arrives at the following expression for the diffusive velocity,

$$w = \frac{gA}{2\pi}\left(\frac{4\pi}{3}\right)^{2/3} (\rho/m_h)^{-1/3} (R_* T)^{-1/2}, \tag{4.5}$$

where R_* is the stellar radius.

Schatzman uses this equation to calculate some representative values for the diffusion velocity. For the specific case of oxygen, using values of $T = 10^7$K, $N_h =$

6×10^{26} cm^{-3}, and $g = 10^9$ cm sec^2, he arrives at a diffusion velocity of $w \sim 2 \times 10^{-7}$ cm/sec. Given a stellar size of 0.01 $R_\odot$, or 10^8 cm, this further leads to diffusion equilibrium times (in this context, the time it would require the element to cross the region of interest) of about 2×10^6 yr for the outer layers, and 10^8 to 10^9 yr for the entire star. For comparison, a young, hot white dwarf (T_{eff} ~140,000K) will cool to ~60,000K in 2 million years, and to ~20,000 K in 10^8 years. While these diffusion timescales show that the composition could be altered over the time of evolution, Schatzman actually concludes that diffusion alone could *not* modify the surface composition, because any hydrodynamic motion would offset the small diffusion velocities.

4.3 The Modern View of the Diffusion Equation

While essentially correct, the above view needs adaptation for use in full evolutionary models. In particular, the time dependent change in the diffusion velocity at each layer within a model needs to be calculated. Thus in this "modern view" the physics of diffusion is set in terms adaptable to numerical computations.

The time-dependent change in number density due to diffusion is fairly simple; for any given element with a number density n, the rate of change is given (in spherical symmetry), by

$$\frac{\partial n}{\partial t} = -\frac{1}{r^2}\frac{\partial (w r^2 n)}{\partial r} \tag{4.6}$$

where w is the diffusive velocity, and n is the number density. One of the difficulties with this equation is that it is a partial differential equation, explicitly containing the time derivative. The structure equations, at heart, are a set of ordinary differential equations, solved for a static sequence of models. This implies a completely different

approach is necessary for diffusion.

The diffusion velocities w obviously play a key role in the solution of the diffusion equation. While the appearance of the diffusion equation is relatively simple – and its solution correspondingly difficult – the diffusion velocities are almost exactly the opposite. The diffusion velocities are given by Burgers (1969), Equation [18.1], where I have simplified by ignoring thermal effects and magnetic fields. The diffusive velocity $\mathbf{w}_j$ of a species j is then determined by

$$\sum_{i}^{M} K_{ij}(\mathbf{w}_i - \mathbf{w}_j) = \nabla p_j - \frac{\rho_j}{\rho}\nabla p - Z_j n_j e\mathbf{E} \tag{4.7}$$

where the sum is taken over the M elements in the mixture and electrons. K_{ij} are the resistance coefficients, $\mathbf{E}$ is the electric field, and all other symbols have their usual meaning. For a mixture of M elements, equation [4.7] gives a set of M independent equations for $M+2$ unknowns. There are $M+1$ densities, (M elements + electrons), but since $K_{ij} = K_{ji}$, the equations are not all independent; the electric field $\mathbf{E}$ is treated as another unknown.

The resistance coefficients K_{ij}, inversely related to the diffusion coefficients used by some authors (see Eqn. [4.37]), can be viewed as representing a viscous force resisting the diffusive movement. They are derived from consideration of inter-atomic collisions and scattering. The resistance coefficients used here were obtained from the calculations of Paquette et al.(1986a, PPFM), who used a static screened Coulomb potential to calculate the impact integrals. They published their results as analytic fitting functions for the coefficients. Our resistance coefficients are computed from their fitting tables, eliminating the need for extensive calculations or less precise approximations.

Though it might be possible to arrive at an analytic solution for the diffusion

velocities to compare with Schatzman, this would not be very illustrative. The very nature of this work is an examination of the *dynamical* nature of diffusion. The diffusion velocities, as will be seen, vary widely within a star. To calculate a single velocity, or extrapolate a timescale from this velocity, would be an inadequate comparison. Instead, velocities calculated from Eqn. [4.5] will be compared to the numerical solutions in the next section.

4.4 Solving the Diffusion Equation

4.4.1 Numerical methods

With the paucity of treatments of dynamical diffusion, there are no "standard methods" for the diffusion equation in white dwarfs. The works which have the most sophisticated treatment for diffusion, Pelletier et al.(1986), Muchmore (1984), and Iben & MacDonald (1985), all follow different approaches. Further, in addition to simply solving the diffusion equation, there was an additional constraint that was placed on the method to be used here: it had to be incorporated within a working stellar evolution code, ISUEVO. This strongly encouraged the selection of a finite difference method, rather than a finite element method such as used by Pelletier et al.(1986).

The first simplification made is the assumption of spherical symmetry. The effect of this is to replace ∇f with $\frac{1}{r^2}\frac{\partial r^2 f}{\partial r}$. Non-spherical effects in diffusion are most likely of lower order of importance than non-sphericity in dynamical processes, although the study of Vauclair and Reisse (1977) indicates that circulation from rotation may be important. However, since the equilibrium, model is constrained under spherical symmetry, consistency requires that diffusion be treated as spherically symmetric.

The equation for the diffusive velocities, Equation [4.7] is not a linearly independent system, since we have M equations and $M+2$ unknowns. So we follow the method used in Muchmore (1984) and IM, and introduce the steady-state constraints of no net mass flow and no net current, that is,

$$\sum_{i}^{M+1} A_i w_i = 0 \tag{4.8}$$

$$\sum_{i}^{M+1} Z_i e w_i = 0 \tag{4.9}$$

Despite its apparent complexity, the set of equations [4.7, 4.8-4.9] gives a simple linear system of equation for the diffusive velocities for all elements present. In practice, subroutines from the Numerical Analysis Group (NAG) are used to solve this linear system, although nearly any linear equation solver library would suffice.

In order to solve the diffusion equation, we invoke a simple technique known as the method of lines. First, the spatial derivative in Equation [4.6] is discretized with centered differences, as follows: [1]

$$\frac{\partial n_j}{\partial t} = -\frac{1}{r_j^2} \frac{n_{j+1} w_{j+1} r_{j+1}^2 - n_{j-1} w_{j-1} r_{j-1}^2}{2(r_{j+1} - r_{j-1})} \tag{4.10}$$

We then, as in IM, invoke the boundary conditions that

$$n \to 0 \quad \text{as} \quad r \to R_*,$$

and

$$\frac{\partial n}{\partial r} \to 0 \quad \text{as} \quad r \to 0$$

For N layers in the model, this gives $n_{N+1} = 0$ and $n_0 = n_1$, where layers $N+1$ and 0 are "pseudo-layers" considered for the application of adding boundary

[1] In the following section, the subscripts j represent the quantity at layer j within the model, contrary to the earlier notation, where subscripts referred to element j.

conditions. We then have following set of equations:

$$\frac{\partial n_1}{\partial t} = -\frac{1}{r_1^2}\frac{n_2 w_2 r_2^2}{2r_2} \tag{4.11}$$

$$\frac{\partial n_j}{\partial t} = -\frac{1}{r_j^2}\frac{n_{j+1}w_{j+1}r_{j+1}^2 - n_{j-1}w_{j-1}r_{j-1}^2}{2(r_{j+1}-r_{j-1})} \quad 2 \le j \le N-1 \tag{4.12}$$

$$\frac{\partial n_N}{\partial t} = \frac{1}{r_N^2}\frac{n_{N-1}w_{N-1}r_{N-1}^2}{2(r_{N+1}-r_{N-1})} \tag{4.13}$$

For each element in the model, this gives a system of N *ordinary* differential equations to be integrated for some timestep δt. For a typical model, there are about 300 zones.

To integrate equations [4.11-4.13], the entire system is integrated by a numerical library subroutine DEBDF. This is a backward differentiation formula initial value problem integrator, part of the DEPAC library by Shampine and Watts (1979). This integrator was selected because of its ability to handle stiff differential systems, as well as its simplicity to implement in the evolution code. The integration must be carried out separately for each element in the model.

This method was chosen for several reasons. First, the spatial discretization could be simply carried out using the existing model grid, which allows the diffusion computation to be incorporated much more easily into the evolution code. Second, it allowed for treatment of as many elements in a mixture as desired. And third, it allows the use of an existing software library, with known numerical behavior, for the integration of the ordinary differential equations.

The differential equations are assumed stiff for the solution scheme. This is partially justified by the observation of Pelletier et al.(1986) that diffusion timescales can vary widely throughout the star. Even if incorrect, this assumption only affects the numerical method used; a stiff problem solver is typically less efficient on non-stiff

problems. In order to integrate a stiff differential equation, we need to calculate the Jacobian $J_{ij} = \partial f_i / \partial n_j$, of the above system, where f_i are the right-hand sides of equations [4.11-4.13]. Because of the centered differences used in the system, it is a simple banded matrix containing only the ± 1 off-diagonal bands, given by

$$J_{1,2} = \frac{-1}{r^2}\frac{w_2}{2} \tag{4.14}$$

$$J_{i,i-1} = \frac{1}{r_i^2}\frac{w_{i-1}r_{i-1}^2}{2(r_{i+1}-r_{i-1}} \quad 2 \le i \le N-1 \tag{4.15}$$

$$J_{i,i+1} = -\frac{1}{r_i^2}\frac{w_{i+1}r_{i+1}^2}{2(r_{i+1}-r_{i-1})} \quad 2 \le i \le N-1 \tag{4.16}$$

$$J_{N,N-1} = \frac{1}{r_N^2}\frac{w_{N-1}R_{N-1}^2}{2(r_{N+1}-r_{N-1})} \tag{4.17}$$

$$J_{i,j} = 0 \quad \text{otherwise.} \tag{4.18}$$

This also gives another reason for selecting the DEPAC library. It is possible to specify a banded Jacobian matrix structure to the DEBDF routine, thus allowing more efficient computation.

4.4.2 Timestep control and the quasi-static assumption

Since this system must be integrated separately for each element, a "quasi-static" assumption is made. For some timestep δt, the equations are integrated for each element, assuming that changes in the composition profile for one element will not affect the diffusion of another element over the timestep δt. Only after all elements in the mixture have been integrated are the composition profiles updated for the next δt. This assumption constrains the choice of δt.

The cooling timescales of the star are on the order of 10^3 to 10^7 years, depending on the effective temperature. For the thin, outer layers, this is nearly always

much longer than the diffusion timescales, so given an evolutionary timestep Δt, we integrate the diffusion equations for a series of shorter timesteps δt, until we reach Δt. A larger timestep allows the diffusion to be calculated with fewer integrations, thus minimizing computation time. However, a larger timestep also allows for greater change in the composition profiles, thus violating our quasi-static assumption. We therefore begin with an arbitrary 5 year δt timestep. Each element is diffused for δt, and then the maximum relative change in composition at any point for all elements is determined

$$\Delta n_{\max} = \max_i \left(\frac{n_{i,\text{new}} - n_{i,\text{old}}}{n_{i,\text{new}}} \right), \tag{4.19}$$

where

$$n_{i,\text{old}} = \text{initial number density at layer } i \tag{4.20}$$

$$n_{i,\text{new}} = \text{final number density at layer } i \tag{4.21}$$

Given such a maximum $\Delta n_{\max}$, the new timestep is then given by

$$\delta t_{\text{new}} = \frac{0.15}{\Delta n_{\max}} \delta t_{\text{old}}. \tag{4.22}$$

Thus a composition change greater than 15% at *any* point in the model will cause a decrease in the timestep used. This method allows for the timestep to adaptively increase as the compositional structure approaches diffusive equilibrium, and yet maintains the quasi-static nature of the calculation. The values of 5 years and 15% were arbitrarily selected, as a compromise between retaining the quasi-static nature and speed of calculation.

There is also a third timestep here, one used internally within the DEPAC library. When the DEPAC library is called, it is instructed to integrate the diffusion

equation over the timestep δt. The DEPAC integrator uses whatever timestep needed to accomplish this integration and maintain a specified error tolerance. The error tolerances were set at 10^{-4} for the relative error, and 5×10^{-6} for the absolute error. This allowed rapid computation, and is consistent with the error tolerances used in the other parts of the code.

4.5 Diffusion Velocities – Representative Results

Representative diffusion velocities for helium in a PG 1159 model are shown in Figure [4.1]. Also shown in this Figure is the helium composition profile. As can be seen, the diffusion velocity is a smooth curve near the outer layers of the star. The shape of this curve will be explored more in the next section; note for now that the diffusive velocity is higher near the surface, and thus the outer regions will reach diffusive equilibrium before the inner regions. Further, there is the negative spike in the diffusion velocity at the interface between the helium envelope and carbon/oxygen core, at a mass fraction of about $q_s = 10^{-3}$. The negative diffusion velocity is a result of the helium being forced inward by the steep number density gradient at the core boundary.

We can compare the diffusion velocities with those calculated using Eqn. [4.5]. Given a stellar radius for this model of 1.67 $\times 10^9$cm, we can re-write Eqn. [4.5] as

$$w = 1.201 \times 10^{-13} \frac{Ag}{\rho^{1/3} T^{1/2}} \text{ cm/s} \tag{4.23}$$

This allows us to compare the diffusion velocity calculated with Schatzman's method and Burger's formalism directly. A comparison is given for the oxygen diffusion velocity at two locations in the star in Table [4.1]. With its higher Z, oxygen will be

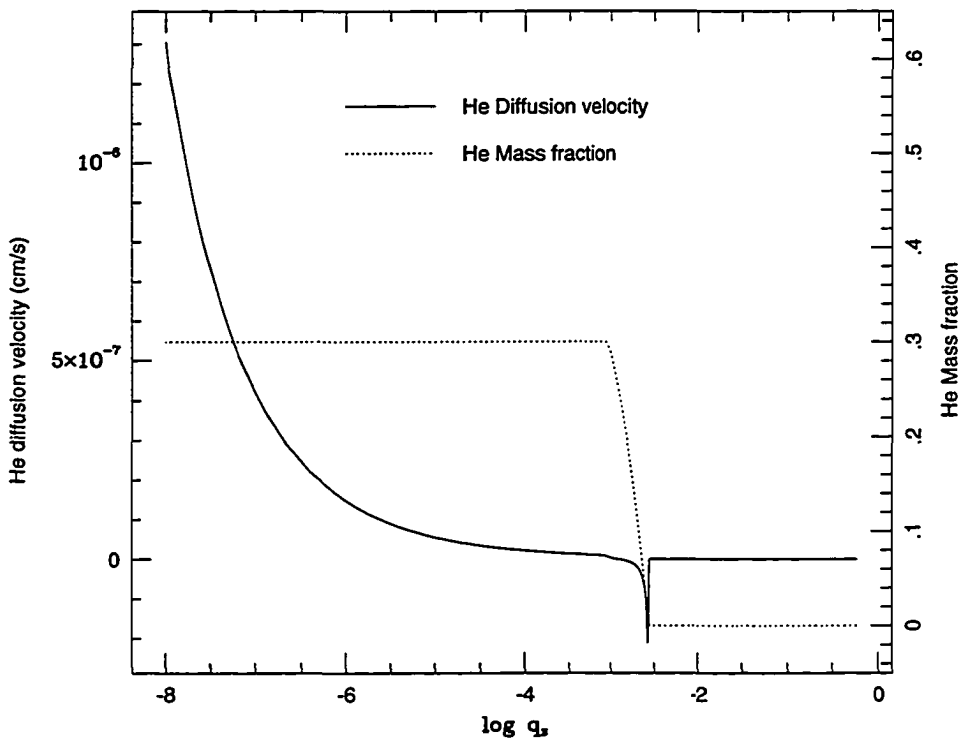

Figure 4.1: Diffusion velocity for PG 1159 model

most likely to conform to the constraint in Eqn. [4.4]. Nearer the center of the star, at $\log q = -3.1$, the diffusion velocities from the two different methods are comparable. As can be seen, however, near the surface, there is a large discrepancy in the two different methods, of nearly an order of magnitude. This is explained by the last column, the condition expressed in Eqn. [4.4]. The limit under which Schatzman's equation is valid ($\Delta < 1$), is violated in both locations. However, this departure is exaggerated near the surface, as Δ increases due to the greatly decreased density. Thus Schatzman's expression in Eqn. [4.5] is inapplicable without further correction over most of the range of physical parameters in this model.

Table 4.1: Oxygen Diffusion Velocity Comparison

$\log q$	$\log g$ (cm/s^s)	$\log \rho$ (gm/cm^3)	log T (K)	w(Schatzman) (cm/sec)	w(model) (cm/sec)	Δ
-3.1	7.675	3.002	7.753	1.206×10^{-9}	4.416×10^{-9}	9.7
-7.0	7.486	-0.288	6.948	2.464×10^{-8}	1.889×10^{-7}	37.1

4.6 Physical Explanation of the Diffusion Velocities

As mentioned in the previous chapter, comparison of these results with other authors is impossible since no other work exists. Instead, we must satisfy ourselves that the results are reasonable by using a more analytic approach, and examine the physical forces which drive the diffusion. The diffusion equations are complex, and understanding the solution in an intuitive way can be difficult. Still, with a little mathematics, the physical basis for these results can be made clearer.

In determining the diffusion velocities, there are two competing processes, the

driving – the differential forces acting on the ions – and the resistance – the viscosity caused by atomic collision. The driving is determined by the physical conditions, mostly temperature, pressure, and number density gradients. The resistance is more a function of inter-atomic interactions and dynamics, but is also dependent on the conditions. The interplay of these two processes determines the resulting diffusion velocity behavior. First, we examine the forces responsible for species separation, then we will examine the resistance to diffusive movement.

4.6.1 The driving forces

To begin with, the right hand side of Equation [4.7] is what I will refer to as the "driving force" of the diffusion, denoted by $-\psi_j$. That is, we have

$$-\psi_j = \nabla p_j - \frac{\rho_j}{\rho}\nabla p - Z_j n_j e\mathbf{E}, \tag{4.24}$$

$$= \nabla(n_j kT) - \frac{\rho_j}{\rho}\nabla p - Z_j n_j e\mathbf{E}, \tag{4.25}$$

$$= kT\nabla n_j + n_j \nabla kT - \frac{\rho_j}{\rho}\nabla p - Z_j n_j e\mathbf{E}. \tag{4.26}$$

At this point, we can identify the term containing ∇n_j as "chemical diffusion", reflecting number density gradients. One might be further tempted to identify the ∇kT term as thermal diffusion, but this is incorrect. Thermal diffusion is the interconnection of diffusion and heat flow, which has been neglected here. This term can be better understood by continuing its breakdown, as follows:

$$-\psi_j = kT\nabla n_j + n_j \nabla \frac{p}{n} - \frac{\rho_j}{\rho}\nabla p - Z_j n_j e\mathbf{E} \tag{4.27}$$

$$= kT\nabla n_j + \frac{n_j}{n}\nabla p - \frac{n_j p}{n^2}\nabla n - \frac{\rho_j}{\rho}\nabla p - Z_j n_j e\mathbf{E}. \tag{4.28}$$

Noting that $\rho_j = m_j n_j$ and $\rho = \mu m_h n$, we have

$$-\psi_j = kT\nabla n_j - n_j kT\nabla \ln n + \frac{(\mu m_h - m_j)n_j}{\mu m_h n}\nabla p - Z_j n_j e\mathbf{E}. \tag{4.29}$$

Hydrostatic equilibrium allows us to replace ∇p with $-\rho g$. Defining the number density fraction $X_j = n_j/n$, we have

$$-\psi_j = kTX_j\nabla n + kTn\nabla X_j - kTX_j\nabla n - (\mu m_h - m_j)n_j g - Z_j n_j e\mathbf{E}. \quad (4.30)$$

The ∇n terms cancel, giving the following:

$$-\psi_j = \overbrace{nkT\nabla X_j}^{1} - \overbrace{(\mu m_h - m_j)n_j g}^{2} - \overbrace{Z_j n_j e\mathbf{E}}^{3}. \quad (4.31)$$

The three terms can be identified with three different driving mechanisms as follows. The first term depends on the fractional number density gradient. This is typically called "ordinary diffusion" or "chemical diffusion". This term depends on the gradient of the fraction number density and not on the total number density. The second term is proportional to the gravitational force; and depends on the difference between the particle mass and the mean mass of the surrounding material. This "gravitational settling" term guarantees that lighter and heavier elements separate. This term is directly proportional to the gravity; this is also in accordance with our intuition, since the pure surface layers observed in white dwarfs indicates that diffusion operates more efficiently in these objects compared to the main sequence. Finally, there is the electric field term, which arises from the fact that diffusion is acting on charged particles. Although not apparent here, this term is related to the gravity as well, since the source of the electric field is a separation of electrons and ions caused by the gravitational field. In practice, the electric field is treated as an additional unknown to be calculated.

The forces driving the diffusion are plotted in Figure [4.2] for the PG 1159 model shown in Figure [4.1]. Clearly, the major force in driving the diffusion is the gravitational force, except for the interface near the core boundary. Near the core,

there is a large contribution from the chemical term, caused by the steep decrease in the helium in the core.

Shown in Figure [4.3] are the driving terms near the surface, where the vertical scale has been expanded roughly by a factor of 100 over the scale in Figure [4.2]. Since the surface of this model has a homogeneous composition, and thus no composition gradients, there is no contribution from the chemical diffusion term. The electrical and gravitational terms dominate.

Examining Figures [4.1]-[4.3] , it is apparent that the greatest diffusion velocity is at the surface, while the greatest driving takes place near the center of the star. In order to resolve this apparent contradiction, we must now take a look at the left hand side of Eqn. [4.7] and examine the behavior of the resistance coefficients.

4.6.2 The resistance coefficients

To fully understand the diffusive motions, we must understand the nature of the resistance coefficients. However, as I will be following the description given in PPFM, who in turn base their work on the formalism of Chapman & Cowling (1970), I will start by deriving the diffusion coefficients, which have a simple relation to the resistance coefficients used here. This is not an analytical analysis of the resistance coefficients; rather, I will derive simplified approximations to illustrate the functional dependence of the resistance coefficients on the stellar parameters.

According to PPFM (their Eqn. [5]), the first approximation[2] to the diffusion

[2] D_1 is the first approximation. While I will not use higher approximations, i.e. $D_2, ...$, I will keep the subscript to keep notation consistent with PPFM.

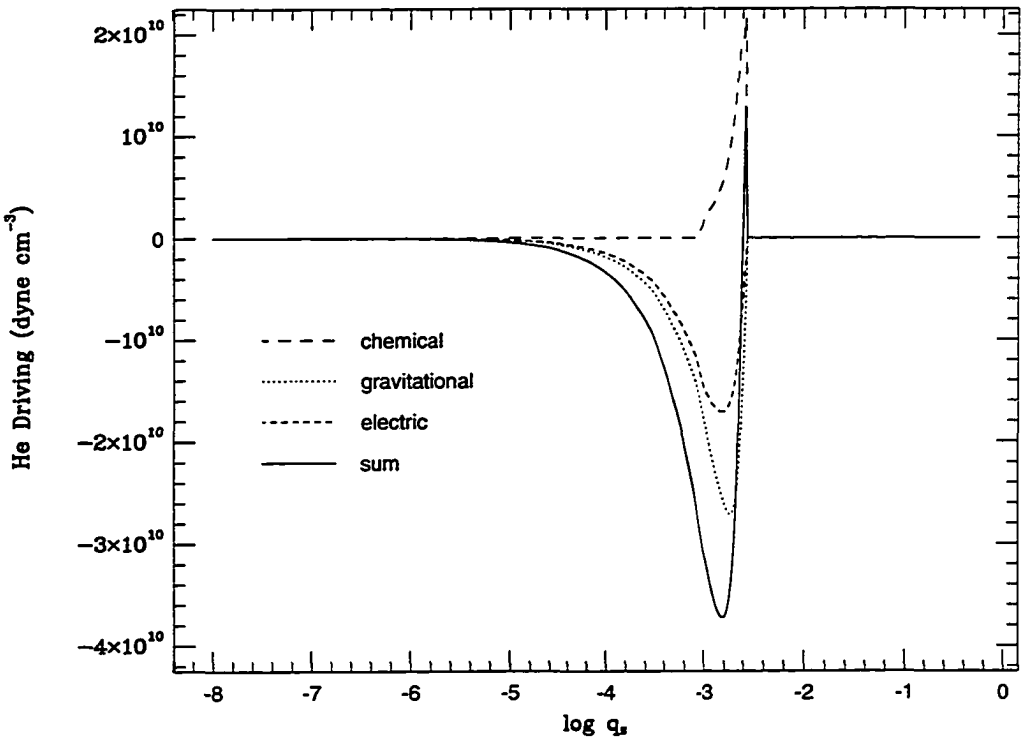

Figure 4.2: Diffusion driving for PG 1159 model

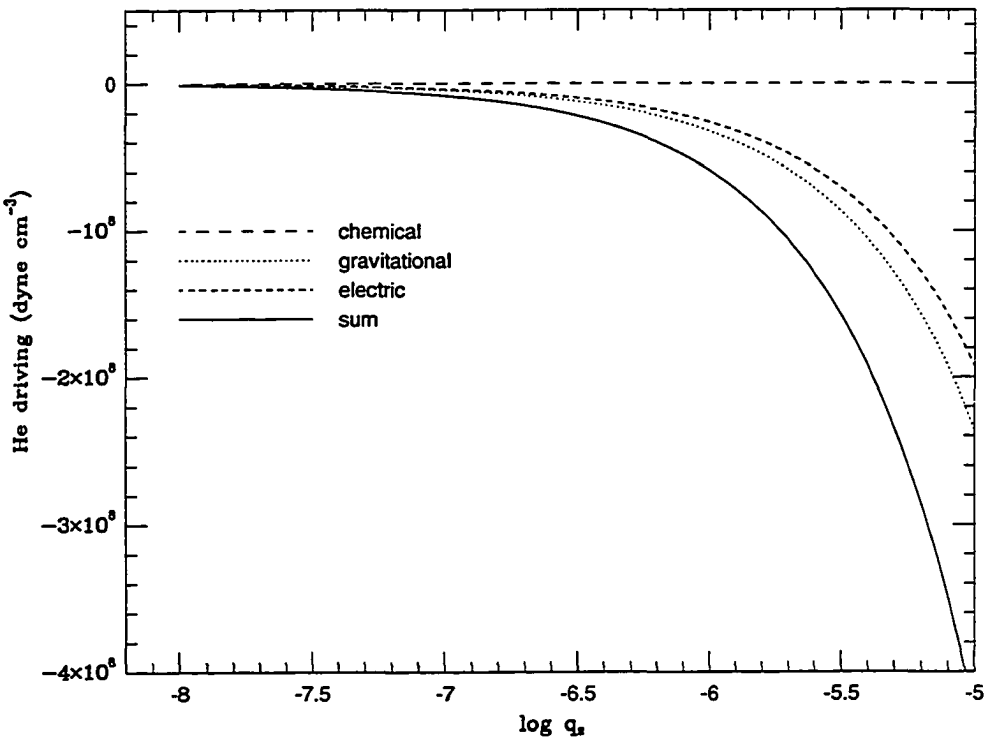

Figure 4.3: Surface diffusion driving for PG 1159 model

coefficient of two elements is given by

$$[D_{st}]_1 = \frac{3E}{2nm}, \tag{4.32}$$

where

$$n = n_s + n_t, \tag{4.33}$$

$$m = m_s + m_t, \tag{4.34}$$

$$E = \frac{kT}{8M_sM_t\Omega_{st}^{(11)}} \quad \text{(PPFM Eqn. [17])} \tag{4.35}$$

$$M_i = \frac{m_i}{m_s + m_t}, (i = s, t) \tag{4.36}$$

where the subscripts s and t refer to each species, and $\Omega_{s,t}^{(11)}$ is the "collision integral," and the superscripts i and j represent moments of the integrals. Since the resistance coefficients are related to the first approximations, we will not be using higher moments of the collision integrals. The resistance coefficients are related to the diffusion coefficients by

$$K_{st} = X_sX_tn\frac{kT}{[D_{st}]_1} \tag{4.37}$$

where X_i is the fractional number density of species i.

The collision integral $\Omega_{st}^{(ij)}$ is in turn given by PPFM Eqns. [18-21] as

$$\Omega_{st}^{(ij)} = \left(\frac{kT}{2\pi mM_sM_t}\right)^{\frac{1}{2}} \int_0^\infty e^{-g^2} g^{2j+3} \phi_{st}^{(i)} dg, \tag{4.38}$$

where

$$\phi_{st}^{(i)} = 2\pi \int_0^\infty (1 - cos^i \chi_{st}) bdb \tag{4.39}$$

and

$$\chi_{st} = \pi - 2\int_{r_{st}^{\min}}^\infty bdr \left\{ r^2 \left[1 - \frac{b^2}{r^2} - \frac{V_{st}(r)}{g^2kT} \right]^{\frac{1}{2}} \right\}^{-1}. \tag{4.40}$$

$V_{st}(r)$ is the interaction potential, and $r_{st}^{\min}$ is the distance of closest approach of the two atoms, given by

$$1 - \frac{b^2}{(r_{st}^{\min})^2} - \frac{V_{st}(r_{st}^{\min})}{g^2 kT} = 0.$$

Despite the apparent complexity, these terms have rather simple physical interpretations, in that they describe a classical collision between two particles interacting with potential $V_{st}(r)$. $\Omega_{st}^{(i,j)}$ are related to collisional cross sections[3] after integrating over Maxwellian velocity distributions. The integrand g in Eqn. [4.38] is a dimensionless velocity. $\phi_{st}^{(i)}$ are collisional cross sections for a given energy, integrated over the impact parameter b. χ_{st} is the scattering angle, integrated over the distance between the particles. Further approximations will simplify these integrals, keeping in mind that our final goal is an understandable expression for the resistance coefficients as a function of the stellar parameters.

The details of what follows can be found in PPFM. First we assume a pure Coulomb potential, of the form $V_{st}(r) = Z_s Z_t e^2/r$; the $\phi_{st}^{(i)}$ integrals are then

$$\phi_{st}^{(1)} = 2\pi \left(\frac{Z_s Z_t e^2}{2kTg^2}\right)^2 \ln(1+\beta_{st}) \tag{4.41}$$

where

$$\beta_{st} = \frac{2kTg^2\lambda_D}{Z_s Z_t e^2} \tag{4.42}$$

and

$$\lambda_D = \left(\frac{kT}{4\pi e^2 \sum_i n_i Z_i^2}\right)^{1/2}. \tag{4.43}$$

[3]The superscripts represent moments of the integral. While most higher order moments are unused, the superscripts are retained to maintain consistency with the notation in PPFM.

λ_D is the Debye length, the effective range of the Coulomb potential in an ionized plasma, where the Coulomb interaction is "screened" by intervening ions. Such a "screened" potential follows the form of

$$V(r) = Z_s Z_t \frac{e^{-r/\lambda_D}}{r^2}.$$

We now make a second approximation, and ignore the velocity dependence of the β_{st} term in Equation [4.41], replacing it with an average value of the dimensionless velocity, $< g^2 >= 2$. This gives (PPFM Eqns. [29], [31], & [33])

$$\phi_{st}^{(1)} = 2\pi \left(\frac{Z_s Z_t e^2}{2kT}\right) \frac{A_{st}^{(1)}}{g^4}, \tag{4.44}$$

$$A_{st}^{(1)} = \ln(1+\gamma_{st}^2), \tag{4.45}$$

and

$$\gamma_{st} = \frac{4kT\lambda_D}{Z_s Z_t e^2}. \tag{4.46}$$

Finally, we integrate over the velocity distribution to obtain the collision integral, which, with the given assumptions, becomes (see PPFM Eqn. [34])

$$\Omega_{st}^{(11)} = \pi \left(\frac{kT}{2\pi m M_s M_t}\right)^{\frac{1}{2}} \left(\frac{Z_s Z_t e^2}{2kT}\right)^2 A_{st}^{(1)}. \tag{4.47}$$

We are nearly there. Remember that the initial goal of this exercise was to arrive at a simplified analytic expression for the resistance coefficients, in order to understand the diffusive behavior. The resistance coefficient, from Eqns. [4.32], [4.35], and [4.37] is given by

$$\begin{aligned} K_{st} &= X_s X_t n \frac{2kTnm}{3E}, \\ &= X_s X_t n^2 \frac{2kTm}{3} \frac{8M_s M_t \Omega_{st}^{(11)}}{kT}, \\ &= \frac{16}{3} X_s X_t n^2 M_s M_t \Omega_{st}^{(11)}. \end{aligned} \tag{4.48}$$

Now, using the the definition of $\Omega_{st}^{(ij)}$ from Equation [4.47], and some algebra, we have

$$K_{st} = \frac{4\pi}{3} X_s X_t n^2 \left(\frac{M_s M_t}{2\pi m (kT)^3}\right)^{\frac{1}{2}} (Z_s Z_t e^2)^2 \ln\left(1 + \frac{4kT\lambda_D}{Z_s Z_t e^2}\right) \quad (4.49)$$

Approximating $m_i \sim A_i m_h$, we have

$$K_{st} = \frac{4\pi}{3} \frac{X_s X_t n_2}{m_h (A_s + A_t)} \left(\frac{A_s A_t}{2\pi (kT)^3 m_h (A_s + A_t)}\right)^{\frac{1}{2}} Z_s^2 Z_t^2 e^4 \times \ln\left(1 + \frac{4kT\lambda_D}{Z_s Z_t e^2}\right) \quad (4.50)$$

$$K_{st} = 3.275 \cdot 10^{10} X_s X_t n^2 Z_s^2 Z_t^2 \left(\frac{A_s A_t}{[T(A_s + A_t)]^3}\right)^{\frac{1}{2}} \times \ln\left(1 + 2.395 \cdot 10^3 \frac{T\lambda_D}{Z_s Z_t}\right) \quad (4.51)$$

I will make another approximation, and neglect the logarithmic term, since the $T^{-3/2}$ dependence will dominate. This leaves us with

$$K_{st} = 3.275 \times 10^{10} \left(\frac{Z_s^4 A_s Z_t^4 A_t}{(A_s + A_t)^3}\right)^{\frac{1}{2}} X_s X_t \frac{n^2}{T^{3/2}} \ \mathrm{gm \cdot cm^{-3} \cdot sec^{-1}}. \quad (4.52)$$

We have now reached the goal of a simple analytic form approximation to the resistance coefficients. Eqn. [4.52] relates the resistance coefficient to the model parameters of density and temperature. While not precise enough for actual modeling – indeed, the entire point of PPFM was to avoid the various approximations used here – it does give us an idea of the behavior of the resistance to diffusion within the stellar interior.

The net result can now be stated quite simply. The diffusion driving force, given by Equation [4.31], depends on the number density. The more atoms of a given species present, the greater the total force. If we neglect the temperature dependence, the

resistance to diffusion given by Equation [4.52] depends on the square of the number density. This is because the resistance depends on the inter-atomic interaction, which goes roughly as the square of the number of ions present. Thus, the highest velocity is found in the lowest density regions, i.e., near the surface.

Now that we have a physical description of the resistance coefficients, let us examine their behavior in the models. The sum of the resistance coefficients, as given by the tables in PPFM, is plotted in Figure [4.4]. The resistance coefficients vary over 10 orders of magnitude between the surface of the model and the core. Where the driving forces increase by roughly a factor of 100 from the surface to $q_s = 10^{-5}$, the resistance coefficients increase by over a factor of 1000. So even though the driving force is weakest at the surface, the resistance to diffusive motion increases faster than the force as a function of depth, and the net effect is the highest diffusion velocity is at the surface.

4.7 Summary: What Just Happened

In this chapter I presented a detailed description of the diffusion equation, and a description of its numerical solution. We have also examined the behavior of the diffusion velocities within our models, and looked at the important physical parameters which govern its behavior. The most important idea is that equilibrium is reached from the outside in, and the governing factor is the resistance to diffusion determined by the resistance coefficients.

As I have shown, diffusion has its greatest impact in the outer layers of the model, where the resistance is lowest. It is in these very layers that we can also probe the structure of stars, using the tools of stellar pulsation theory. In the next

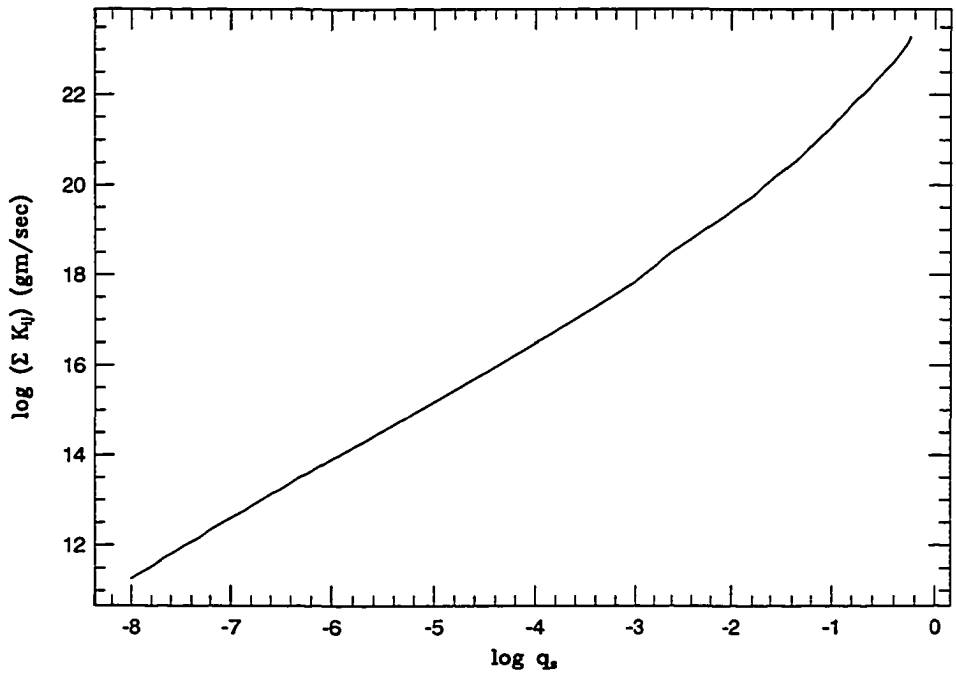

Figure 4.4: Resistance coefficients for a PG 1159 model

chapter we will examine the changes in compositional structure due to the diffusion in an evolving model, and, most importantly, compare the resulting models with observation.

CHAPTER 5. EVOLUTION RESULTS - TRANSFORMATION OF THE HELIUM STARS

The light which reveals to us the existence of the heavenly bodies also bears the secret of their constitution ...

James E. Keeler (1897)

In this Chapter, I describe the results of a calculation of a sequence of helium-rich white dwarf models. This sequence represents the evolution of a PG 1159 star as it cools and becomes a "normal" DB white dwarf. PG 1159 stars are an important starting point because they lie at the top of the white dwarf cooling track. Many of the PG 1159 class – including the prototype PG 1159-035 – are also pulsating stars; these pulsations allow a probe of the interior structure of the star, thus a better understanding of the changes that take place during the evolution of a white dwarf. This Chapter discusses the evolution of the sequence that includes diffusion beginning at the PG 1159 stage. Using this starting model, I show that a direct evolutionary link can exist between the PG 1159 stars and the much cooler DB white dwarfs below the DB gap. The model that results from evolution from the PG 1159 temperature regime to below the DB gap is then subject to the same sort of stringent test passed by the initial model: comparison of its oscillation frequencies with those observed in the pulsating DB white dwarf GD 358.

5.1 The Initial Model

The initial model was designed to model the observed pulsational spectrum of PG 1159, and is based on the evolved core of a post-AGB star. The model was initially evolved to the AGB and the formation of a carbon/oxygen degenerate central core by Iben (1984). This model was removed from the AGB during a thermal pulse, and so is representative of the probable progenitors of DB white dwarfs. Kawaler & Bradley (1994) modified the outer layers of the model in a systematic way, evolving the starting models into the PG 1159 regime for comparisons with the WET observations of this star reported by Winget et al.(1991a). For this investigation, the important point of the initial model is that it is an accurate model of the star PG 1159 that matches the observational constraints both from the spectroscopy of Werner et al.(1991) and from its observed oscillations.

The composition profile of the initial model is shown in Figure [3.1]. The envelope, down to a depth of $\log q = 10^{-3.5}$ is set to a uniform composition of ^{4}He 30%, ^{12}C 35%, and ^{16}O 35% by mass. These abundances are consistent (within the uncertainties) with the atmospheric models of Werner, Heber, & Hunger (1991a), who find (by mass) helium at 0.33, C at 0.5, and O at 0.17. The most important feature of the composition profile is the composition transition at $\log q = -3.5$. This is a direct result of the investigation by Kawaler & Bradley (1994); the location of this transition is determined from the pulsational properties of PG 1159.

By the time the model approaches the PG 1159 regime, nuclear burning has ceased. This allows initial models of stars of different masses to be obtained from the original model by re-integrating the equations of structure, after changing only the mass of the model. In this process, the dependence of fractional luminosity and

composition as functions of the fractional mass are preserved. Some iteration on the surface luminosity is necessary in these integrations to ensure satisfaction of the surface boundary conditions. With this procedure, as long as the mass did not differ too much from the original $0.59M_{\odot}$ model, the resulting models should be accurate representations of stars that have similar evolutionary history through the thermally pulsing AGB.

5.2 The Diffusion Sequence

The results of the evolution and diffusion calculations are described in Dehner & Kawaler (1995). Some of the results presented in that publication are also given here, along with additional data and discussion not presented in Dehner & Kawaler (1995) due to space constraints.

To examine a range of predecessor masses, we computed four evolutionary sequences, ranging from $0.56M_{\odot}$ to $0.62M_{\odot}$. The results of the calculations show lighter elements float to the top, while heavier elements sink to the core. This is summarized in Figure [5.1], which shows the ^{4}He mass fraction for models of several effective temperatures in the $0.58M_{\odot}$ evolutionary sequence. As the model cools, the helium abundance increases in the upper layers; when the model reaches 80,000K the mass fraction of helium at the surface has reach reached nearly unity, and the mass fraction of the He transition zone has reached a depth of $\log q = -5.0$.

The corresponding helium diffusion velocities for this model sequence are shown in Figure [5.2]. As the model evolves, the diffusion velocity drops near the surface. This reflects the increase of the helium composition in these layers, and the decrease of the mean molecular weight. As seen from Eqn. [4.31], as the mean molecular weight

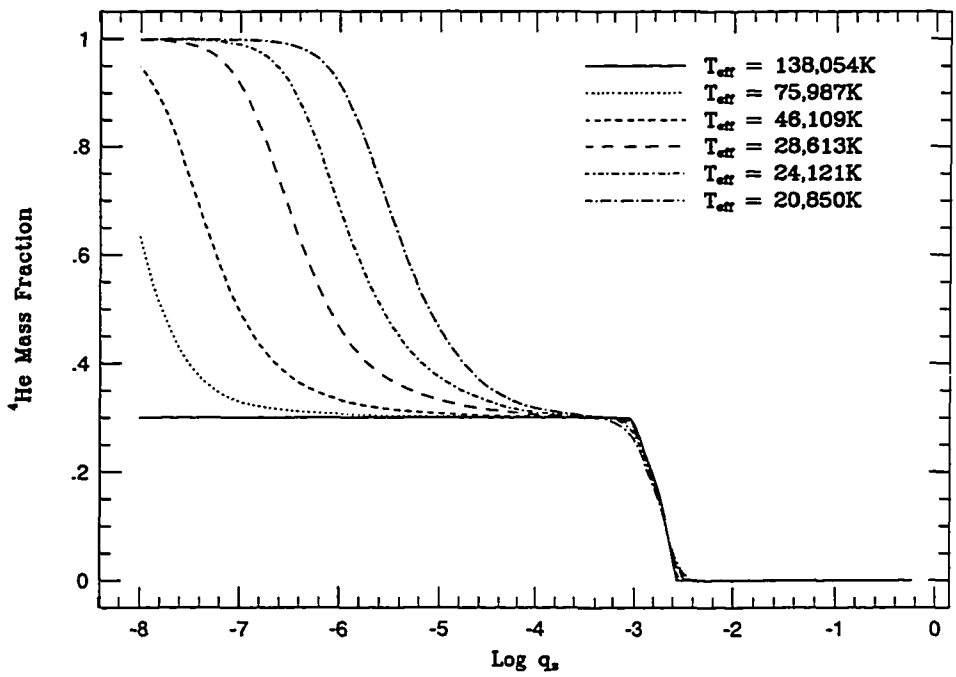

Figure 5.1: Helium composition evolution

μ approaches the atomic weight of helium, the driving force for the diffusion (on helium) will decrease. As the helium fractional abundance increases towards unity, the abundance of other elements will decrease; this decrease will cause a decrease in their driving, due to the number density dependence of the gravitational term. This change in μ can is seen in Figure [5.3], which shows the mean molecular weight μ as a function of mass fraction for the models in Figure [5.2].

The evolution of some of the more important parameters in the 0.58 $M_{\odot}$ sequence are given in Table [5.1]. The location of the helium to carbon transition zone is difficult to define in models where the helium has not yet formed a clear surface layer, until about 41,000K in effective temperature. The log of the surface carbon abundance (by mass) is also given. As can be seen, even at 21,000K, there is still some carbon in the surface layers of the model.

Table 5.1: Evolution of Key Values

T_{eff} (K)	log $L/(L_{\odot})$	Time (Myr.)	log He/C trans.	log surf. C
138,054	2.26	0.000	n/a	-0.46
112,154	1.76	0.045	n/a	-0.50
94,618	1.36	0.144	n/a	-0.55
75,987	0.90	0.409	n/a	-0.70
60,950	0.45	0.892	n/a	-0.92
46,109	-0.09	2.022	n/a	-1.44
41,159	-0.30	2.771	-7.18	-1.71
30,690	-0.85	6.857	-6.60	-2.73
28,562	-0.98	8.984	-6.44	-3.05
25,809	-1.17	14.190	-6.14	-3.61
23,377	-1.35	23,048	-5.82	-4.25
20,850	-1.56	40,781	-5.44	-4.99

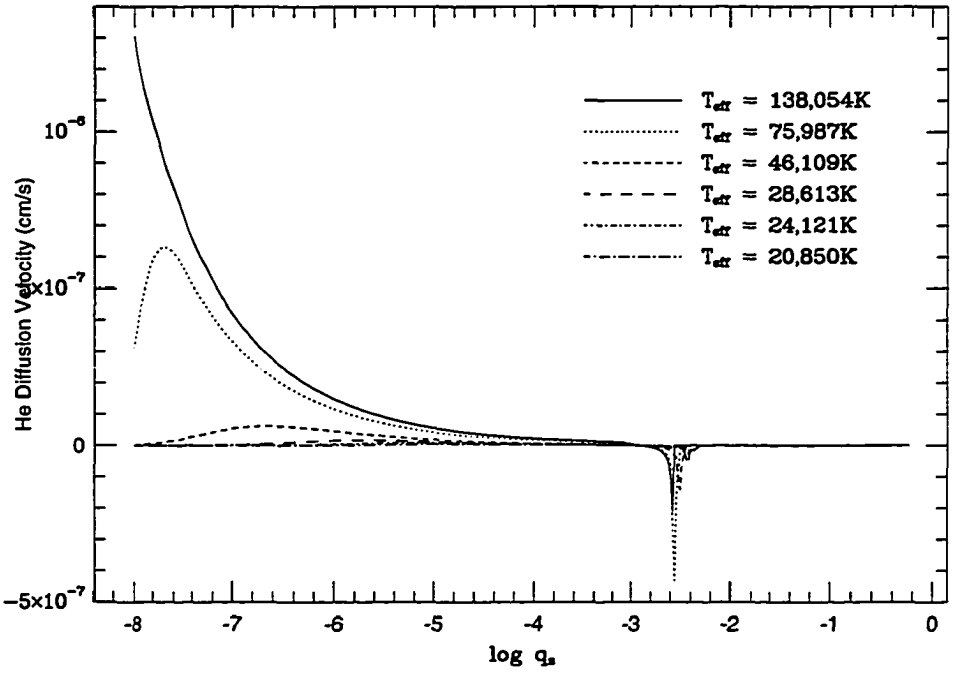

Figure 5.2: Helium diffusion velocity evolution.

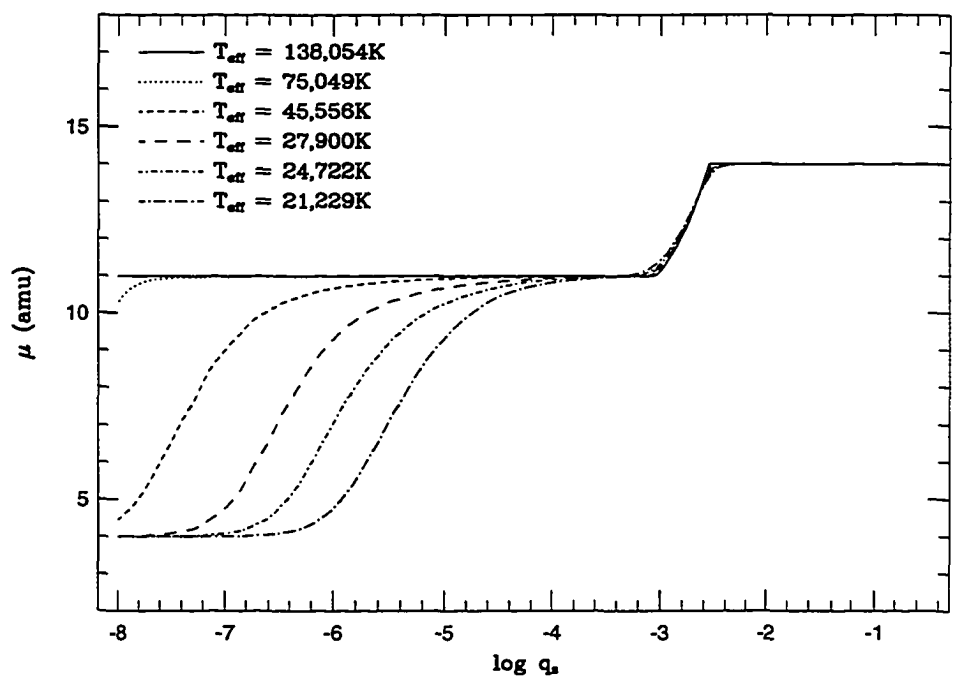

Figure 5.3: Mean molecular weight evolution.

5.3 Comparing with Observation: Pulsations

An important facet of any investigation is comparison with observables. So far, I have taken an initial model – as best determined by observation – and simulated its evolution into a cooler star. The major result so far has been accumulation of helium at the top of the model, with heavier elements sinking deeper. A more in-depth examination is afforded by computation of the nonradial oscillation frequencies of the models that are within the DB instability strip, and comparison of these periods with observations. The nonradial $g-$mode periods for models in the appropriate temperature range are computed using the adiabatic pulsation codes described in Kawaler & Bradley (1994).

As the models approach the hot edge of the DB instability strip, which is at about 28,000K, the transition zone has reached a depth of about $\log q = -6.0$. The depth of this composition transition zone, however, has observational significance. As discussed by, e.g., Kawaler (1990) and Kawaler & Bradley (1994), such a composition transition zone produces a strong density gradient, which in turn acts as a reflecting boundary for some nonradial modes. One signature of nonradial $g-$modes, such as seen in white dwarfs, is that they are equally spaced in period. Those modes which are influenced by the transition zone are "trapped modes"; they show periods that are systematically different than untrapped modes. The signature of trapped modes is that they are closer to the next larger period than normal modes. Thus trapped modes appear as local minima in a plot of periods spacing as a function of period when the the period spacing is computed in a reverse–difference form. The period spacing itself is a function of the mass of the star, and the period difference between trapped modes is determined by the depth of the composition transition zone (see Kawaler &

Bradley 1994, and Bradley & Winget 1994, and their references, for details.)

Photometric observations of GD 358, the prototype DBV, were made by Winget et. al. (1994). These observations were used by Bradley & Winget (1994) in order to model the structure of GD 358. While comparing models to models may be a somewhat dubious pursuit, in this case it is useful since the models were generated by completely different procedures. The models of BW consist of evolved white dwarf cores with static envelopes added which were adjusted to fit the pulsational data. This is similar to the approach of Kawaler & Bradley (1994) for the model of PG 1159 used as the initial model here. My GD 358 model, however, is not constructed to fit any *specific* observations; it is simply the result of the evolutionary calculations.

When comparing the models to the observations, it is useful to compare both the periods and the period spacing. In order to facilitate this comparison for a large number of models, I computed the sum of the squares of the differences between the period, and the same for the period spacing, for all models in the instability range. That is, I computed the sums

$$\sigma_{dP}^2 = \sum^{N} \left(dP_{\rm obs} - dP_{\rm mod}\right)^2 \& \tag{5.1}$$

$$\sigma_{P}^2 = \sum^{N} \left(P_{\rm obs} - P_{\rm mod}\right)^2 \tag{5.2}$$

where the sum is taken over all observed periods. The inverse of these quantities are plotted in Figure [5.4] for all models, where the best match will be shown by peaks in the diagram. The best model, although somewhat a matter of debate, is the $0.58M_{\odot}$ model with $T_{\rm eff}$=24,210K. With this model, the periods and the period spacing both fit well to GD 358.

Now, we compare the pulsational spectra of our models with that observed by

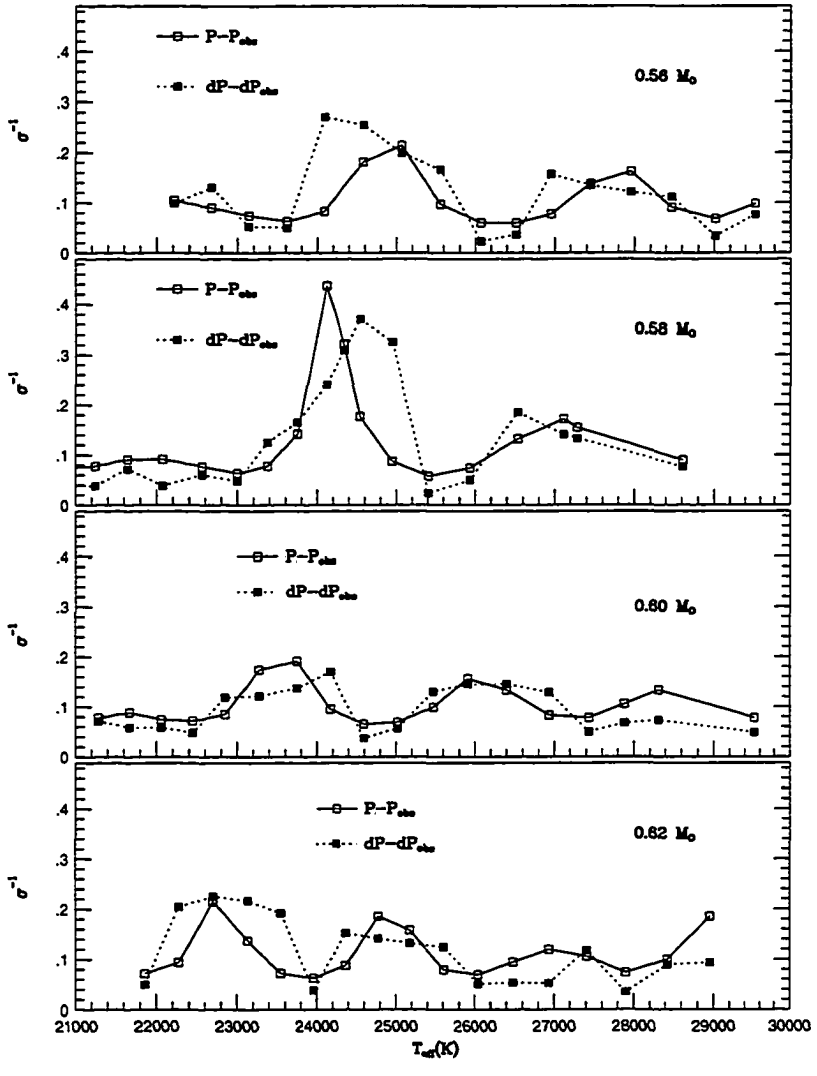

Figure 5.4: Model grid to observation comparison.

Table 5.2: Period comparison

k	Evolved	BW	GD 358
5	298.641	301.803	
6	340.390	339.975	
7	382.116	377.734	
8	423.444	420.505	423.27
9	461.782	462.336	464.23
10	494.362	499.181	(501.59)
11	534.622	535.575	(541.75)
12	577.982	575.938	(576.76)
13	619.120	616.119	618.28
14	659.920	658.426	658.35
15	699.238	701.370	700.64
16	734.684	733.988	734.30
17	775.708	770.358	770.57
18	817.524	812.507	

the WET data and as modeled by BW. All three spectra are shown in Figure [5.5]. The hollow triangles represent data points where the identification of pulsational modes was uncertain. A listing of the periods in our best model, BW's model, kindly provided by Paul Bradley, and the observed periods in GD 358, from Winget et al.(1994), is given in Table [5.2].

The pulsational behavior of the evolved model and the BW model is similar. While there is some discrepancy at the shorter periods around 450 s, the longer periods show the same behavior. Further, the global characteristics of luminosity and temperature are close; as shown in Table [5.3], the evolved model falls well within the range of values calculated for GD 358 using the model grid of BW. So while the BW model is a superior fit to the data, the evolved model is similar to the model of BW in many respects.

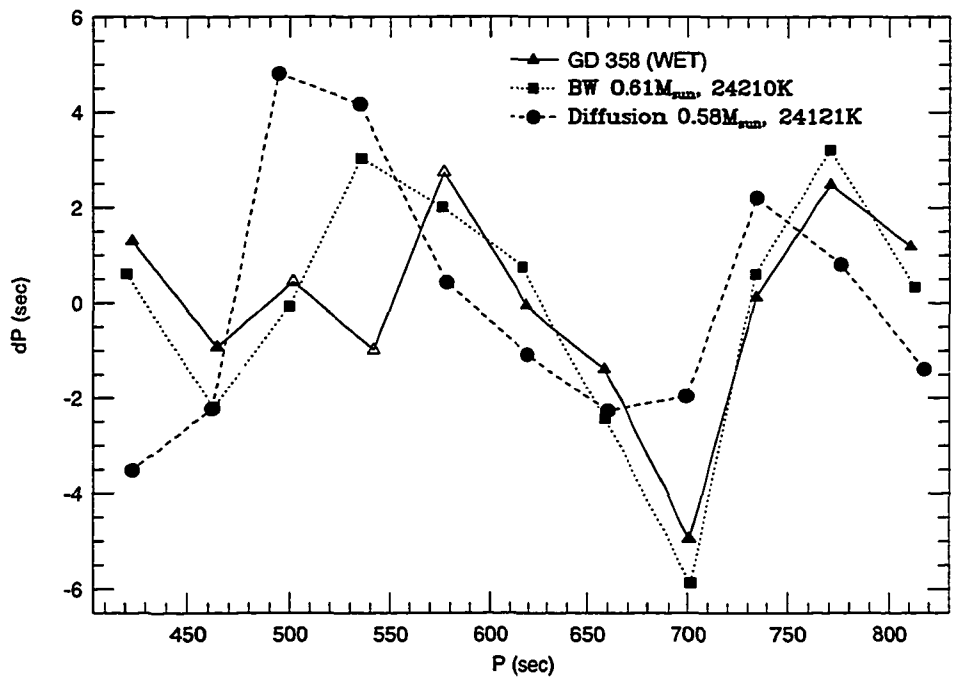

Figure 5.5: Period spacing comparison.

Table 5.3: Comparison of model characteristics

	Diffusion	BW best	BW range
$T_{eff}(10^3K)$	24.121	24.210	24±1
M ($M_\odot$)	0.58	0.61	0.61±0.03
log ($L/L_\odot$)	-1.294	-1.308	$-1.30^{+0.09}_{-0.12}$
log (M_{He}/M_*)	-6.0	-5.82	$-5.70^{+0.18}_{-0.30}$

The carbon in PG 1159 behaves essentially opposite of the helium; it slowly sinks to the core of the star. However, even in the coolest model the surface carbon never reaches zero; there always remains some trace abundance at the surface. Recent observations of GD 358 by Provencal et al.(1995) (private communication) indicate trace carbon abundances, as observed by HST ultraviolet observations. Atmospheric models by P. Thejll indicate that the carbon is present with a ratio of log n(C)/n(He) = -5.5 (Provencal, 1995), while in our models the residual carbon abundance gives a log ratio of -4.5. Further, they predict a somewhat higher surface temperature then I do, at $T_{eff} \sim$ 28,000K. While there is a modest discrepancy here, it is apparent that the carbon abundance can be explained by a diffusive tail, without invoking more exotic scenarios such as radiative levitation or accretion.

5.4 Conclusions: the PG 1159 — DB link

This model sequence demonstrates how a PG 1159 star may evolve into a DBV star like GD 358. The key factor in this conclusion is the pulsational data of GD 358, and the comparison with the model properties. Not only does the pulsational spectrum fit the observations, but the model is also consistent with the independently derived model of BW. This is significant because BW is specifically constructed to fit

the observational data, while my model is simply evolved from the PG 1159 stage.

This then shows one definite path in white dwarf spectral evolution, between PG 1159 and GD 358. It shows at least one possible predecessor of GD 358, and a fate of PG 1159 stars. Further, with the identification of these stars as the same star at different evolutionary states, this simplifies considerations of previous stages of stellar evolution. Post-AGB evolutionary models now have to account for one less type of white dwarf, if the PG 1159 and DBV stars are the same.

A key weakness in this investigation is the lack of hydrogen in the models. Because of this, the models maintain their helium rich appearance at all evolutionary stages. This is in direct conflict with the existence of the DB gap. The simple existence of this gap indicates that *all* white dwarfs must contain (or acquire) hydrogen during their cooling lifetime, before reaching T_{eff} ~45,000K. While the spectroscopic analysis of PG 1159 by Werner et al.(1991a) indicates very little hydrogen, the consequences of hydrogen in the evolution of a PG 1159 model are explored in the next Chapter.

CHAPTER 6. THE HYDROGEN MODELS

Second verse, same as the first – a little bit louder and a little bit worse

Traditional

In this chapter, I describe calculations of the evolution of a PG 1159 model with a small amount of hydrogen added. As discussed in previous Chapters, observations constrain the hydrogen content of the surface of PG 1159 to be very small, less than 5% by mass. The previous Chapter demonstrated that PG 1159 stars can be the ancestors of the DB stars except for the fact that such a link requires that the DB gap be ignored. Adding a small amount of hydrogen to the PG 1159 models could in principle lead to their becoming DA stars at the appropriate temperature range; this raises the interesting possibility that PG 1159 stars could represent the progenitors of all white dwarfs, as has been suggested in the so–called "single–channel" models of white dwarf chemical evolution (see, for example, Shipman 1989, and Liebert et al.1987). In order to investigate the effects of hydrogen on the evolution, a small amount was added to the surface of the initial model.

6.1 The Initial Model

The initial model for investigating hydrogen was based on the PG 1159 model discussed previously. There were three major constraints that were considered when

adding the hydrogen to the model. First, the total hydrogen mass was to be less than $10^{-10}M_{\odot}$. This limit is determined from Liebert et al.(1987), who argue only a very thin hydrogen surface layer can be convectively overturned at the red edge of the DB gap. Second, the surface abundance of the hydrogen was to be (at most) 5% by mass, to be consistent with the spectroscopic observations as modeled by Werner et al.(1991a). Finally, the hydrogen was not to extend deep enough into the stellar envelope to ignite; it was assumed that the models had evolved to the stage where nuclear burning would cease. While this last assumption may be somewhat arbitrary, it allowed a reasonable starting model to be generated.

Starting with the $0.58M_{\odot}$ PG 1159 model, I first extended the surface layers out to a mass fraction of 10^{-14}, so that layers cool enough and thin enough to contain the hydrogen actually existed in the model. Then, 5 % by mass of the helium was replaced with hydrogen in the outer layers of the model, down to a temperature of 10^6K, after which the hydrogen abundance was further reduced by a factor of $(10^6/T)^4$. The temperature dependence of the hydrogen composition was to prevent nuclear burning from occurring with the newly introduced hydrogen, and was used to mimic hydrogen depletion in the deeper layers by nuclear burning. Nuclear burning did occur, but at a nearly insignificant rate. The total hydrogen added was $2.13 \times 10^{-12}M_{\odot}$. Finally, the model was evolved for very short timesteps ($\sim$ 1 year) without diffusion in order for the structure to settle to hydrostatic equilibrium.

6.2 Evolutionary Behavior

The results for the hydrogen echo the results for the helium, except at a *much* faster timescale. The faster timescale in the outer layers[1] is a result of decreased resistance to the diffusive motions, which in turn is caused by the decreased density, as discussed in Chapter 4. In this model, the hydrogen surface abundance had increased by a factor of 10 in around 100 years, as shown in Figure [6.1]. Such an enhanced abundance would have been detectable, as discussed by Werner et al.(1991a). This contradiction will be addressed later in this Chapter.

The evolution of some quantities of interest are shown in Table [6.1]. Note that both hydrogen and helium are increasing at the surface, at the expense of the carbon and (not shown) oxygen. Also note that the effective temperature is increasing with time. This is because the star has not quite relaxed into its new configuration, and therefore has not really settled onto the white dwarf cooling track yet. If a larger timestep had been used, an evolutionary timestep of about a few thousand years, this temperature increase would not be apparent. This only further underscores the quickness at which diffusion acts in the surface layers of this model, as compared to the evolutionary time.

The carbon abundance in this model behaves as in the previous non-hydrogen model, decreasing drastically as a function of time. At the surface layer, the final model shown in Figure [6.1], at 195 years, has a carbon mass fraction of 5.8×10^{-2}, much lower than that calculated by Werner et al.(1991). This is also inconsistent with the observations. One is then left with the unavoidable conclusion that the

[1] In the helium model sequence, I was not concerned with surface abundances, but thickness of the helium envelope. Thus those models did not extend as far out.

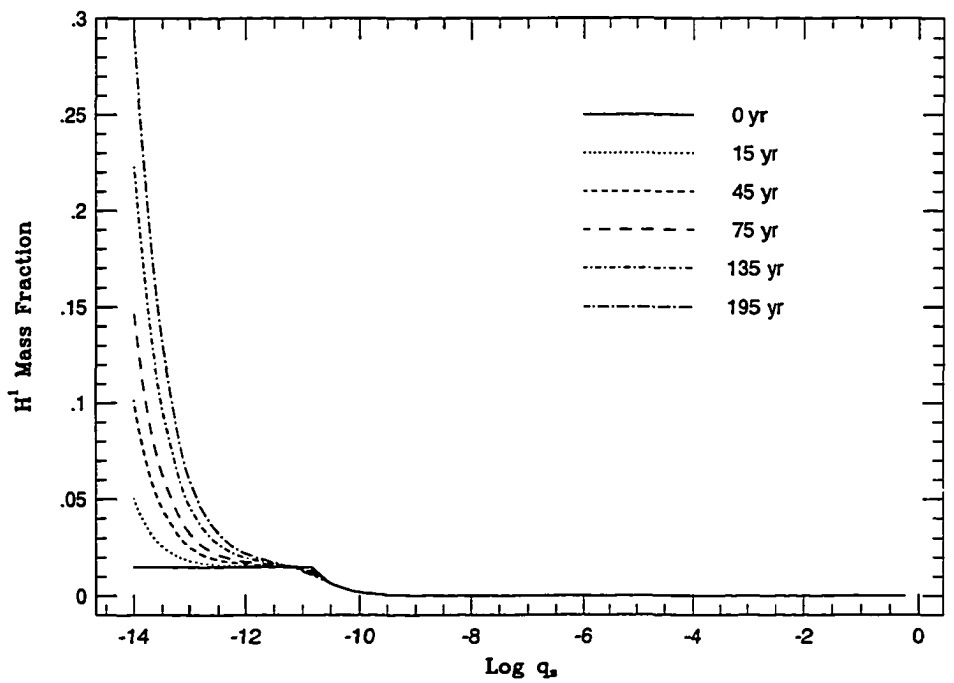

Figure 6.1: Hydrogen composition evolution

Table 6.1: Hydrogen model evolution – surface abundances by mass

Time (yr)	T_{eff} (K)	Surf. H	Surf. He	Surface C
0	137,932	0.015	0.285	0.350
15	138,215	0.050	0.378	0.291
35	138,432	0.086	0.450	0.242
55	138,599	0.117	0.500	0.204
75	138,744	0.147	0.537	0.172
115	138,986	0.200	0.584	0.121
155	139,180	0.249	0.607	0.085
195	139,332	0.292	0.612	0.058

diffusion models are completely at odds with the observed abundances of PG 1159 when hydrogen is present in the outer layers and all other assumptions (e.g., no mass loss) are retained.

6.3 Resolving the Contradiction

Despite the optimistic title of this section, there is (currently) no resolution to the contradiction between theory and observation. While I can suggest some mechanisms which may account for this difference, and provide some quantitative description, there is no conclusive solution. Perhaps the best that can be said is that this difference demonstrates the existence of some process neglected or as yet unidentified in the current description.

Identification of the coolest PG 1159 star may provide a clue as to when this mechanism shuts off and allows the elemental separation to proceed unimpaired. The survey by Dreizler et al.(1994, summarized in Dreizler et al.1995) indicates that, while most PG 1159 stars are at temperatures above 100,000K, there are a few objects that

show PG 1159 abundance patterns at temperatures as low as 65,000K.

6.3.1 Mass loss

One possible explanation for this is the presence of mass loss in PG 1159. We can determine at least an order of magnitude of the required mass loss by examining the diffusion velocities. To begin, the diffusion velocities are shown in Figure [6.2]. The velocities near the top of the model are near 0.001 cm/s. We can estimate the mass flow rate from the formula

$$\dot{M} = 4\pi R^2 \rho v.$$

Using R $\sim$ 0.01R$_\odot$, and $\rho \sim 3{\times}10^{-6}$gm $\cdot$ cm^{-3}, this latter from near the top of the models, one calculates $\dot{M} \sim 3 \times 10^{-16}M_\odot$/yr. A mass loss as small as this would be undetectable, at least by direct means such as distorted line profiles.

In Chapter 2 I discussed the work of Pauldrach et al.(1988) on radiatively driven winds and mass loss in PNNi; Table [2.2] shows some of their results. This table shows that the mass loss rates from the PNNi are much greater than required to suspend diffusion. If we extrapolate this table to the PG 1159 stars, with higher surface gravity, we can suggest that as the star cools, and the gravity increases, the mass loss will decrease, eventually allowing diffusion to continue unimpeded. Further, there are the results of Werner et al.(1995), which indicates possible mass loss from two very hot DO stars. While these results are preliminary, i.e., there is no quantitative determination, this is an intriguing discovery. Whatever process is responsible for the mass loss requires rates large enough to prevent diffusion, and yet small enough so that some hydrogen is still retained, which can later float to the surface.

It is worth noting that even in the absence of surface hydrogen, mass loss would also delay the purification of the surface helium layer. However, since mass loss driven by a radiative wind will decrease quickly with decreasing luminosity, the results for the PG 1159 - DB sequence would be virtually unchanged; most of the separation occurs at temperatures well below the PG 1159 range.

6.3.2 Dynamical motions

Another possibility is that of hydrodynamic fluid circulation in the upper envelope mixes the material, and prevents the settling of material. Such mixing only need take place within a small part of the star to prevent - or at least delay - diffusion. Examination of such a process, however, requires dynamical calculation beyond the scope of this work.

6.3.3 Magnetic fields

Yet another possibility may be effects from magnetic fields. Magnetic fields were neglected in the development of the equations describing diffusion largely due to the difficulty involved. Magnetic field terms remove the spherical symmetry, and result in a much more complicated system. We can still gain a rough idea of the required magnitude of the magnetic field by examining the dependence of the diffusion driving force on the magnetic term, which was neglected in the previous discussion. This dependence is given approximately by [cf. Burgers (1969), Eqn. 18.1]

$$-\psi_{s,\mathrm{mag}} = \mathbf{j}_s \times \mathbf{B}/c \tag{6.1}$$

$$\mathbf{j}_s \approx Z_s e n_s w_s \tag{6.2}$$

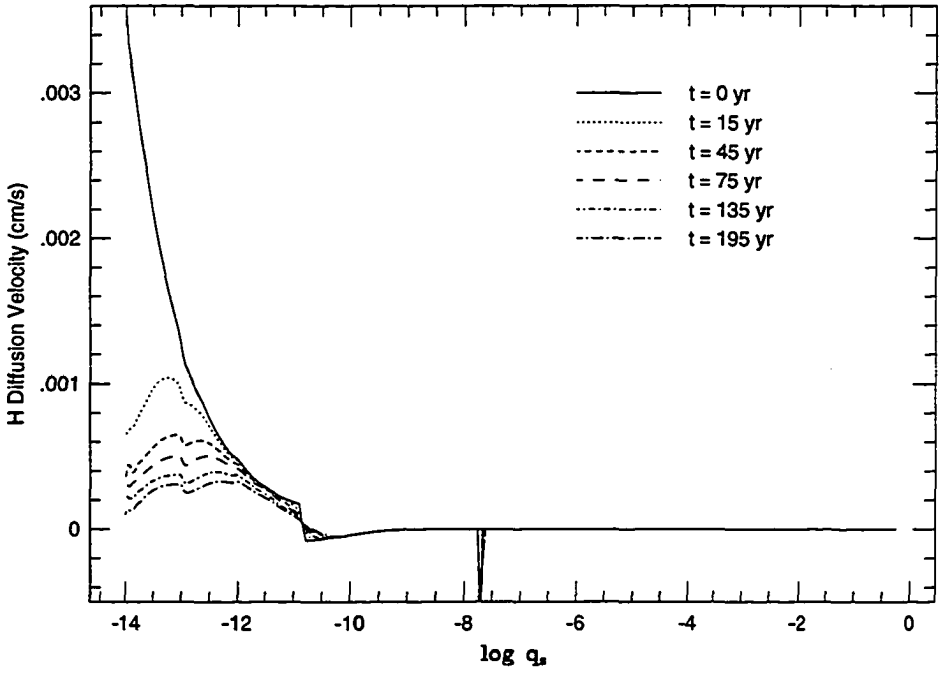

Figure 6.2: Hydrogen diffusion velocities

where $\psi_{s,\mathrm{mag}}$ is the magnetic driving force, $\mathbf{j}_s$ is the current due to element s, Z_s, n_s, w_s are the charge, number density, and diffusion velocity of element s, $\mathbf{B}$ is the magnetic field, and c is the speed of light. As a first estimate, I will require that the magnitude of the magnetic driving term be equal to the sum of the other driving terms. Using the surface values from the model for hydrogen of $n = 4.013 \times 10^{16}$ cm^{-3}, $w = 6.640 \times 10^{-3}$ cm/s, and $\psi = -5.481$ dyne/cm^3, this gives $j = 1.280 \times 10^5$ esu/s, and $B = 1.284 \times 10^6$ Gauss, or about 1 MG.

The observations of PG 1159 by Winget et al.(1991) give an upper limit of 6000G for a magnetic field of PG 1159; obviously, 1 MG is out of the question. Schmidt & Smith (1995) report on a survey for the number of magnetic white dwarfs. While they focus on the cooler DA white dwarfs, they find that about 4.0% $\pm$ 1.5% of all white dwarfs have a magnetic field, with field strengths ranging from $\sim 3 \times 10^4$G to 10^9G. This small number of magnetic white dwarfs makes it unlikely that magnetic forces play a strong role in resolving the hydrogen diffusion problem.

6.3.4 Radiative levitation

It is possible that radiative effects may play a role in the heavy element abundances in PG 1159 stars. However, it is unlikely that radiative forces will solve the current problem. Radiative forces in PG 1159 stars have been studied most recently by Unglaub & Bues (1995, 1996), and they find that radiative forces are insufficient to maintain the observed abundance. Further, they note that radiative force scale as the inverse of the number density, and so it is difficult to invoke radiative forces to maintain more than a trace abundance of heavy elements in a stellar atmosphere.

6.4 Conclusions

Calculations of diffusion in a PG 1159 model containing hydrogen show that hydrogen would diffuse to the surface on very short timescale. Within a period of ~100 years, hydrogen rises to the surface of the model in abundances much larger than the currently observed upper limit. This increase in hydrogen is accompanied by a decrease in carbon and oxygen, which drops their abundance to far less than that observed in the PG 1159 stars.

The reason for this disagreement is unclear. One skeptical explanation is that the diffusion calculations themselves are fatally flawed. The results of the previous Chapter, however, indicate that there must be some validity to the methodology. The most likely possibility is the inhibition of diffusion at early times through mass loss. If this is the case, the temperature limit where pure surface abundance white dwarfs begin to appear may give some clue about what process causes mass loss, and when this process ceases to be important.

CHAPTER 7. CONCLUSIONS AND SUMMARY: WHERE HAVE WE COME?

We shall not cease from our exploring. And the end of our exploring will be to arrive where we started and know the place for the first time.

- T. S. Eliot (1942)

Here I review and summarize the work in this Dissertation. It should be remarked on that all of the section titles in this Chapter are questions. The process of answering questions – the purpose of this investigation – opens new questions, and these new questions are what broaden our horizons of inquiry.

7.1 Summary: What has happened

In this Dissertation, I have attempted to explore the effects of diffusion and evolution on helium-surface white dwarf stars. In a fundamental manner, the effects of diffusion are shown by the nearly pure hydrogen or helium surfaces of white dwarfs. However, a more quantitative examination of these effects, made possible by the probing of deeper layers through seismological analysis, is in order.

In the second Chapter, I described current thoughts and directions in stellar evolution, and how white dwarfs fit into this picture. White dwarfs are the remnants of stellar evolution, and so they serve as an archaeological sign of the history of

star formation. White dwarfs themselves are not "dead" however; they still continue to evolve and change over time. Relating the properties of white dwarfs to their precursor stars is one of the most important goals of this – or any – investigation involving these compact stars. And as the oldest stars, the faintest white dwarfs also determine the age of stellar populations. Using white dwarfs to determine these ages is the second purpose for the study of white dwarfs.

In the third and fourth Chapters, I described the computational techniques used to model white dwarfs. The physical processes describing white dwarf evolution are fairly well understood, and the numerical techniques for modeling these processes equally well established. The structural changes that come about with evolution have been modeled by many other authors, and comparison with these works shows that ISUEVO is a state–of–the–art tool for these investigations. The diffusion processes, however, are less well modeled, so such a comparison is more difficult. In this case, I demonstrated that the results are physically meaningful, using analytic arguments and considering the driving forces and the resistance.

Finally, I presented the results of the computations, showing the effects of diffusion during evolution. Starting with a model of the hot, pulsating white dwarf PG 1159, I modeled its evolution down to a much cooler stage, where the pulsating, helium rich white dwarfs known as the DBVs live. The fact that these stars pulsate is pivotal in this investigation, since these pulsations allow a direct measurement of the interior layers of a star. In this case, when the PG 1159 model cooled to the DBV stage, the helium floating to the surface had the same thickness as the measured helium layer in the DBV GD 358. This strongly indicates that the PG 1159 stars are (or can be) predecessors of the DBV stars, despite the large disparity in surface

composition and structure.

However, this conclusion is challenged by the presence of the DB gap, a temperature range where there are no known helium–rich white dwarfs. Since the PG 1159 model contained no hydrogen, consistent with observations, it must retain its helium rich appearance all through its evolution, which is inconsistent with the existence of the gap. To address this inconsistency, I added a small amount of hydrogen to the PG 1159 model and computed a new evolutionary sequence. In this sequence, the hydrogen floated to the surface so quickly that it would be visible while the star was still in the PG 1159 stage. This implies the existence of some mechanism which impedes the diffusion process, at least temporarily. One likely candidate is mass loss, since only a very low rate is needed. Mass loss is also known to occur in planetary nebula nuclei, which are believed to be the immediate predecessors of PG 1159 stars, at rates much greater than that needed to swamp diffusion.

7.2 What does it mean?

First, I have established an evolutionary relationship between the PG 1159 stars and the DBV stars. This reduces the number of pre-white dwarf evolutionary channels which are necessary to produce these object. If a model or mechanism can produce a PG 1159 star from a main sequence star, then this will naturally produce the cooler DBV stars.

Many models of white dwarfs use stratified compositions, with a a transition zone between layers of different composition given by an equilibrium profiles, such as that of Arcoragi & Fontaine (1980). These results show that this approach is suspect. Diffusive equilibrium is reached from the surface of the star inward, due to

the behavior of the resistance coefficients. The composition profile seen in GD 358, with the helium transition zone at $\sim 10^{-6} M_*$, is not developed until the model has cooled to the DBV instability strip.

Also explained in this model is trace abundances of metals such as carbon. These metals need not be dredged up from lower levels, but will still remain in the upper layers of the star. this is because the diffusive driving force depends on the number density of the element, so as the element is depleted, the driving force decreases. The resistance, however, is more dependent on the total number density, and so does not decrease as quickly.

I have also demonstrated that there is still a mystery about the young, hot PG 1159 stars. Previous results (e.g.Unglaub & Bues 1995) cannot explain the abundance of metals in these objects. My diffusion calculations are consistent with these studies, since I predict that metals, particularly carbon and oxygen, will drop to well below observed abundances in a very short time. Again, however, mass loss can perhaps provide the solution to this problem; the same degree of mass loss that is needed to prevent the hydrogen rising to the surface preserves the metal abundance in the atmosphere and below; thus PG 1159 shows metals, and the PG 1159 stars will show metals until their mass loss rates drop to below the critical value presented in chapter 6.

7.3 Where do we go from here?

One of the fundamental question about white dwarfs stems from the observed division between hydrogen-rich white dwarfs and helium-rich white dwarfs. Do these types of white dwarfs form and evolve with (mostly) separate channels? Many inves-

tigators, such as Sion (1986), propose a two-track evolutionary sequence for white dwarf stars, with separate channels for DA and DB white dwarfs. The division between hydrogen and helium white dwarfs would then stem from the formation process, with the composition being determined by earlier stages of evolution. For example, the suggestion by Iben (1984), that the difference is determined by the conditions under which a star leaves the AGB. A star leaving the AGB during a thermal pulse will lose its outer hydrogen envelope, and so become a DB.

This two-track model is complicated, however, by the existence of the DB gap. The simple existence of the gap implies that all young, hot white dwarfs must contain some amount of hydrogen. The existence of helium rich white dwarfs above and below the gap implies that there must exist some temperature-dependent mechanism for changing the surface composition. Liebert et al.(1987) suggest a combination of gravitational settling (to initially bring the hydrogen to the surface) followed by convective mixing to accomplish this. It is in the hopes of modeling such a process, and explaining the DB gap, that this investigation is ultimately aimed.

Another facet of diffusion in white dwarfs, which has not been discussed so far, is the effect on cooling timescales. While it is neglected in this investigation, the occurrence of diffusion could have a strong impact on white dwarf cooling. First of all, diffusion by gravitational settling is an addition source of energy to the cooling white dwarf; second, changing the surface composition by diffusion will change the opacities in the outer layers, and affect the rate at which a star loses energy. And as shown by Wood (1990), the apparent ages of white dwarfs are affected by the thickness of the surface helium layer. Calculation of the white dwarf luminosity function should therefore take into account the changing thickness of the surface

layer as these stars evolve.

These complications show that this dissertation is just a beginning. The tools and techniques developed herein have a much wider applicability in investigating questions of astrophysical interest. Understanding white dwarfs is one of the keys to a better knowledge of stars in general and stellar evolution. The inquiries into white dwarfs began over 200 years ago, with their initial discovery by Herschel (1782, 1785). Since then, the understanding of these stars has involved widening areas both inside and outside of astrophysics; Fowler (1926) discovered the applicability of Fermi–Dirac statistics in explaining their interiors. Beaudot et al.(1967) showed how the elusive neutrinos are an important mechanism for cooling in white dwarfs.

In this dissertation, I have added a new piece of physics to the description of white dwarf evolution. This has answered some questions about white dwarf ancestry, such as the relationship between PG 1159 and GD 358. This has in turned raised other questions about physical processes within these objects: where is the hydrogen in PG 1159? In the end, the questions that are raised are the more important than the answers, for it is the questions which lead us on to new discoveries.

BIBLIOGRAPHY

If I have seen further, it is because I have stood on the shoulders of giants.

– Isaac Newton

Adams, W. W. 1959, PASP, 27, 236

Arcoragi, J.-P., & Fontaine, G. 1980, ApJ, 242, 1208

Beaudet, G., Petrosian, V., & Salpeter, E.E. 1967, ApJ, 150, 979

Becker, S.A., & Iben, I. Jr. 1979, ApJ, 232, 831

Bergeron, P., Saffer, R. A., & Liebert, J. 1992, ApJ, 394, 228

Bergeron, P., Wesemael, F., & Liebert, J. 1990, ApJ, in press

Blöcker, T. 1995, White Dwarfs: Proceedings of the 9th European Workshop on White Dwarfs, eds. D. Koester & K. Werner, (Berlin: Springer–Verlag), p68

Blöcker, T., & Schönberner, D. 1991, A&A, 244, L43

Böhm, K.H., & Cassinelli, J. 1971, Astr. Ap., 12, 21

Böhm-Vitense, E. 1958, Zs. Ap., 46, 108

Bond, 1862, Astron. Nach., 1353, listed in 1862, MNRAS, XXII, 5

Bowen, G.H., & Willson, L.A., 1991, ApJ, 375, L58

Bowers, R.L., & Deeming, T. 1984, Astrophysics I: Stars (Boston: Jones and Bartlett Publishers, Inc.)

Burgers, J.M. 1969, Flow Equations for Composite Gases, (New York: Academic Press)

Chandrasekhar, S. 1939, An Introduction to Stellar Structure, (Chicago: University of Chicago Press)

Chayer, P., Fontaine, G., & Wesemael, F. 1989, White Dwarfs, Proc. IAU colloquium No. 114, ed. G. Wegner, (Berlin: Springer-Verlag), p253

Chayer, P., Fontaine, G., & Wesemael, F. 1990, White Dwarfs, proc. of the NATO Advance Research Workshop, Seventh European Workshop on White Dwarfs, eds. Vauclair and Sion, (Dordrecht: Kluwer), p229

Clark, A. G., 1862, MNRAS, XXII, 5

Clayton, Donald D., 1994, Principles of Stellar Evolution and Nucleosynthesis,(Chicago: University of Chicago Press)

Clerke, Agnes M. 1887, Popular History of Astronomy, (Edinburgh: A & C Black)

Clerke, Agnes M. 1903, Problems in Astrophysics, (London: Adam & Charles Black)

Cole, P.W., & Dupree, R.G., 1980, ApJ, 239, 284

Cole, P.W., & Dupree, R.G., 1981, ApJ, 247, 607

Cox, J.P., & Giuli, R.T 1968, Principles of Stellar Structure (New York: Gordon and Breach)

D'Antona, F., & Mazzitelli, I. 1990, Ann. Rev. Astron. Astrophys., 28, 139

Dehner, B.T., & Kawaler, S.D. 1995, ApJ, 445, L141

Dorman, B., Rood, R.T., & O'Connell, R.W. 1993, ApJ, 419, 596

Dreizler, S., Werner, K., & Heber, U. 1995, White Dwarfs: The 9th European Workshop on White Dwarfs, eds. D. Koester and K. Werner (Berlin: Springer-Verlag) p160

Dreizler, S., Heber, U., Jordan, S., & Engels, D. 1994, Hot Stars in the Galactic Halo, ed S.J. Adelman, (Cambridge: Cambridge University Press) p228

Dupuis, J., Pelletier, C., Fontaine, G., & Wesemael, F., 1989, White Dwarfs, Proc. IAU colloquium No. 114, ed. G. Wegner, (Berlin: Springer-Verlag), p359

Eddington, A. S. 1922, MNRAS, 82, 431

Eggleton, P., Faulkner, J., & Flannery, B. 1973, Astron. Astrophys., 23, 325

Eliot, T. S., 1942, "Little Gidding"

Fontaine, G., Brassard, Bergeron, P., & Wesemael, F. 1992, Proc. of the 8th European Workshop on White Dwarfs, ed. M. Barstow, (Kluwer: Dordrecht), in press

Fowler, R. H. 1926, MNRAS, 87, 114

Harris, M.J., Fowler, W.A., Caughlan, G.R., & Zimmerman, B.A., Ann. Rev. Astron. Astro., 21, 165

Gathier, R. & Pottasch, S. R., 1989, A&A, 209, 369

Hanson, C. J., & Kawaler, S. D., 1994, Stellar Interiors: Physical Principals, Structure, and Evolution, (New York: Springer-Verlag)

Herschel, F. W., 1782, Phi. Trans. R. Soc. Lon., 72, 112

Herschel, F. W., 1785, Phi. Trans. R. Soc. Lon., 75, 40

Hertzsprung, E., 1915, Ap. J., 42, 115

Hoffleit, D. 1982, The Bright Star Catalog, Fourth Revised Edition (New York: Yale University Observatory)

Hubbard, W., & Lampe, M. 1969, ApJSupp, 18, 297

Iben, I. Jr. 1975, ApJ, 196, 545

Iben, I. Jr. 1984, ApJ, 277, 333

Iben, I. Jr., & Laughlin, G. 1989, ApJ, 341, 312

Iben, I. Jr., 1991, ApJSupp, 76, 55

Iben, I. Jr., & MacDonald, J., 1985, ApJ, 296, 540

Iben, I. Jr., & Renzini, A., 1983, Ann. Rev. Astron. Astrophys., 21, 271

Iben, I. Jr, & Renzini, A. 1984, Phys. Reports, 105, 329

Iben, I. Jr,, & Tutukov, A. V. 1984, ApJ, 282, 615

Itoh, N., Hayashi, H., & Kohyama, Y. 1993, ApJ, 418, 405

Kawaler, S.D., Hansen, C.J., & Winget, D.E. (1985), ApJ, 295, 547

Kawaler, S.D. 1990, Confrontation Between Stellar Pulsation and Evolution, eds. C. Cacciari and G. Clementini, (San Francisco: Astronomical Society of the Pacific), p494

Kawaler, S.D., & Bradley, P. 1994, ApJ, 427, 415

Kawaler, S.D. 1996, Stellar Remnants, eds. G. Meynet and D. Shaerer, (Berlin: Springer-Verlag)

Keeler, James E. 1897, ApJ, 6, 271

Kepler, S.O., & Nelan, E.P. 1993, AJ, 105, 608

Kepler, S.O. 1995, private communication

Kippenhahn, R., Weigert, A., & Hofmeister, E. 1967, Meth. Comp. Phys., 7, 53

Lambert, J.D. 1991, Numerical Methods for Ordinary Differential Systems (Chichester: John Wiley & Sons)

Liebert, J. 1986, Hydrogen Deficient Stars and Related Objects, eds. K. Hunber, D. Schönberner & N.K. Rao (Dordrecht: D. Reidel) Liebert, J. 1980, Ann. Rev. Astron. Astrophys., 18, 363

Liebert, J., Dahn, & Monet 1988, ApJ, 332, 891

Liebert, J., Fontaine, G., & Wesemael, F. 1987, Mem. S. A. It., 58, 17

McCook, K., & Sion, E.M. 1987, ApJSupp, 65, 603

MacDonald, J. 1992, ApJ, 394, 619

MacDonald, J., & Vennes, S. 1991, ApJ, 371, 719

McGraw, J. T., Starrfield, S. G., Liebert, J., & Green, R.F. 1979, IAU Colloq. 53, White Dwarfs and Variable Degenerate Stars, ed. H. M. Van Horn & V. Weidemann (Rochester: Univ. Rochester), 377

Mestel, L., 1952, MNRAS, 112, 583

Muchmore, D., 1984, Ap.J., 278, 769

Munkata, M., Kohyama, Y., & Itoh, N., 1985, 296, 197

Nather, R. E., Winget, D. E., Clemens, J. C., Hansen, C. J., & Hine, B. P., 1990, ApJ, 361, 309

Paczynski, B. 1970, Acta Astron., 6, 426

Paquette, C., Pelletier, C., Fontaine, G., & Michaud, G. 1986a, ApJS, 61, 177

Paquette, C., Pelletier, C., Fontaine, G., & Michaud, G. 1986b, ApJS, 61, 197

Pauldrach, A., Puls, J., Kudritzki, R. P., Méndez, R. H., & Heap, S. R., 1988, A & A, 207, 123

Pelletier, C., Fontaine, G., Wesemael, F., and Michaud, G. 1986, ApJ, 307, 242

Press, W.H., Flannery, B.P., Teukolsky, S.A., & Vetterling, W.T. 1989, Numerical Recipes: The Art of Scientific Computing [Fortran Version], (Cambridge: Cambridge University Press) Provencal, J. 1995, Private communication

Provencal, J.L, & Shipman, H.L., 1995, White Dwarfs: Proceedings of the 9th European Workshop on White Dwarfs, eds. D. Koester and K. Werner (Berlin: Springer-Verlag) p298

Rogers, F.J., & Iglesias, C.A. 1992, ApJSupp, 79, 507

Schatzman, E. 1958, White Dwarfs, (North Holland: Amsterdam)

Schmidt, G., & Smith, P.S. 1995, ApJ, 448, 305

Schönberner, D. 1983, ApJ, 272, 708

Schwarzchild, M., 1958 Structure and Evolution of Stars, (Dover: New York)

Shipman, H. 1987, The Second Conference on Faint Blue Stars, IAU Col. No. 95, eds. Philip, Hayes, Liebert, (Schenectady: L. Davis)

Shipman, H., Thejll, Bhatia, & Liebert, J. 1991, White Dwarfs, proc. of the NATO Advance Research Workshop, Seventh European Workshop on White Dwarfs, eds. Vauclair, G. and Sion, E., (Dordrecht: Kluwer), p229

Sion, E.M. 1984, ApJ, 282, 612

Sion, E. 1986, PASP, 98, 821

Tassoul, M., Foutaine, G., & Winget, D.E. 1990, ApJSupp, 72, 335

Thejll, P., Vennes, S., & Shipman, H., 1991, ApJ, 370, 355

Unglaub, K., & Bues, I. 1995, White Dwarfs: Proceedings of the 9th European Workshop on White Dwarfs, eds. D. Koester and K Verner, (Berlin: Springer–Verlag) p118

Unglaub, K., & Bues, I. 1996, A&A, in press

Vauclair, G., & Liebert, J. 1987, Scientific Accomplishments of the IUE, ed. Kondo, Y., (Reidel Publishing Company), 355

Vauclair, G., & Reisse, C. 1977, A&A, 61, 415

Vennes, S., Pelletier, C., Fontaine, G., & Wesemael, F. 1987, The Second Conference on Faint Blue Stars, IAU Col. No. 95, eds. Philip, Hayes, Liebert, (Schenectady: L. Davis), p665

Wesemael, F., & Truran 1982, ApJ, 260, 807

Weidemann, V. 1990, Ann. Rev. Astron. Astrophys., 28, 103

Werner, K. 1991, A&A, 251, 147

Werner, K., 1995 WET Workshop Werner, K., Heber, U., & Hunger, K., 1991a, A&A, 244, 437

Werner, K., Heber, U., & Hunger, K. 1991b, White Dwarfs, proc. of the NATO Advance Research Workshop, Seventh European Workshop on White Dwarfs eds. G. Vauclair and E. Sion, (Dordrecht: Kluwer), p219

Werner, K., Hermann, W.-R., Heber, U., Napiwotzki, R., Rauch, T. & Wessolowski, U. 1992, A&A, 259, L69

Werner, K., & Koester, D. 1992, Proc. Kiel/CCP7 Workshop on Atmospheres of Early-Type Stars, eds. U. Heber, C. S. Jeffery, Lecture Notes in Physics, (Springer: Berlin), p273

Werner, K., Rauch, T., Dreizler, S., & Heber, U. 1995, White Dwarfs: The 9th European Workshop on White Dwarfs, eds. D. Koester & K. Werner (Berlin: Springer–Verlag), p171

Wesemael, F. 1979, A&A, 72, 104

Wesemael, F., Green, R. F., & Liebert, J., 1985, ApJSupp, 58, 379

Winget, D. E., & Fontaine, G.,1982, Pulsations in Classical and Cataclysmic Variable Stars, ed. J. P. Cox and C. J. Hansen

Winget, D. E., & Van Horn, H. 1987, The Second Conference on Faint Blue Stars, IAU Col. No. 95, eds. Philip, Hayes, Liebert, (Schenectady: L. Davis), p363

Winget, D. E., et al., 1991, ApJ, 378, 326

Winget, D. E., et al., 1994, ApJ, 430, 839

Wood, M. 1992, ApJ, 386, 539

Wood, M., & Winget, D. E. 1989, White Dwarfs, Proc. IAU colloquium No. 114, ed. G. Wegner, (Berlin: Springer-Verlag), p282

Wood, M., Winget, D. E., & Van Horn, H. 1987, The Second Conference on Faint Blue Stars, IAU Col. No. 95, eds. Philip, Hayes, Liebert, (Schenectady: L. Davis), p639

APPENDIX A. SYMBOLS DEFINITIONS

The following table lists the symbols used, their meanings, and the units.

symbol	meaning	units
r	radial coordinate	cm
R	radial coordinate $r/R_\odot$	dimensionless
ρ	density	$gm \cdot cm^{-3}$
κ	(specific) opacity	$cm^2 \cdot gm^{-1}$
n	number density	cm^{-3}
w	diffusion velocity	$cm \cdot s^{-1}$
K	resistance coefficient	$gm \cdot cm^{-3} \cdot s^{-1}$
ϵ	energy generation	$ergs \cdot gm^{-1} \cdot s^{-1}$

APPENDIX B. DIFFUSION SOURCE CODE

This appendix contains the Fortran source code listing of the diffusion subroutines used with ISUEVO. This source code is writting in Fortran-77, but contains a "#include" statement, and is intended to be C-pre-processed. Not included in this listing are:

1. NAG linear equation subroutines, which are proprietary and unavailable for publication
2. DEPAC differential equation integrator, which is publicly available.
3. certain values in "block data collision", to save space.
4. source code for the C subroutines "priter" and "iplot", which are interactive X-windows display utilities.

B.1 Main Diffusion Code

```
c subroutines to do diffusion for the stellar evolution code ISUEVO.
c ISUEVO was written by Steven D. Kawaler, Iowa State University.
c This diffusion code was written by Benjamin T. Dehner.  Since the
c comments and bugs in here are mine, should, God forbid, anything
c work right, I'll take credit for that too.
c Support subroutines for this found in file dvels.f

#include "isuevo.h"
```

```
      subroutine diffuse
      implicit double precision (a-h,o-z)
      parameter (neqmax = jmax)
      parameter (lrw = 250+14*neqmax)
      parameter (liw = 55 + neqmax)
c Common block STRUC contains model structure
      common/STRUC/h(jmax,30),comp(jmax,15),sr(jmax),nj,modno
c Common block OLD contains the old values of everything
      common/OLD/hold(jmax,30),compold(jmax,15),srold(jmax),njold
c Common block GLOB contains global model parameters
      common/GLOB/fms,dmdt,xat0,z,alfa,time,dtime,pcl,tcl,fls,teffl
c Common block CONST contains fundamental physical constants
      COMMON/CONST/CMS,CRS,CLS,CG,CSB,CPI,CP4,CCL,CME,CH,CNA,
     1 CEV,CK,CSYR
      common /model/ dt,ttimed,numits,it,nel
      common /diffus/w(jmax,nelmax),rc(nelmax,nelmax)
      common /denses/ xn(jmax,nelmax),r(jmax)
      common /index/ielnum(nelmax),newiel(nelmax),newx(nelmax),
     1  newnel
      common /clamps/ xntot(jmax),xnlow
      dimension rwork(lrw),iwork(liw),xtemp(jmax),info(15)
      dimension xnold(jmax,nelmax),xnnew(jmax,nelmax)
      dimension rtol(jmax),atol(jmax), iamhere(nelmax)
      character title*40,lines*20
      external rhtside,jac   ! these declarations needed for DEPAC

      xmh = 1.673d-24  ! hydrogen mass
c
c nel: number of elements to do diffusion for
c ielnum: 'comp' array element to do diffusion for.
c first, set how many elements to worry about, and which ones:
      nel = 12
      do i = 1,12
       ielnum(i) = i
      enddo

c initialize display stuff.
      lines = 'xxx'
      call priter(6,lines)
```

```
      print *,'starting diffusion'
      write(title,'(20hISUEVO: Diffusion to,x,1pe9.3,x,5hyears)')
     1  dtime/csyr
      call priter(1,title)

c set up number density arrays.  with nel=number of elements
c must convert from mass fraction used in 'comp' array.

      do k = 1,nj
       xne = 0.d0
       xntot(k) = 0.d0
       do i = 1,nel
        xn(k,i) = comp(k,ielnum(i))*dexp(h(k,5))/acomp(ielnum(i))/xmh
        xntot(k) = xn(k,i)+xntot(k)
        xne = xne + zcomp(i)*xn(k,i)
       enddo
       xn(k,nel+1) = xne
      enddo
      do k = 1,nj
       r(k) = crs*dexp(h(k,1))
      enddo
c
c see how many elements are in model
c below are clamps to consider whether element is "present" for
c purposes of whether or not to diffuse it.
      xngone = 1.d-10  ! element considered not present
      xntrace = 1.d-6  ! element considered "trace"

c now.  what do we do if it's trace?
c most people just use static, but instead we'll use some relaxed
c error tolerances.

      do jj = 1,nel
       xnsum = 0.d0
       iamhere(jj) = 0
       do lay = 1,nj
        xnsum = xnsum + xn(lay,jj)/xntot(lay)
       enddo
       if(xnsum.ge.xngone) iamhere(jj) = 1
       if(xnsum.ge.xntrace) iamhere(jj) = 2
```

```
      enddo
      iamhere(nel+1) = 2      ! don't forget electrons
c
c now initialize some other stuff
      xnlow = 1.d-9           ! fractional number density, below which
c                             !  is element ignored for velocity calc.
      ttimed = 0.d0           ! total time diffused
      numtot = 0              ! total number of iterations taken
      ismallit = 4            ! number of small dt initial iterations
      dtmin = 10.d0*csyr      ! min time step after ismallit iteration
      dtmax = 5.d4*csyr       ! max time step
      dtmfac = 5.d0           ! max change in timestep
      dtstart = 5.d0*csyr     ! time step for first ismallit iterations
      dt = dtstart            ! begining diffusion timestep
      numits =  20000         ! approx. max iterations -- not an
    ! essential number.

c set elements to be plotted if plot is asked for
      nplot1 = 1
      nplot2 = 4

c begin time loop:
      do it = 1,numits+1
       numtot = numtot + 1
c following is to break out of loop when reach ttimed = dtime
       if(ttimed+dt.ge.dtime)then
        dt = dtime-ttimed
        it = numits + 1
       endif
       if(dt.le.0.d0)go to 100
       ttimed = ttimed + dt

c display stuff.
       write(lines,'(10hiteration ,i6)')numtot
       call priter(2,lines)
       write(lines,'(8httimed: ,1pe9.3)')ttimed/csyr
       call priter(4,lines)
       write(lines,'(4hdt: ,1pe9.3)')dt/csyr
       call priter(3,lines)
```

```
      call iplot(1,1,4,0)

c begin element loop
     do iel = 1,nel+1
c line 20 is at end of element loop.
      if(iamhere(iel) .eq. 0) go to 20

      write(lines,'(9helement: ,i3)')iel
      call priter(5,lines)

c set up temporary array
      do ii = 1,nj
       xtemp(ii) = xn(ii,iel)
      enddo
      ipar = iel
      rpar = 0.d0
      istart = 0
c following are parameters for DEBDF code; see DEBDF source for an
c  explanation of what this tells it to do.
c DEBDF is part of the DEPAC library, which  was written by
c L. F. Shampine and H. A. Watts, and is documented in
c SAND79-2374 "DEPAC -- Design of a User Oriented Package of ODE
c Solvers",  which I would guess is a Sandia Labs publication.
      t = 0.d0
      tout = dt
      info(1) = 0
      info(2) = 1
      info(3) = 0
      info(4) = 0
      info(5) = 1
      info(6) = 1
      neq = nj
      iwork(1) = 1
      iwork(2) = 1
c set error tolerances:
c  special case for layers with low number densities
      do jj = 1,nj
       if(xtemp(jj)/xntot(jj).lt.1.d-5)then
        rtol(jj)=2.d-3              ! increased relative tolerance
        atol(jj) = 2.5d-7*xntot(jj)  ! decreased absolute tolerance
```

```
         else
          rtol(jj) = 1.d-4
          atol(jj) = 5.d-6*xntot(jj)
         endif
        enddo
c relax tolerances more for "trace" elements
        if(iamhere(iel).eq.1)then
         do jj = 1,nj
          rtol(jj) = 5.d0*rtol(jj)
          atol(jj) = 2.d0*atol(jj)
         enddo
        endif

c  For each element, we discretize the spatial derivatives, and
c hand the time-dependant ODE to this program to integrate

10      call debdf(rhtside,neq,t,xtemp,tout,info,rtol,atol,idid,rwork,
     1  lrw,iwork,liw,rpar,ipar,jac)

c idid is a debdf diagnostic -- check for problems
        if((idid.eq.-1).and.(istart.lt.2))then
         info(1) = 1
         istart = istart + 1
         write(*,15)iel,t/csyr,it,ttimed/csyr
15       format('trying more debdf iterations, element ',i2,' t = ',
     1   1pe10.3,' iteration',i5,' ttimed =',1pe10.3)
         go to 10
        endif

        do ii = 1,nj
         if(xtemp(ii).lt.0.d0)xtemp(ii) = 0.d0
         xnnew(ii,iel) = xtemp(ii)
        enddo

c unrecoverable error:  report problem and quit.
        if(idid.lt.0)then
         print *,'error in debdf, idid = ',idid
         print *,'error at element iel = ',iel
         print *,'error in iteration ',it,', at t = ',t/csyr
         print *,'ttime = ',ttimed/csyr
```

```
        call crash(xnnew)
       endif

c end element loop -- kicked here if element wasn't present
20     continue
       enddo

c find maximum changes in xn -- used for finding new dt
       dxnrel = 0.d0
       dxnabs = 0.d0
       do ii1 = 1,nel+1
        if(iamhere(ii1).gt.0)then
         do ii2 = 1,nj
          dxn = dabs(xn(ii2,ii1)-xnnew(ii2,ii1))
          if(xn(ii2,ii1).gt.0.d0)then
           thsdx = dxn/xn(ii2,ii1)
           dxnrel = dmax1(thsdx,dxnrel)
           if(thsdx.eq.dxnrel)idxel = ii1
           if(thsdx.eq.dxnrel)idxlay = ii2
          endif
          dxnabs = dmax1(dxn,dxnabs)
          xn(ii2,ii1) = xnnew(ii2,ii1)
          if(dxnabs.eq.dxn)then
           idabel = ii1
           idablay = 112
          endif
         enddo
        endif
       enddo

c now, from maximum change in xn, find new time step:
c (with clamps of dtmin < dt < dtmax)
       dtold = dt
       if(it.gt.ismallit)then
          dt = dt*1.5d-1/dxnrel
          if(xn(idablay,idabel).lt.xnlow*xntot(idablay))
     1     dt = 0.75d0*dt
          dt = dmin1(dt,dtmax)
          dt = dmax1(dt,dtmin)
          dt = dmin1(dt,dtmfac*dtold)
```

```
       endif

c now put data back into comp arrays, for plotting.
       do lay = 1,nj
        rho = 0.d0
        do i = 1,nel
         rho = xn(lay,i)*acomp(ielnum(i)) + rho
        enddo
        do i = 1,nel
         comp(lay,ielnum(i)) = xn(lay,i)*acomp(ielnum(i))*
     1     (1.d0-z)/rho
        enddo
       enddo

c end of time loop:
      enddo

100   continue

      do il = 1,nj
       test = 0.d0
       do ie = 1,nel
        test = test + comp(il,ie)
       enddo
       if(test.gt.1.d0+1.d-6)then
        print *,'Large mass fraction',test,' layer',il
        stop
       endif
      enddo

c done
       print '(a21,i5,a11)',' diffusion completed ',numtot,
     1  ' iterations'
       call priter(6,title)
       call priter(1,title)
       write(lines,'(13hDone difusion)')
       call priter(2,lines)
       return
       end
```

```
c <<<<<<<<<<<<<<<< rhtside - rhtside >>>>>>>>>>>>>>>>>>>
      subroutine rhtside(x,u,uprime,rpar,ipar)
c set up rhs (discretized spatial derivatives) for DEBDF initial
c value problem solver.
      implicit double precision (a-h,o-z)
      dimension u(nj),uprime(nj)
c Common block STRUC contains model structure
      common/STRUC/h(jmax,30),comp(jmax,15),sr(jmax),nj,modno
c Common block GLOB contains global model parameters
      common/GLOB/fms,dmdt,xat0,z,alfa,time,dtime,pcl,tcl,fls,teffl
c Common block CONST contains fundamental physical constants
      COMMON/CONST/CMS,CRS,CLS,CG,CSB,CPI,CP4,CCL,CME,CH,CNA,
     1 CEV,CK,CSYR
      common /model/ dt,ttimed,numits,it,nel
      common /diffus/w(jmax,nelmax),rc(nelmax,nelmax)
      common /denses/ xn(jmax,nelmax),r(jmax)
      common /index/ielnum(nelmax),newiel(nelmax),newx(nelmax),
     1  newnel
      common /clamps/ xntot(jmax),xnlow
      iel = ipar
c put updated number density u back into xn for call to dvels
      do ii = 1,nj
       if(u(ii).lt.0.d0)u(ii) = 0.d0
       xn(ii,iel) = u(ii)
      enddo
      call dvels
c rpar is the signal that dvels has been called.  No need to call
c it both here and in JAC.  Note that dvels is not optimized for this
c problem, since it solves for all nel velocities, and we only need
c one at a time.
      rpar = 1.d0

      uprime(1) = -r(2)*w(2,iel)*u(2)/r(1)**2/2.d0
      do il = 2,nj-1
       rp1 = r(il+1)
       rm1 = r(il-1)
       delr = 2.d0 * (rp1 - rm1)
       uprime(il) = -(rp1**2*w(il+1,iel)*u(il+1) - rm1**2*
     1  w(il-1,iel)*u(il-1))/r(il)**2/delr
      enddo
```

```
      uprime(nj) = r(nj-1)**2*w(nj-1,iel)*u(nj-1)/2.d0/r(nj)**2/
     1 4.d0/(r(nj)-r(nj-1))

      return
      end
c <<<<<<<<<<<<<<<<< JAC -- JAC -- JAC >>>>>>>>>>>>>>>>>
      subroutine jac(x,u,pd,nrowpd,rpar,ipar)
c evalucate jacobian of finite difference system for debdf.  Since we
c have told debdf that this is a banded system with +1 -1 from
c diagonal (which it is) we must use "irow" funtion defined below.
      implicit double precision (a-h,o-z)
c Common block STRUC contains model structure
      common/STRUC/h(jmax,30),comp(jmax,15),sr(jmax),nj,modno
c Common block GLOB contains global model parameters
      common/GLOB/fms,dmdt,xat0,z,alfa,time,dtime,pcl,tcl,fls,teffl
c Common block CONST contains fundamental physical constants
      COMMON/CONST/CMS,CRS,CLS,CG,CSB,CPI,CP4,CCL,CME,CH,CNA,
     1 CEV,CK,CSYR
      common /model/ dt,ttimed,numits,it,nel
      common /diffus/w(jmax,nelmax),rc(nelmax,nelmax)
      common /denses/ xn(jmax,nelmax),r(jmax)
      common /index/ielnum(nelmax),newiel(nelmax),newx(nelmax),
     1  newnel
c
      dimension u(nj),pd(nrowpd,nj)
c following function statement for storing of banded matrix:
      irow(i,j) = i - j + 3
c
      iel = ipar
c rpar is signal that dvels was called from sub. rhtside
      if(rpar .lt. 5.d-1) then
       do ii = 1,nj
        if(u(ii).lt.0.d0)u(ii) = 0.d0
        xn(ii,iel) = u(ii)
       enddo
       call dvels
      endif

      pd(irow(1,2),2) = -r(2) * w(2,iel)/2.d0/r(1)**2
```

```
      do ii = 2,nj-1
       denom = 2.d0*r(ii)**2*(r(ii+1)-r(ii-1))
       pd(irow(ii,ii-1),ii-1) = r(ii-1)**2*w(ii-1,iel)/denom
       pd(irow(ii,ii+1),ii+1) = -r(ii+1)**2*w(ii+1,iel)/denom
      enddo

      pd(irow(nj,nj-1),nj-1) = r(nj-1)*w(nj-1,iel)/
     1 2.d0/r(nj)**2/2.d0/(r(nj)-r(nj-1))
      rpar = 0.d0
      return
      end
c ****************
      subroutine crash(xn)
      common/STRUC/h(jmax,30),comp(jmax,15),sr(jmax),nj,modno
      common /index/ielnum(nelmax),newiel(nelmax),newx(nelmax),
     1  newnel
      dimension xn(jmax,nelmax)
       do lay = 1,nj
        rho = 0.d0
        do i = 1,nel
         rho = xn(lay,i)*acomp(ielnum(i)) + rho
        enddo
        do i = 1,nel
         comp(lay,ielnum(i)) = xn(lay,i)*acomp(ielnum(i))*
     1    (1.d0-z)/rho
        enddo
       enddo
      open(unit=45,file='crash.bin',form='unformatted',
     1  status='unknown')
      call binout(45)
      stop
      end
```

B.2 Diffusion Velocity Code

Following is the source code for the subroutines which calculate the diffusion velocity.

```
c various subroutines to calculate the diffusive velocity.  dvels
c does the main work of finding diffusive velocities, with support
c from rescoef (finds resistance coefficients) and some NAG
c subroutines (F07ADF & F07AEF) to do matrix solutions.  For use
c with the ISUEVO stellar evolution program.
c Ben Dehner

#include "isuevo.h"

c  <<<<<<<<<<<<<<<<  rescoef - rescoef - rescoef  >>>>>>>>>>>>>>>>
      subroutine rescoef(ilay)
c use formalism from Paquette, Pelletier, Fontaine and Michaud (1986)
c Ap. J. Supp. v61 p177 (referred to as PPFM in this subroutine) to
c calculate diffusion coefficient.  Then puts all resistance
c coefficients in matrix rc.
      implicit double precision (a-h,o-z)
      common /model/ dt,ttimed,numits,it,nel
      common /coefs/ctab1(4,50),ctab5(4,50),expnd1(2),expnd2(2)
      common /diffus/w(jmax,nelmax),rc(nelmax,nelmax)
      common /denses/ xn(jmax,nelmax),r(jmax)
      common /index/ielnum(nelmax),newiel(nelmax),newx(nelmax),
     1  newnel
      common /clamps/ xntot(jmax),xnlow
c Common block STRUC contains model structure
      common/STRUC/h(jmax,30),comp(jmax,15),sr(jmax),nj,modno
c Common block OLD contains the old values of everything
      common/OLD/hold(jmax,30),compold(jmax,15),srold(jmax),njold
c Common block GLOB contains global model parameters
      common/GLOB/fms,dmdt,xat0,z,alfa,time,dtime,pcl,tcl,fls,teffl
c Common block CONST contains fundamental physical constants
      COMMON/CONST/CMS,CRS,CLS,CG,CSB,CPI,CP4,CCL,CME,CH,CNA,
     1 CEV,CK,CSYR
      data e /4.803d-10/
      data amu /1.6602d-24/
c
      t = dexp(h(ilay,3))
c
      xnz2 = 0.d0
      do ii = 1,newnel+1
       do jj = 1,newnel+1
```

```
        rc(ii,jj) = 0.d0
       enddo
       xnz2 = xnz2 + xn(ilay,newx(ii))*zcomp(newiel(ii))**2
      enddo

c find debye screening length (Eqn 2)
      debye = dsqrt(ck*t/4.d0/cpi/e**2/xnz2)

      do 1000 irow = 1,newnel+1
      if(xn(ilay,newx(irow)).lt.xnlow*xntot(ilay)) go to 1000
       z1 = zcomp(newiel(irow))
       a1 = acomp(newiel(irow))
       xn1 = xn(ilay,newx(irow))

       do 1900 icol = irow+1,newnel+1
        if(icol.eq.irow) go to 1900
        if(xn(ilay,newx(icol)).lt.xnlow*xntot(ilay)) go to 1900
        z2 = zcomp(newiel(icol))
        a2 = acomp(newiel(icol))
        xn2 = xn(ilay,newx(icol))
        xnatom = xn1 + xn2
c
c 1: find screening length lambda
c   -- larger of Debye length (eqn. 2) and average inter-ionic
c      distance (see text p180)
      xl = (3.d0/4.d0/cpi/xnatom)**(1.d0/3.d0)
      xlam = dmax1(debye,xl)

c now find collision integral omega, use table as necessary
c i, find fitting function f (PPFM eqn. 70)
c   from PPFM:  gam12 = Eqn 33;  psi12 = Eqn 68;  eps12 = Eqn 66
      gam12 = 4.d0*ck*t*xlam/z1/z2/e**2
      psi12 = dlog(dlog(1.d0+gam12**2))
      eps12 = cpi*(z1*z2*e**2/2.d0/ck/t)**2*dsqrt(ck*t/
     1  (2.d0*cpi*amu*a1*a2/(a1+a2)))

      if(psi12.lt.-7.d0)then
       write(*,301)ilay,psi12,gam12,t,xlam
301    format('psi12 out of range, i= ',i4,' psi12 = ',1pe12.4,
     1   ' gam12 = ',1pe12.4,/,' T = ',1pe12.4, ' xlam = ',1pe12.4)
```

```
        psi12 = -7.d0
       endif

c find fitting function F; use table & eqn. 70 if -7 < psi < 3:
       if(psi12.le.3.d0)then
        nbin = int((psi12+7.d0)/2.d-1) + 1
        psin = 2.d-1*dble(nbin-1) - 7.d0
        psin1 = 2.d-1*dble(nbin) - 7.d0
        if(z1*z2.gt.0.d0)then
         xlnf = ctab1(1,nbin)*(psin1 - psi12)**3 + ctab1(2,nbin)*
     1    (psi12 - psin)**3 + ctab1(3,nbin)*(psin1-psi12) +
     2    ctab1(4,nbin)*(psi12-psin)
        endif
        if(z1*z2.lt.0.d0)then
        xlnf = ctab5(1,nbin)*(psin1 - psi12)**3 + ctab5(2,nbin)*
     1    (psi12- psin)**3 + ctab5(3,nbin)*(psin1-psi12) +
     2    ctab5(4,nbin)*(psi12-psin)
        endif
        f = dexp(xlnf)
       endif

c use eqns 73-74 if psi >3
        if(psi12.gt.3.d0)then
         if(z1*z2.gt.0.d0)f = expnd1(1)*dexp(psi12) + expnd1(2)
         if(z1*z2.lt.0.d0)f = expnd2(1)*dexp(psi12) + expnd2(2)
        endif

c ii, now we know f, get omega (PPFM eqn. 65)
        omega = eps12*f

c now, finally, compute diffusion coefficient
c    ee from PPFM eqn 17,  dc from PPFM eqn 5
        ee = ck*t/(8.d0*a1*a2/(a1+a2)**2*omega)
        dc = 3.d0*ee/2.d0/(a1+a2)/amu/(xn1+xn2)

c and resistance coefficient (PPFM 22)
        rc(irow,icol) = ck*t*xn1*xn2/(xn1+xn2)/dc
        rc(icol,irow) = rc(irow,icol)
        if((icol.eq.newnel+1).and.(rc(irow,icol).eq.0.d0))then
         print *,'irow',irow,' icol',icol,' rc',rc(irow,icol)
```

```
        print *,'newnel',newnel,' ilay',ilay
        continue
       endif
1900  continue
1000  continue
c check for 0 resistance coefficients for electrons.
c     sume = 0.d0
c     do ii = 1,newnel+1
c      sume = sume + rc(ii,newnel+1)
c     enddo
c     if(sume.lt.1.d-10)then
c      print *,'0 electron rc'
c      continue
c     endif
      return
      end
c <<<<<<<<<<<<< acomp -- acomp -- acomp >>>>>>>>>>>>>>>>>>>>
      double precision function acomp(i)
c returns atomic weight of comp array element i.  nel+1 is a flag for
c electrons.
      implicit double precision (a-h,o-z)
      common /model/ dt,ttimed,numits,it,nel
      atmp = -1.d0
      if(i.le.4) atmp = dble(i)
      if(i.eq.5) atmp = 6.d0
      if(i.eq.6) atmp = 7.d0
      if(i.eq.7) atmp = 7.d0
      if(i.eq.8) atmp = 12.d0
      if(i.eq.9) atmp = 13.d0
      if(i.eq.10) atmp = 14.d0
      if(i.eq.11) atmp = 15.d0
      if(i.eq.12) atmp = 16.d0
      if(i.eq.(nel+1)) atmp = 5.443d-4
      if(atmp.le.0.)then
       print *,'acomp: do not recognize i = ',i
       stop
      endif
      acomp = atmp
      return
      end
```

```
c<<<<<<<<<<<<<< zcomp -- zcomp -- zcomp >>>>>>>>>>>>>>>>>>>>>>>>
      double precision function zcomp(i)
c return charge z for comp array element i
C  ASSUMING COMPLETE IONIZATION!
      implicit double precision(a-h,o-z)
      common /model/ dt,ttimed,numits,it,nel
      ztmp = 0.d0
      if((i.eq.1).or.(i.eq.2)) ztmp = 1.d0
      if((i.eq.3).or.(i.eq.4)) ztmp = 2.d0
      if((i.eq.5).or.(i.eq.6)) ztmp = 3.d0
      if(i.eq.7) ztmp = 4.d0
      if((i.eq.8).or.(i.eq.9)) ztmp = 6.d0
      if((i.eq.10).or.(i.eq.11)) ztmp = 7.d0
      if(i.eq.12) ztmp = 8.d0
      if(i.eq.(nel+1)) ztmp = -1.d0
      if(dabs(ztmp).lt.5.d-1)then
       print *,'ztmp: do not recognize i= ',i
       stop
      endif
      zcomp = ztmp
      return
      end
c<<<<<<<<<<<<<<<< dvels -- dvels -- dvels >>>>>>>>>>>>>>>>>>
      subroutine dvels
c subroutine to solve for diffusion velocities.  Solves set of linear
c equations given by eqns (8), (9), and (10) in Iben and McDonald,
c ApJ 296, 540, 1985  (in this subroutine, referred to as IM)
      implicit double precision(a-h,o-z)
c Common block STRUC contains model structure
      common/STRUC/h(jmax,30),comp(jmax,15),sr(jmax),nj,modno
c Common block OLD contains the old values of everything
      common/OLD/hold(jmax,30),compold(jmax,15),srold(jmax),njold
c Common block GLOB contains global model parameters
      common/GLOB/fms,dmdt,xat0,z,alfa,time,dtime,pcl,tcl,fls,teffl
c Common block CONST contains fundamental physical constants
      COMMON/CONST/CMS,CRS,CLS,CG,CSB,CPI,CP4,CCL,CME,CH,CNA,
     1 CEV,CK,CSYR
      common /model/ dt,ttimed,numits,it,nel
      common /diffus/w(jmax,nelmax),rc(nelmax,nelmax)
      common /denses/ xn(jmax,nelmax),r(jmax)
```

```
      common /index/ielnum(nelmax),newiel(nelmax),newx(nelmax),
     1  newnel
      common /clamps/ xntot(jmax),xnlow
      dimension dlxndr(jmax,nelmax),dltdr(jmax)
      dimension tmp(jmax),t(jmax),rho(jmax),tl(jmax),tmp2(jmax)
      dimension rhs(nelmax+2),xksum(nelmax+2)
      dimension eqmatrix(nelmax+2,nelmax+2),eqold(nelmax+2,nelmax+2)
      dimension ipiv(nelmax+2),wold(jmax,nelmax)
      data modold /0/


c 1st, initialize some derivatives for RHS of IM eqn 10.
c      only need to do this part once per model.
      if(modold .ne. modno) then
       xmh = 1.673d-24
       const = xmh * cg
       do j = 1,nj
        rho(j) = dexp(h(j,5))
        tl(j) = h(j,3)
        t(j) = dexp(h(j,3))
       enddo
       call kderiv(r,tl,dltdr,nj,'r','tl')
       modold = modno
      endif

      do j = 1,nj
       xntot(j) = 0.d0
       do i = 1,nel
        xntot(j) = xntot(j) + xn(j,i)
       enddo
      enddo
      do j = 1,nel+1
       do ii = 1,nj
        wold(ii,j) = w(ii,j)
        tmp(ii) = xn(ii,j)
       enddo
       call kderiv(r,tmp,tmp2,nj,'r','xn')
       do ii=1,nj
        if(xn(ii,j).gt.0.d0)dlxndr(ii,j)=tmp2(ii)/xn(ii,j)
        if(xn(ii,j).le.0.d0)dlxndr(ii,j)=0.d0
```

```
       enddo
      enddo

c find diffusive velocities by setting up matrix for each layer.
c first, find out how many elements of the ones we wanted to do are
c present in this layer:
c newx: gives the xn array element we are worried about
c newiel: gives the comp function arguements we are worried about
      do 1000 ilay = 1,nj

      newnel = 0
      do k = 1,nel
       w(ilay,k) = 0.d0
       if(xn(ilay,k).gt.xnlow*xntot(ilay))then
        newnel = newnel + 1
        newiel(newnel) = ielnum(k)
        newx(newnel) = k
       endif
      enddo
      if(newnel.lt.2)go to 1000
c take care of electrons:
      newx(newnel+1) = nel + 1
      newiel(newnel+1) = nel + 1

c now set up matrix for diffusive velocities.
c   Have newnel+2 unknowns in system:
c    (newnel) elements, array elements 1-newnel,
c    electrons, array element (newnel+1)
c    electric field. array element (newnel+2)

c find resistance coefficitents:
      call rescoef(ilay)

c find out if electrons are diffusing anywhere
      sume = 0.d0
      noel = 0
      do j = 1,newnel
       sume = sume + dabs(rc(j,newnel+1))
      enddo
      if(sume .lt. 1.d-30)then
```

```
       newnel = newnel - 1
c      noel = 1
      endif
c
      do j=1,newnel+1
       xksum(j) = 0.d0
       do jj = 1,newnel
        xksum(j) = rc(j,jj) + xksum(j)
       enddo
      enddo

c  1st (newnel) rows are equations for diffusive velocities
c  (IM Eqns 10).  I am not using the "electron" equation from
c  Eqns 10; must leave one equation out since the complete system
c  is not independant; see the text in IM.
      do irow = 1,newnel
       do icol = 1,newnel+1
        if(icol.ne.irow) eqmatrix(irow,icol) = -rc(irow,icol)/
     1   xn(ilay,newx(irow))
        if(icol.eq.irow) eqmatrix(irow,icol) = xksum(irow)/
     1    xn(ilay,newx(irow))
       enddo
       eqmatrix(irow,newnel+2)=-zcomp(newiel(irow))
      enddo

c  no net mass flow equation -- row (newnel + 1), (IM eqn 8):
      do icol = 1,newnel+1
       eqmatrix(newnel+1,icol) = acomp(newiel(icol))*
     1   xn(ilay,newx(icol))
      enddo
      eqmatrix(newnel+1,newnel+2) = 0.d0

c  no net current equation -- row (newnel + 2) (IM eqn 9):
c   -- note this condition is NOT physically valid.  See J. M.
c      Burgers, "Flow Equations for Composite Gasses" (Academic
c      Press, NY: 1969), chapter 5, section 32

      do icol = 1,newnel+1
       eqmatrix(newnel+2,icol) = zcomp(newiel(icol))*xn(ilay,
     1  newx(icol))
```

```
      enddo
      eqmatrix(newnel+2,newnel+2) = 0.d0
c
c set up right hand side:  1st newnel elements are RHS from IM
c Eqn 10 last 2 are from mass & current conditions eqns 8 and 9

      do irow = 1,newnel
       rhs(irow) = -acomp(newiel(irow))*const*(fms-sr(ilay))*cms/
     1  r(ilay)**2 - ck*t(ilay)*dltdr(ilay)-ck*t(ilay)*
     2  dlxndr(ilay,newx(irow))
      enddo
      rhs(newnel+1) = 0.d0
      rhs(newnel+2) = 0.d0

c ******
c store matrix for debugging, in case of a problem below
      do ii = 1,newnel+2
       do jj = 1,newnel+2
        eqold(ii,jj) = eqmatrix(ii,jj)
       enddo
      enddo
c ******
c the following calls are to some NAG library subroutines.  The first
c one does LU-decomposition of the matrix, the second solves
c the equations.
      nn1 = newnel + 2
      nn2 = nelmax + 2
      info = 0
      call f07adf(nn1,nn1,eqmatrix,nn2,ipiv,info)
      if(info.lt.0.or.noel.eq.1)then
       print *,'eqmatrix: '
       do iii = 1,newnel+2
        write(*,'(15(1pe8.1,x))')(eqmatrix(iii,jjj),jjj=1,newnel+2)
       enddo
       print *,'eqold:'
       do iii = 1,newnel+2
        write(*,'(15(1pe8.1,x))')(eqold(iii,jjj),jjj=1,newnel+2)
       enddo
       print *,'xn:'
       do iii = 1,newnel+1
```

```
         write(*,'(i2,x,1pe12.4)')newx(iii),xn(ilay,newx(iii))
        enddo
        print *,'error ',info,' in LU decomposition in dvels'
        print *,'noel =',noel
        print *,'layer ',ilay,' iteration',it
        print *,'newnel = ',newnel
        print *,'rc'
        do iii = 1,newnel+1+noel
         write(*,'(12(1pe12.4,x))')(rc(iii,jjj),jjj=1,newnel+1+noel)
        enddo
c
c       call iplot(-1,0,ilay,sr,wold)
        call iplot(4,13,ilay,sr,xn)
        pause
       endif

       call f07aef('N',nn1,1,eqmatrix,nn2,ipiv,rhs,nn2,info)
       if(info.ne.0)then
        print *,'error ',info,' in backsubstitution in dvels'
        print *,'layer ',ilay,' iteration',it
        pause
       endif
c finished, put diffusive velocities in w array
       do k = 1,newnel+1
        w(ilay,newx(k)) = rhs(k)
       enddo
c find electron diffusive velocity, backsubstitute into current eqn.
c      xsum = 0.d0
c      do k = 1,newnel
c       xsum = xsum + zcomp(newiel(k))*rhs(k)
c      enddo
c      w(ilay,nel+1) = -xsum/zcomp(nel+1)
c done, next layer
1000   continue
c
       return
       end
c
c  <<<<<<<<<<<<<<<  kderiv - kderiv - kderiv  >>>>>>>>>>>>>>>>>>>
       subroutine kderiv(x,f,dfdx,n,xvar,yvar)
```

```
c stolen from Kurucz's ATLAS program.   (R. L. Kurucz, "ATLAS: A
c Computer Program for Calculating Model Stellar Atmospheres",
c Smithsonian Astrophysical Observatory Special Report 309,
c Mar 3, 1970)
c
c  assumes that any zero in x occurs at an endpoint.
      implicit real*8 (a-h,o-z)
      character*(*) xvar,yvar
      dimension x(*),f(*),dfdx(*)
c  If x-axis has two consecutive points that are equal, then
c  derivatives cannot be obtained and program must be stopped.
      do 10 j=2,n
       xtest=x(j)-x(j-1)
       if(xtest .eq. 0.d0) then
        write(*,5) xvar,yvar,j,dble(n)
    5   format(/2x,'x-axis has 2 points equal in a derivative'
     1   ' calculation.',/3x,'x-axis variable is ',a12,/3x,'y-axis',
     2   ' variable is ',a12,/3x,'error occurred at depth ',i4,
     3   ' out of ',1pe10.3,' depth points.',
     4   /,' j ',a12,'(j)')
        stop 'kderiv: oops'
       endif
   10 continue
c
      dfdx(1)=(f(2)-f(1))/(x(2)-x(1))
      n1=n-1
      dfdx(n)=(f(n)-f(n1))/(x(n)-x(n1))
      if(n .eq. 2) return
      s=dabs(x(2)-x(1))/(x(2)-x(1))
      do 20 j=2,n1
       scale=dmax1(dabs(f(j-1)),dabs(f(j)),dabs(f(j+1)))/dabs(x(j))
       if(scale .eq. 0.d0) scale=1.d0
       d1=(f(j+1)-f(j))/(x(j+1)-x(j))/scale
       d=(f(j)-f(j-1))/(x(j)-x(j-1))/scale
       if(dabs(d) .lt. 1.d-7) then
        tan=0.d0
       else
        tan=d/(s*dsqrt(1.d0+d**2)+1.d0)
       endif
       if(dabs(d1) .lt. 1.d-7) then
```

```
        tan1=0.d0
       else
        tan1=d1/(s*dsqrt(1.d0+d1**2)+1.d0)
       endif
   20  dfdx(j)=(tan1+tan)/(1.d0-tan1*tan)*scale
      return
      end
c  <<<<<<<<<<<<<  collision - collision - collision  >>>>>>>>>>>>>
      block data collision
c collision integral fitting tables, for use with resistance
c coefficient calculations.  All from Paquette, Pelletier, Fontaine
c and Michaud (1986) ApJSupp, 61, 177 (1986)  (in this subroutine
c referred to as PPFM)

      implicit double precision (a-h,o-z)
      common /coefs/ctab1(4,50),ctab5(4,50),expnd1(2),expnd2(2)
c following data from PPFM, Table 1. (repulsive potentials)
      data ctab1 / omitted /
c these from PPFM equation [73a] (repulsive potentials)
      data expnd1 /1.00141d0, -3.18209d0/
c this data from PPFM table 5: (attractive potentials)
      data ctab5/ omitted /
c and this from PPFM eqn. [74a] (attractive potentials)
      data expnd2 /1.01101d0, -3.19815d0/
      end
```

B.3 Include File

Include file, isuevo.h

```
/* common defintions and limits for ISUEVO */
#define JMAX 999       /* maximum number of layers   */
#define jmax 999

#define NELMAX 15    /* maximum number of elements */
#define nelmax 15    /* change this with care      */
```

```
                    /* don't change at all -- the nuclear   */
                    /* buring rates in burn2.f have many    */
    /* arrays with cross sections and other */
                    /* constants.                           */

/* below are structure definitions for the C code.  I don't know what
   will happen if we try to compile this with Fortran ... */

#if !defined(LANGUAGE_FORTRAN)

typedef struct model_file MOD_FILE;
typedef struct pulsation_file PLS_FILE;

/* model file structure */
struct model_file {
 double fms;
 double dmdt;
 double xat0;
 double z;
 double alfa;
 double tim;
 double dtime;
 double pcl;
 double tcl;
 double fls;
 double teffl;
 int nj;
 int modno;
 double sr[JMAX];
 double h[JMAX][7];
 double comp[JMAX][NELMAX];
};

/* pulsation file structure */
struct pulsation_file {
 int nj;
 double r[JMAX];
 double mass[JMAX];
 double l[JMAX];
 double t[JMAX];
```

```
 double rho[JMAX];
 double p[JMAX];
 double eps[JMAX];
 double kappa[JMAX];
 double cv[JMAX];
 double chi_rho[JMAX];
 double chi_t[JMAX];
 double eps_rho[JMAX];
 double eps_t[JMAX];
 double kappa_rho[JMAX];
 double kappa_t[JMAX];
 double del[JMAX];
 double del_ad[JMAX];
 double mu[JMAX];
 double h1[JMAX];
 double he4[JMAX];
 double c12[JMAX];
 double o16[JMAX];
 };

/* "struc" common block structure */
struct common_struc {
 double h[30][JMAX];
 double comp[NELMAX][JMAX];
 double sr[JMAX];
 int nj;
 int modno;
 };

/* "glob" common block structure */
struct common_glob {
 double fms;
 double dmdt;
 double xat0;
 double z;
 double alfa;
 double time;
 double dtime;
 double pcl;
 double tcl;
```

```
 double fls;
 double teffl;
 };

/* "const" common block structure */
struct common_const {
 double cms;
 double crs;
 double cls;
 double cg;
 double csb;
 double cpi;
 double cp4;
 double ccl;
 double cme;
 double ch;
 double cna;
 double cev;
 double ck;
 double csyr;
 };

/* diffusion common block */
struct common_diffus {
 double w[NELMAX][JMAX];
 double rc[NELMAX][NELMAX];
 };

/* in order to see these common block, C code compiled with the
   Fortran code must contain the lines below.  The trailing
   underscore "_" is due to Fortran naming conventions.  Common
   block elements are then refered to as members of their respective
   structure.

   extern struct common_struc struc_;
   extern struct common_glob glob_;
   extern struct common_const const_;
*/

#endif     /* end of non-Fortran stuff */
```